Esmaeil Jahanshahi

Control Solutions for Multiphase Flow

Linear and nonlinear approaches to anti-slug control

Thesis for the degree of philosophiae doctor

Trondheim, October 2013

Norwegian University of Science and Technology
The Faculty of Natural Sciences and Technology
Department of Chemical Engineering

NTNU

Norwegian University of Science and Technology

Thesis for the degree of philosophiae doctor

The Faculty of Natural Sciences and Technology
Department of Chemical Engineering

ISBN 978-82-471-4670-5 (printed version)
ISBN 978-82-471-4671-2 (electronic version)
ISSN 1503-8181

Doctoral theses at NTNU, 2013:271

Printed by Skipnes

SUMMARY

Severe-slugging flow in offshore production flowlines and risers is undesirable and effective solutions are needed to prevent it. Automatic control using the top-side choke valve is a recommended anti-slug solution, but many anti-slug control systems are not robust against plant changes and inflow disturbances. The closed-loop system becomes unstable after some time, and the operators turn off the controller. In this thesis, the focus is on finding robust anti-slug solutions using both linear and nonlinear control approaches. The study includes mathematical modeling, analysis, OLGA simulations and experimental work.

First, a simplified dynamical four-state model was developed for a severe-slugging pipeline-riser system. The new model, and five other models existing in the literature, were compared with results from the OLGA simulator. OLGA is a commercial package based on rigorous models and it is widely used in the oil industry. The new four-state model is also verified experimentally. Furthermore, the pipeline-riser model was extended to a well-pipeline-riser system by adding two new state variables.

Next, the simplified dynamical models were used for controllability analysis of the system. From the controllability analysis, suitable controlled variables and manipulated variables for stabilizing control were identified. A new mixed-sensitivity controllability analysis was introduced in which a single γ-value quantifies the robust performance of the control structure. In agreement with previous works, subsea pressure measurements were found to be the best controlled variables for an anti-slug control. The top-side valve is usually used as the manipulated variable, and two alternative locations also were considered. It was found that a subsea choke valve close to the riser base has the same operability as the top-side choke valve, while a well-head valve is not suitable for anti-slug control.

Three linear control solutions were tested experimentally. First, $\mathcal{H}_\infty$ control based on the four-state mechanistic model of the system was applied. $\mathcal{H}_\infty$ mixed-sensitivity design and $\mathcal{H}_\infty$ loop-shaping design were con-

sidered for this. Second, IMC design based on a identified model was chosen. The resulting IMC controller is a second-order controller that can be implemented as a PID controller with a low-pass filter (PID-F). Finally, PI-control was considered and PI tuning values were obtained from the proposed IMC controller. It was shown that the IMC (PID-F) controller has good performance and robustness, matching the model-based $\mathcal{H}_\infty$ controller, and it does not need a mechanistic model and it is easier to tune.

Four nonlinear control solutions were tested; three of them are based on the mechanistic model and the fourth one is based on identified models. The first solution is state feedback with state variables estimated by nonlinear observers. Three types of observers were tested experimentally and it was found that the nonlinear observers could be used only when the using the top-side pressure measurement. The second solution is an output-linearizing controller using two directly measured pressures. The third nonlinear controller is PI control with gain adaptation based on a simple model of the static gain. The last nonlinear solution is a gain-scheduling of three IMC controllers which were designed based on identified models. The gain-scheduling IMC does not need a mechanistic model and shows better robustness compared to the other nonlinear control solutions.

ACKNOWLEDGEMENTS

This work could not have been completed without the assistance of several individuals. First and foremost is my supervisor, Prof. Sigurd Skogestad. Prof. Sigurd Skogestad has been a real source of motivation during this work. His doors were always open for suggestions and guidance and his passion for learning has truly inspired me. He has definitely left a lasting impression on me as a both a person and as a researcher. Next, I would really like to thank my co-supervisor Prof. Ole Jørgen Nydal (Department of Energy and Process Engineering). He provided access to the multi-phase flow laboratory and we always had fruitful discussion about slug flow.

Special thanks goes to Esten Ingar Grøtli (Department of Engineering Cybernetics) who introduced me to the world of Nonlinear Estimation and Nonlinear Control, and was co-author for two of conference publications. I would also like to acknowledge with gratitude, the master students who contributed to this project: Anette Helgesen, Knut Åge Meland, Mats Lieungh, Henrik Hansen, Terese Syre, Mahnaz Esmaeilpour and Anne Sofie Nilsen.

I greatly appreciate help from the NTNU technical and laboratory staff who helped to build the experimental rig for the anti-slug control, specially Geir Finnøy who implemented the electronics and the data acquisition system of the experimental rig.

I gratefully acknowledge the funding source that made this work possible. This work has been financed by SIEMENS AS, Oil & Gas Solutions through the project SIEMENS-NTNU Research Cooperation Oil and Gas Offshore. I would like to thank the project manager from Siemens Dr. Anngjerd Pleym who helped in the timely completion of this work with assistance in the scheduling.

It was an absolute privilege to have the company of Process Systems Engineering group members most of whom became my close friends and I will always cherish the tremendous warmth I received from them. They

helped create an environment of sharing, as we learned together the lessons of life as well as Process Control.

Finally, I would like to thank my parents, Rahmatollah and Mahtalat Jahanshahi who have always stood by me, even though living far away.

Esmaeil Jahanshahi
October 2013
Trondheim, Norway

Contents

Chapter 1

INTRODUCTION

The world energy demand has been increasing rapidly due to further industrialisation and emerging new industrial giants such as China and India. In spite of recent developments in new energies, fossil fuels are still the most important source of energy and is expected to remain so. Because of increased demand, the crude oil price has stayed above 100 US$ during the past decade. Since the resources are limited, many technologies have been developed to maximize the production from existing petroleum reservoirs. Production from unconventional sources like Oil Sands in Canada, which was not economically feasible before, is possible now.

The first fields that were explored in the history of oil and gas were easy to produce and not very technically demanding. However, as these resources are drained, the demand for more advanced technology is growing. One interesting fact is that even if the newly discovered offshore fields are located at places with deeper water, the depth of the reservoir formations tend to be smaller. The result is that the reservoirs have low energy, meaning lower temperatures and lower pressure and therefore making it more difficult to exploit them. The driving force for producing the oil and gas is then smaller making the fields more prone to slugging, and the low temperatures makes it more difficult to avoid solids formation, like hydrates and waxes [63].

Safe and economical transport of the produced oil and gas by subsea pipelines is a big challenge in offshore oil production. This has led to advances in multiphase transport technology and the emergence of the multidisciplinary field of "Flow Assurance". In this Chapter, first, we briefly introduce the main processes involved in offshore oil production. Next, we discuss challenges related to flow assurance at offshore oilfields. One of these challenges is severe-slugging flow which provides the main motivation for this thesis.

1.1 Offshore Oil Production

The main process units involved in offshore oil production are the reservoir, subsea oil wells, subsea manifolds, flowlines, risers and separators. We will briefly introduce these processes.

1.1.1 Petroleum reservoir

A reservoir is a rock formation of sedimentary origin (with very few exceptions) containing liquid and/or gaseous hydrocarbons. The reservoir rock is porous and permeable, and the structure is bounded by impermeable barriers which trap the hydrocarbons. The vertical arrangement of the fluids in the structure is governed by gravitational forces. Figure 1.1 shows a cross-section of a typical hydrocarbon reservoir (classic anticline) [9]. Petroleum reservoirs are broadly classified as oil or gas reservoirs. These broad classifications are further subdivided depending on [3]:

- The composition of the reservoir hydrocarbon mixture
- Initial reservoir pressure and temperature
- Pressure and temperature of the surface production

Usually a single pressure value is referred to as the *reservoir pressure* or the *formation pressure*, and a single temperature is referred to as the *reservoir temperature*. For example, the Elgin Franklin field in the North Sea has a reservoir pressure of 1000 bar and a temperature of 200 °C [69]. Some reservoirs contain heavy oils that require artificial lift for production. The cold temperatures in deepwater or in the Arctic also play a role in how well the oil flows. Sometimes water or produced gas is injected into the reservoir to maintain the pressure and force the oil to flow toward the production wells.

1.1.2 Subsea oil wells

An oil well generally refers to any boring through the earth that is designed to find and acquire petroleum hydrocarbons. In particular, it is a producing well with oil as its primary commercial product. Oil wells almost always produce some gas and frequently produce water. Most oil wells eventually produce mostly gas or water [66].

Subsea wells are essentially the same as onshore wells. Mechanically however, they are placed in a Subsea structure (template) that allows the wells to be drilled and serviced remotely from the surface, and protected

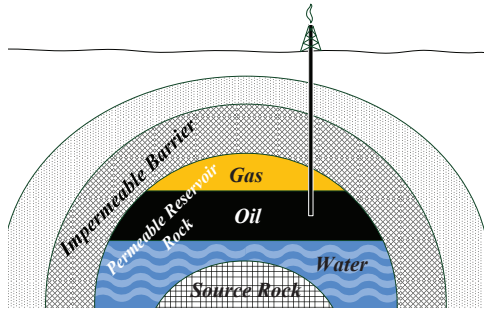

Figure 1.1: Cross-section of a typical hydrocarbon reservoir

from damage, e.g. from trawlers. The wellhead is placed in a slot in the template where it mates to the outgoing pipeline as well as hydraulic and electric control signals. Operations are handled from the surface where a hydraulic power unit (HPU) provides hydraulic power to the subsea installation via an *umbilical*. The umbilical is a composite cable containing tension wires, hydraulic pipes, electrical power and control and communication signals [11]. The oil, water and gas sometimes travel from the reservoir to the surface under their own pressure (natural drive). A well in which the formation pressure is sufficient to produce oil at a commercial rate without requiring a pump is called a *natural flowing well*. Most reservoirs are initially at pressures high enough to allow a well to flow naturally. If reservoir pressures are low, however, artificial lift is employed. Artificial lift can be in the form of in-well or seafloor pumps and is sometimes accompanied with in-well heating and/or gas lift systems.

1.1.3 Subsea processing

A subsea processing unit (Figure 1.2) separates water from the produced multiphase mixture and injects the water back to a disposal reservoir. In addition, it includes a booster to send oil and gas with a higher pressure through the subsea flowlines. Produced sand from the well also is treated by the subsea processing system. Removing the water helps to improve recovery from low-pressure reservoirs by reducing the head pressure in risers and hence the back pressure on oil wells. The recovery rate of Tordis field of Norway has increased from 49% to 55% by use of the subsea processing system. Moreover, injecting the water into the reservoir reduces the water emission from topside facilities to the sea [70].

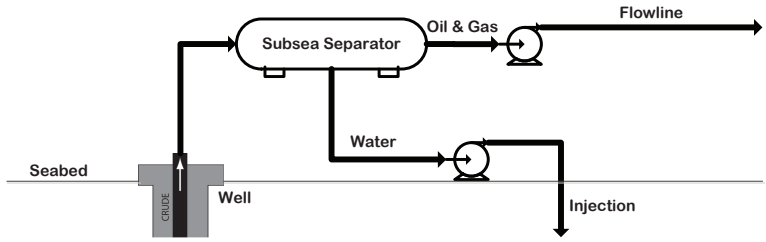

Figure 1.2: Schematic presentation of a subsea processing system

1.1.4 Subsea pipelines and risers

Pipelines (and risers) are the blood vessels of the oilfield; they are used for a number of purposes in the production of offshore hydrocarbon resources (see Figure 1.3). These include e.g. [4]:

- Export (transportation) pipelines;
- Flowlines to transfer product from platforms to export lines;
- Water injection or chemical injection flowlines;
- Flowlines to transfer product between platforms, subsea manifolds and satellite wells;
- Pipeline bundles.

In offshore field development, pipelines are a major cost and many criteria, depending on depth and temperature must be taken into account in their design. A riser system is essentially a conductor pipe connecting the well-head at the seabed to the topside facility. There are basically two kinds of risers; namely rigid risers and flexible risers. A hybrid riser is the combination of both. The six main configurations for flexible risers are shown in Figure 1.4. Configuration design drivers include a number of factors such as water depth, host vessel access/hang-off location, field layout such as number and type of risers and mooring layout, and in particular environmental data and the host vessel motion characteristics [4].

1.1.5 Topside separators

The function of the topside facilities is to separate the oil well stream into three “components” or phases (oil, gas, and water), and process these phases into marketable products or dispose them in an environmentally acceptable

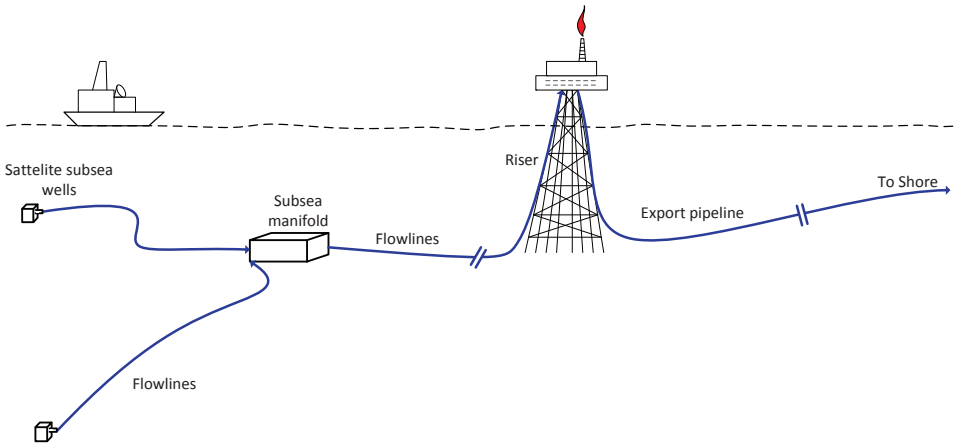

Figure 1.3: Subsea pipelines and riser

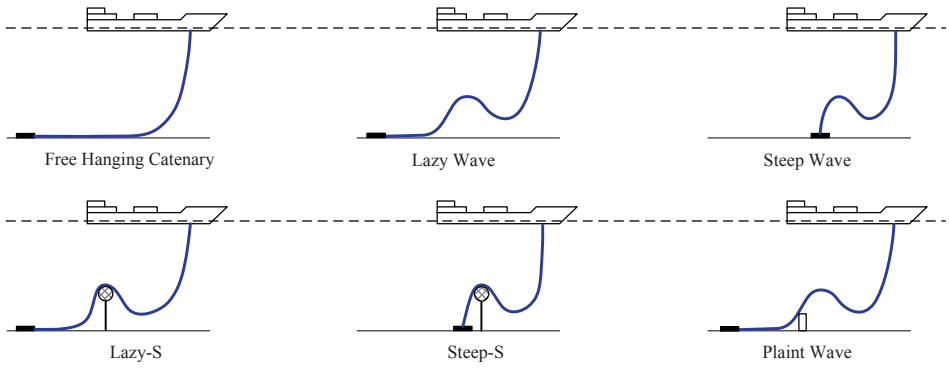

Figure 1.4: Flexible riser configurations

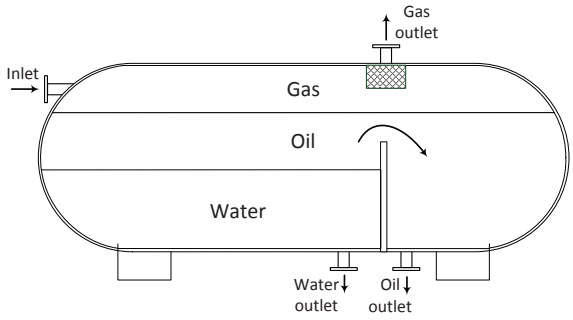

Figure 1.5: Topside three-phase separator

manner. In the separators, gas is flashed from liquids and "free water" is separated from the oil. This should remove enough light hydrocarbons to produce a "stable" crude oil with volatility (i.e., vapor pressure) to meet sales criteria. Separators are classified as two-phase if they separate gas from the total liquid stream and three-phase if they also separate the liquid stream into its crude oil and water components [65]. Figure 1.5 shows a three-phase separator. During the early years of the oil industry the gas was burnt in flares, but today the gas is usually compressed and treated for sale or injection.

In Figure 1.5, two level controllers regulate the levels of water and oil in the separator and one pressure controllers regulate the pressure of the gas by actuating their corresponding outlet valves. Because of the coupling between the two levels and the pressure, the separator is an interesting multi-variables control problem. The level switches and other safety logics are also important requirements in operation.

1.2 Flow Assurance Challenges

"Flow assurance" is a relatively new term in the oil and gas industry. It refers to ensuring successful and economical flow of the hydrocarbon stream from the reservoir to the point of sale and is closely linked to multiphase flow technology.

The concept of Flow Assurance developed because traditional approaches are inappropriate for deepwater production due to extreme distances, depths, temperatures or economic constraints. The term Flow Assurance was first used by Petrobras in the early 1990s as "Garantia do Escoamento" [Portuguese], literally meaning "Guarantee of Flow", or Flow Assurance [32].

Flow assurance is an extremely diverse subject matter, encompassing

many separate and specialized subjects and embracing all kinds of engineering disciplines. Besides network modeling and transient multiphase simulation, flow assurance involves handling solid deposits, such as gas hydrates, asphaltene, wax, scale and naphthenates (oil and condensate). Flow assurance is the most critical task during deep-water production because of the high pressures and low temperature involved. The financial loss from production interruption or asset damage due to flow assurance mishap can be astronomical. What compounds the flow assurance task even further is that these solid deposits can interact with each other and cause blockage of the pipelines and result in flow assurance failure.

Flow Assurance is applied during all stages of system selection; detailed design, surveillance, troubleshooting operation problems and increased recovery in late life etc.

1.2.1 Hydrates

Gas hydrates are crystalline materials where water molecules form a framework containing cavities which are occupied by individual gases or gas mixtures (e.g. methane, ethane, propane, isobutane and inorganic molecules such as CO_2 and H_2S). Hydrates form when light hydrocarbons meet with water, typically at temperatures less than 5°C and at elevated pressures.

Hydrates are similar to snow in appliance and structure, but since the gaseous molecules "stabilize" the water crystalline structures, hydrates are formed before the appearance of snow. Hydrates can cause blockage in gas flowlines, and an effective way is needed to inhibit their formation. The most common solution is use of a chemical "inhibitor" such as MEG (Mono-Ethylene Glycol) or Methanol. Another prevention measure which is used together with chemicals, is insulation of pipelines. In some fields, insulation can be used to keep the temperature above hydrate formation temperature. The calculation of thermal insulation requires thermal calculations which can be extensive.

If, despite of prevention strategies, hydrates are formed, it is important to have means to remove the blockages in the system. Depressurization is the most effective remediation mean. Direct electrical heating can be a solution in critical places. It is used in the Åsgard field of Norway.

"Cold flow" is an alternative technology on hydrate prevention in pipelines at deepwater production. This technology aims to eliminate the need for injection of chemicals and heating under normal operating conditions at seabed. Cold flow is based on slurry transport of hydrate particles and possibly other solids, like wax. However, it will only occur when we have reached steady-state operating conditions. The main goal for this technology is to

have a solution which allows subsea field development based on long mulitphase wellstream transport. The only problem that one may have is at the start-up and shut-in of cold flow technology operations. These operations can be managed by use of chemicals, or pipe insulation and heating. Whatever system will be selected for start-up and shut-in operation, it will add cost and complication to deepwater production facilities [53]. Both NTNU and SINTEF have done research work in the area cold flow technology.

1.2.2 Wax

Wax is a class of hydrocarbons that are natural constituents in any crude oil and most gas condensates. Waxy oils may create problems in oil production for three main reasons [32]:

- Restricted flow due to reduced inner diameter in pipelines and increased wall roughness
- Increased viscosity of the oil
- Settling of wax in storage tanks

For any pipeline experiencing wax deposition, there has to be a wax control strategy. Most often, the wax control strategy simply consists of scraping the wax away from the pipe wall by regular pigging. Sometimes, substantial quantities of wax are removed from the line. In one case, several tonnes of wax were collected in the pig trap at Statfjord field in the Norwegian Sea.

1.2.3 Asphaltenes

Asphaltenes are usually the heaviest fractions of the crude oil and are defined by their solubility characteristics. They are soluble in aromatic solvents such as toluene but precipitate upon addition of n-alkanes such as n-heptane. During production, asphaltenes are also known to precipitate as a result of change in pressure, temperature and or composition of the fluid.

From literature and past history, it is known that asphaltene precipitation is more likely to occur in an under-saturated, light reservoir fluid than a heavy hydrocarbon system. It is also noteworthy that problems due to asphaltenes occur in a two-step process: (i) precipitation from the reservoir fluid, and (ii) deposition of the precipitated asphaltene particles. They cause production rate decline and various other operational problems, such as higher viscosity and water oil emulsion, etc. It is a key risk to handle in flow assurance and production chemistry.

Presently, The main focus of research activities is to understand asphaltene behaviour. New techniques are being developed to measure asphaltene deposition but are not in common use in the industry. It is a consensus in the industry that the "prevention" approach is the best to tackle possible problems caused by solids deposition [46].

1.2.4 Scales

Oilfield scale is mainly deposits of inorganic salts such as carbonates and sulphates of barium, strontium or calcium. Scale may also be salts of iron like sulphides, carbonates and hydrous oxides. Scales reduce transport capacity of flowlines and they can cause plugging. Scale inhibitors are chemicals which stop or interfere with the nucleation, precipitation and adherence of mineral deposits. Scale dissolvers are chemicals which dissolve scale by complexing with ions like barium, strontium, calcium and iron. Other techniques like electromagnetic inhibitor exist too [79].

1.2.5 Corrosion

When "carbon steel" pipes are used in transporting oil and multiphase flow containing a fraction of water, there is usually a high risk of corrosion. The decision to use carbon steel is usually economic, in order to minimise capital expenditure, and its use usually requires implementing a full internal corrosion management strategy to control corrosion levels through the system life.

Various mechanisms have been postulated for the corrosion process. All involve the formation of carbonic acid ion or biocarbonate when CO_2 is dissolved in water.

$$CO_2 + H_2O \rightarrow CO_3^{2-} + 2H^+$$

$$CO_2 + H_2O \leftrightarrow HCO_3^- + H^+$$

Including iron the overall reaction is:

$$CO_2 + H_2O + Fe \rightarrow FeCO_3 + H_2$$

This process can lead to corrosion of the material at a rate which is greater than that from general acid corrosion having the same pH value. The mechanism of corrosion is dependent on the quantity of CO_2 dissolved in the water phase, and predictions of corrosion levels are currently based on the knowledge of CO_2 partial pressure and the use of correlations such as DeWaard-Milliams [45].

1.2.6 Emulsions

Under a combination of low ambient temperature and high fluids viscosity due to inversion water cut conditions, stable emulsions can occur between the water and oil phases. This can impair separation efficiency at the processing facility and thus cause loss in production [45].

Under these conditions there may be need to inject de-emulsifiers at the subsea facilities and also to ensure that sufficient pressure is available to re-start the system following an unplanned shutdown.

1.2.7 Slugging flow

The combined transport of hydrocarbon liquids and gases can offer significant economic savings over the conventional, local, platform-based separation facilities. The flow behavior of two-phase flow is much more complex than that of single-phase flow. Two-phase flow is a process involving the interaction of many variables. The gas and liquid phases normally do not travel at the same velocity in the pipeline because of the differences in density and viscosities. For an upward flow, the gas phase which is less dense and less viscous tends to flow at a higher velocity than the liquid phase. On the other hand, in terrains with a downward slope the liquid flows with a higher velocity than the gas. Although the analytical solutions of single-phase flow are available and the accuracy of prediction is acceptable in industry, multiphase flow predictions, even when restricted to a simple pipeline geometry, are in general quite complex [4]. Some of the flow patterns that occur in a horizontal pipeline for different velocities of flow are shown in Figure 1.6, and flow patterns in vertical pipelines are presented in Figure 1.7.

Slug flow is one of the flow patterns occurring in multiphase pipelines as shown in Figure 1.6 and Figure 1.7. It is characterized by a series of liquid plugs (slugs) separated by a relatively large gas pockets. Slug flow can be caused by any of the following:

- **Hydrodynamic slugs -** this form of slugging occurs in horizontal pipelines due to differences in velocities of the different phases. Liquid builds up and forms slugs which are short, but with a high frequency. This type of slugging causes less problems than “severe slugging”.

- **Riser slugging -** this type of slugging is induced by the presence of a vertical riser. The liquid blocks the entrance to the riser so that the gas can not enter into the riser. This is the case until the pressure of the upstream gas exceeds the gravitational pressure of the liquid in

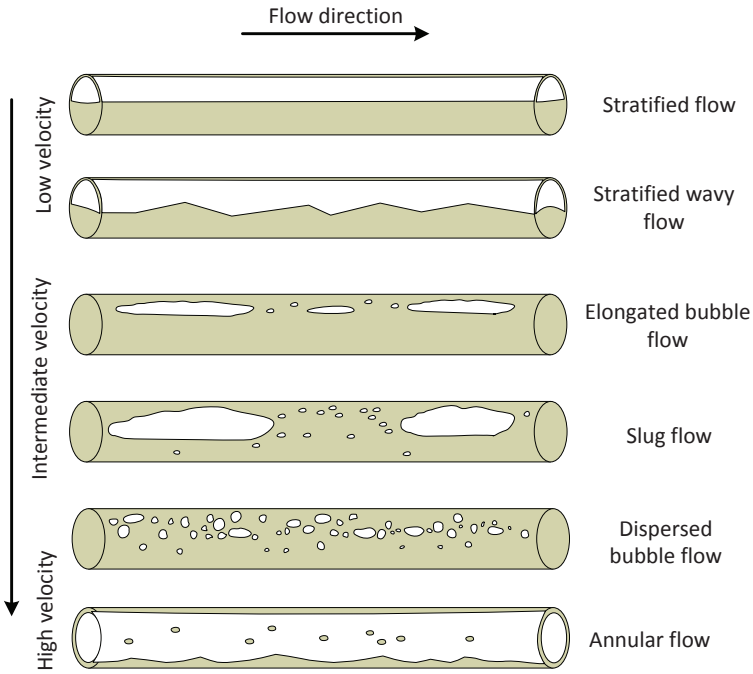

Figure 1.6: Flow patterns in a horizontal pipeline for different velocities

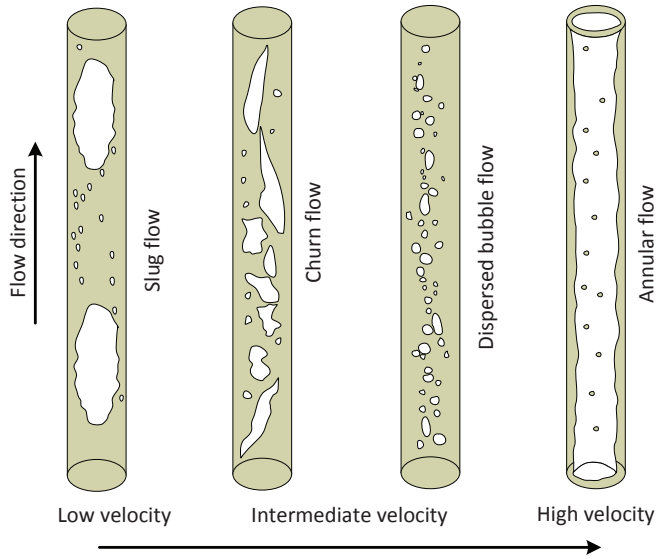

Figure 1.7: Flow patterns in a vertical pipeline for different velocities

the riser column. This type of slugging causes long liquid slugs and large pressure variations. It is also known as "severe slugging".

- **Terrain-induced slugging -** induced by irregular surface of the seabed, liquid tends to accumulate at places with lower elevations. This can cause blockage of the gas flow in the pipe.
- **Operational-based slugging -** one example is pig-induced slugging that happens when a pig is running for cleaning the wax.
- **Casing heading slugs in gas-lifted wells -** this type of slugging is similar to the riser slugging, but gas is compressed in the annulus of the well.
- **Density-wave slugs in long risers and wells -** accumulation of gas at the bottom of the riser (well) makes a region with low-density and this region travels upward.

Slugging in production pipelines and risers has for many years been a major operational problem in subsea oil-gas fields developments. The slugging can result in severe fluctuations in pressure and flow rate (gas and liquid) at both the wells end and the receiving host processing facilities. This causes many problems, e.g. [43]:

- Oscillations are not in agreement with smooth operation
- Safety aspects and shutdown risks
- The total oil and gas production must usually be less than the systems design capacity to allow for the peak production
- Unstable mode often decreases sharply the lift gas efficiency for gas-lifted wells
- Difficulties with gas-lift allocation computation due to instabilities
- Drawbacks on facilities, well operations and equipments

1.3 Riser Slugging

The riser-slugging instability is one of the main flow assurance challenges discussed in the previous section. In the following, we describe the mechanism of the riser slugging in details. Next, we summarise the conventional solutions to prevent the riser slugging. Finally, automatic control is introduced as an anti-slug solution with a large potential of economical benefit.

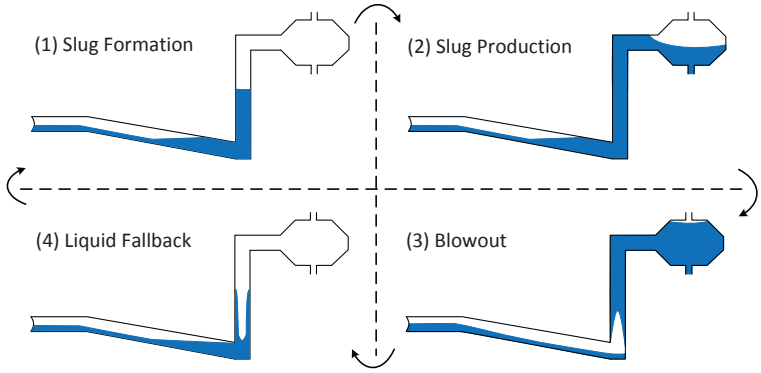

Figure 1.8: Schematic of severe slugging in flowline-riser systems

1.3.1 Mechanism of riser slugging

A downward inclination of the pipeline ending to the riser increases the possibility of the riser slugging. This enables liquid to accumulate in the entrance to the riser, and causes liquid to block the entrance in to the riser. This leads to compression of the gas in the pipeline and finally expansion of the gas in the riser when the gas pressure is higher than the hydrostatic head in the riser [44]. The mechanism of riser slug formation can be described by the following four steps:

- **Step 1 -** Liquid accumulates in the riser low-point due to gravity. This is the case if the gas and liquid velocities are low enough to allow for it.
- **Step 2 -** As long as the hydrostatic head of the liquid in the riser is higher than the pressure drop over the riser the slug continues to grow as gas can not penetrate the liquid blocking the entrance.
- **Step 3 -** When the pressure drop over the riser exceeds the hydrostatic head, the liquid is pushed out of the riser.
- **Step 4 -** When all the liquid has left the riser the velocities are so small that liquid falls back in to the low-point of the riser and starts to accumulate again.

The four steps are illustrated in Figure 1.8 (adapted from [63]).

The flow pattern in risers is not always severe slugging. However, it depends on inflow conditions, topside choke valve, geometry and dimensions of the riser as well as the separator pressure. Flow regime maps are used to

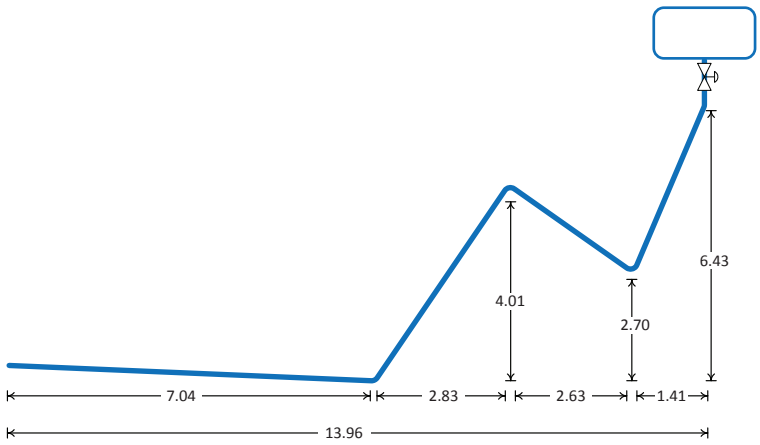

Figure 1.9: Experimental setup for S-riser at NTNU

study the stability of the flow in risers where the flow regime is shown for different values of gas superficial velocity U_{sg} and liquid superficial velocity U_{sl}. One example of such maps is shown in Figure 1.10. This flow regime map was obtained from experiments on a setup for S-riser at multiphase flow laboratory of NTNU [59]. The Geometry and dimensions of the riser are given in Figure 1.9 and the separator is at the atmospheric pressure. Two types of severe-slugging flow are observed at low velocities of liquid and gas inflows. Severe slugging I gives slugs with larger amplitudes (about 1.8 *bar* peak of inlet pressure) compared to those of severe slugging II (about 1.4 *bar* peak of the inlet pressure). By increasing the inflow velocities the flow regime changes to transient slugging with small but high frequency slugs. The flow becomes stable for sufficiently large inflow rates which can be dispersed bubble or annular flow regimes.

1.3.2 Conventional anti-slug solutions

Slug catcher: A slug catcher is a vessel with sufficient buffer volume to store the largest slugs expected from the upstream system. The slug catcher is located between the outlet of the riser and the processing facility. The buffered liquids can be drained to the processing equipment at a much slower rate to prevent overloading the system. As slugging is a periodical phenomenon, the slug catcher should be emptied before the next slug arrives. To design the slug catcher many criteria depending of flow rates and length of the slugs are considered. This solution increases the capital cost and the slug catcher tank occupies space on the platform.

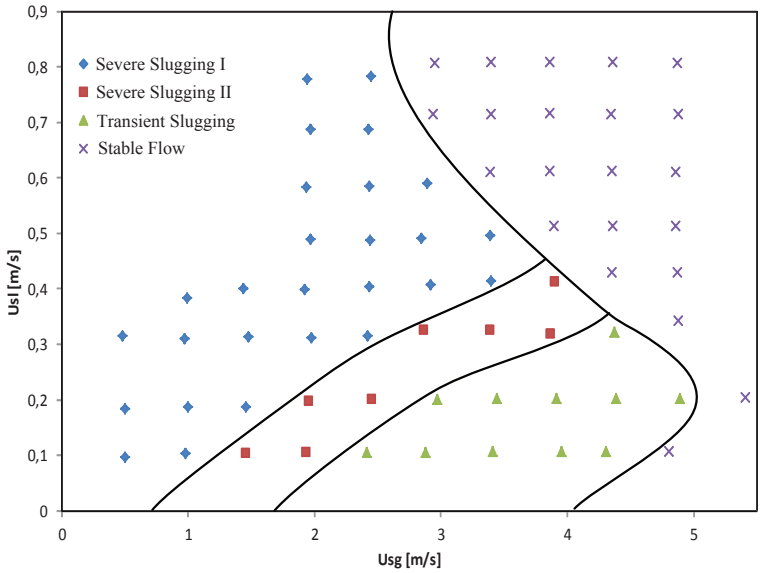

Figure 1.10: Flow regimes occurring in S-riser

Topside Choking: Closing the topside choke valve can eliminate severe-slugging [68]. However, this increases back pressure of the subsea oil wells and decreases the production rate. Topside chocking was one of the first methods proposed to prevent the severe slugging phenomenon in 1973 [82]. It was observed that increased back pressure could eliminate severe slugging but would reduce the flow capacity severely.

Riser Base Gas Injection: This method provides artificial lift for the liquids, moving them steadily through the riser. This technique can alleviate the problem of severe slugging by changing the flow regime from slug flow to annular or dispersed flow, but does not help with transient slugging. It is one of the most frequently used methods for current applications [57].

The riser base gas injection method was first used to control hydrodynamic slugging in vertical risers. However, it was dismissed as not being economically feasible due to the cost of a compressor for pressurizing the gas for injection and the piping required to transport the gas to the base of the riser [67]. Loss and Joule–Thomson cooling are the potential problems resulting from high-injection gas flow rates.

To reduce amount of the injected gas, automatic feedback control can be used. Control of the hold-up at top of the riser by manipulating the gas injection valve has been proposed in [52].

Full Separation: Another solutions is "full separation" where liquid

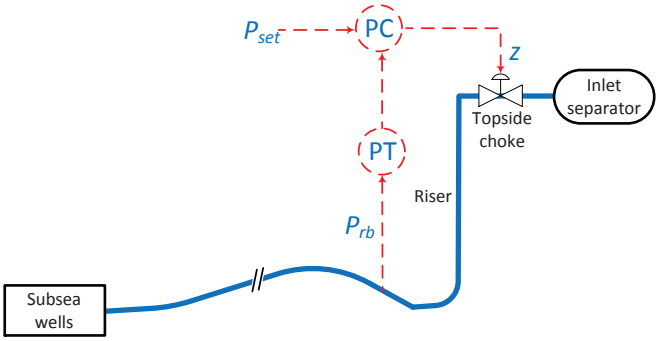

Figure 1.11: Preventing slug flow by control of riser base pressure

phases and gas are separated at the subsea and transported to the topside facilities by separate risers. However, this method is not economical.

1.3.3 Automatic control solution

Most of the researchers in fluid dynamics believe that the boundaries between flow regimes shown in Figure 1.10 are given by nature and cannot be moved without changing riser geometry or the boundary conditions. However, automatic feedback control can change the dynamics of a given steady-state operating point from unstable to stable. By use of automatic control, it is possible to stabilize a normally unstable "non-slugging" flow regime at conditions that the system would give the "slugging" flow regime without control. In other words, we are able to change the boundaries between the flow regimes.

The first successful use of automatic feedback control to prevent slug flow was reported in 1996 [10]. The French company Total used anti-slug control to prevent severe slugging in the Dunbar 16 inches multiphase pipeline located in the North Sea. They controlled the riser base pressure by manipulating the topside choke valve as shown in Figure 1.11. In 2000, ABB reported a similar use of automatic control to prevent slugging in the pipeline between Hod and Valhall platforms in the North Sea [30]. They used a combination of feedforward control and dynamic feedback control in a cascaded structure.

Figure 1.12 shows a bifurcation diagram of the experimental S-riser presented in Section 1.3.1. The bifurcation diagram illustrates the behavior of the system over the whole working range of the choke valve [77]. The solid lines show the maximum and minimum of the slugging oscillation and the average value. The dashed line shows the unstable non-slug steady-state

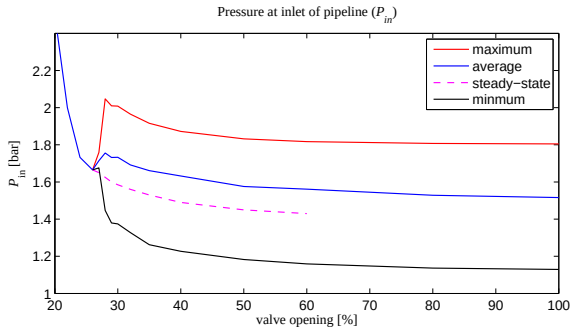

Figure 1.12: Bifurcation diagram of the experimental setup for S-riser [59]

that becomes slugging flow without control. If we manually close the choke valve sufficiently the inlet pressure increases and the flow becomes stable. For the present experimental setup, the critical value of the relative valve opening for the transition between a stable non-oscillatory flow regime and riser slugging is $Z = 26\%$.

The unstable steady-state is like equilibrium of an inverted pendulum and it can be stabilized by dynamic feedback control. The steady-state pressure is lower than the average pressure and the system can operated on lower pressure set-point by use of anti-slug control. This leads to a higher production rate from subsea oil wells and economical benefits [60].

1.4 Motivation

Existing anti-slug control systems are often not operating in practice because of robustness problems; the closed-loop system becomes unstable after some time, for example because of inflow disturbances or plant changes. The operators turn off the controller and instead use manual choking when the control system becomes unstable. The main objective of our research is to find robust solutions for anti-slug control systems. The nonlinearity at different operating conditions is one source of plant change, because gain of the system changes drastically for different operating conditions. In addition, the time delay is another problematic factor for stabilization. A robust controller must have a good gain margin in presence of plant changes and a good delay margin (phase margin) for transportation delay in long flowlines. Furthermore, the system should not drift away from the design operating point (setpoint tracking or performance).

First, we aim at finding a good control structure, that is finding controlled variables, manipulated variables and parings that give a robust

closed-loop system for stabilizing control. Next, we consider both linear and nonlinear approaches for the controller design. PID and PI controllers are commonly used in industry and we seek tuning rules based on closed-loop step test for robust anti-slug control. Then, we consider nonlinear model-based control design to counteract nonlinearity of the system. We compare both the linear and the nonlinear approaches and find advantages and disadvantages of each.

1.5 Organization of Thesis

Chapter 1 (this chapter) gives an introduction to offshore oil production and flow assurance challenges associated with multiphase transport at offshore oil fields. Then, the slugging flow is described in more details and solutions to prevent slugging flow are reviewed.

Chapter 2 presents simplified dynamical models for severe slugging. A new simplified model for pipeline-riser systems is presented, and this model is extended to well-pipeline-riser system. The suggested models are compared to results from OLGA simulator and experiments.

Chapter 3 deals with selection of suitable controlled variables for stabilizing control by use of controllability analysis of the system. Control structures to prevent slugging flow in well-pipeline-riser system and gas lift oil wells are suggested.

In Chapter 4, we consider three different manipulated variables (control valves) for the well-pipeline-riser system. We choose the suitable manipulated variable for anti-slug control by use of controllability analysis. Then, we validate the result by OLGA simulations and experiments.

Chapter 5 proposes a new closed-loop model identification and Internal Model Control (IMC) design for anti-slug control. Furthermore, the PID and PI tunings are obtained from the IMC controller. The proposed model identification and tuning rules are tested experimentally.

In Chapter 6, nonlinear model-based control designs are considered. First, we use state estimation by three different observers and state-feedback. Then, the feedback linearization design by measured outputs is applied. Next, a gain scheduling of three IMC controllers is compared to the two nonlinear model-based approaches.

In Chapter 7, the main conclusions and remarks of this thesis are summarized along with some suggestions for further work.

1.6 List of Contributions

1.6.1 Conference publications

1. E. Jahanshahi, S. Skogestad, Closed-loop model identification and PID/PI tuning for robust anti-slug control In: *10th IFAC International Symposium on Dynamics and Control of Process Systems (DYCOPS)*. Mumbai, India, December 2013.

2. E. Jahanshahi, S. Skogestad, Comparison between nonlinear model-based controllers and gain-scheduling Internal Model Control based on identified model. In: *52nd IEEE Conference on Decision and Control (CDC)*. Florence, Italy, December 2013.

3. E. Jahanshahi, S. Skogestad, E. I. Grøtli. Nonlinear model-based control of two-phase flow in risers by feedback linearization. In: *9th IFAC Symposium on Nonlinear Control Systems (NOLCOS)*. Toulouse, France, September 2013.

4. E. Jahanshahi, S. Skogestad, M. Lieungh. Subsea solution for anti-Slug Control of multiphase risers. In: *European Control Conference (ECC)*. Zürich, Switzerland, July 2013.

5. E. Jahanshahi, S. Skogestad, E. I. Grøtli. Anti-slug control experiments using nonlinear Observer. In: *American Control Conference (ACC)*. Washington D.C., USA, June 2013.

6. E. Jahanshahi, S. Skogestad, A. H. Helgesen. Controllability analysis of severe slugging in well-pipeline-riser systems. in: *IFAC Workshop - Automatic Control in Offshore Oil and Gas Production*. Trondheim, Norway, May 2012.

7. E. Jahanshahi, S. Skogestad, H. Hansen. Control structure design for stabilizing unstable gas-lift oil wells. in: *International Symposium on Advanced Control of Chemical Processes (ADCHEM)*, Singapore, July 2012

8. E. Jahanshahi and S. Skogestad, Simplified dynamical models for control of severe slugging in multiphaser risers. in: *Proceeding of the*

18th International Federation of Automatic Control (IFAC) World Congress 1634–1639. Milan, Italy, September 2011.

1.6.2 Journal publications

1. E. Jahanshahi, S. Skogestad, Simplified dynamical models for control of severe slugging flow in offshore oil production, *In Preparation.*

2. E. Jahanshahi, S. Skogestad, Control structure design for stabilizing control: anti-slug control at offshore oilfields, *In Preparation.*

3. E. Jahanshahi, S. Skogestad, Linear control solutions for anti-slug control at offshore oilfields, *In Preparation.*

4. E. Jahanshahi, S. Skogestad, Nonlinear control solutions for anti-slug control at offshore oilfields, *In Preparation.*

1.6.3 Patents

1. Title: Pipeline-riser system and method of operating the same
   Patent No. 13174514.3 - 1605
   'Subsea solution for anti-slug control at offshore oilfields'
   Inventors: Sigurd Skogestad, Esmaeil Jahanshahi

2. Title: Method of operating a pipeline-riser system
   Patent No. 13174513.5 - 1605
   'Closed-loop model identification and PID/PI tuning for robust anti-slug control'
   Inventors: Esmaeil Jahanshahi, Sigurd Skogestad

3. Title: Robust PID tuning based on relay-feedback and IMC design
   'Robust PID tuning based on relay-feedback and IMC design'
   Inventors: Esmaeil Jahanshahi, Selvanathan Sivalingam, Brad Schofield

Chapter 2

SIMPLIFIED DYNAMICAL MODELS

Instead of elaborated models such as those used for simulation purposes (e.g. OLGA simulator), a simple dynamical model with few state variables is desired for model-based control design. We propose a new simplified dynamic model for severe slugging flow in pipeline-riser systems. The proposed model, together with five other simplified models found in the literature, are compared with results from the OLGA simulator. The new model can be extended to other cases, and we consider also a well-pipeline-riser system. The proposed simple models are able to represent the main dynamics of severe slugging flow and compare very well with OLGA simulations and experiments.

2.1 Introduction

Slugging has been recognised as a serious problem in offshore oilfields and many efforts have been made in order to prevent this problem [10], [30]. The severe slugging flow regime usually occurs in pipeline-riser systems that transport oil and gas mixture from the seabed to the surface. This problem, also referred to as "riser slugging", is characterised by severe flow and pressure oscillations. Slugging problems have also been observed in gas-lifted oil wells where two types of instabilities, casing heading and density wave instability, have been reported [31].

The irregular flow caused by slugging can cause serious operational problems for the downstream surface facilities, and an effective way to handle or remove riser slugging is needed. The conventional solution is to reduce the opening of the top-side choke valve (choking), but this may reduce the

production rate especially for fields where the reservoir pressure is relatively low. Therefore, a solution that guarantees stable flow together with the maximum possible production rate is desirable. Fortunately, automatic control has been shown to be an effective strategy to eliminate the slugging problem and different slug control strategies have tested experimentally [25]. Anti-slug control is an automatic feedback control system that aims at stabilising the flow in the pipeline at the same operating conditions that uncontrolled would yield riser slugging [75]. This control system usually uses the top-side choke as the manipulated variable and the riser base pressures as the controlled variable.

There have been some research on riser slugging using the OLGA simulator to test anti-slug control [21], but for controllability analysis and controller design a simpler dynamical model of the system is desired. The focus of this chapter is on deriving the simple dynamical models which capture the essential behaviour for control. For control, it is more important to capture the main dynamics for the onset of slugging, not the slugging itself. The aim is to avoid the slug flow regime and instead operate at a steady (non-slug) flow regime. Therefore, The shape and length of the slugs are not main concerns in this modeling.

Five simplified dynamical models for the pipeline-riser systems were found in the literature. The "Storkaas model" [76] is a three-dimensional state-space model which has been used for controllability analysis [77]. The "Eikrem model" is four dimensional state-space model [80], [17]. Another simplified model, referred to as the "Kaasa model" [49], only predicts the pressure at the bottom of the riser. The "Nydal model" [55] is the only model that includes friction in the pipes. The most recently published simplified model is the "Di Meglio model" [13], [14]. In addition, we present a new four-state model which includes useful features of the other five models. The six models are simulated in the time domain and compared to results from the more detailed OLGA model in the following five aspects, listed in order of importance:

- Critical valve opening for onset of slugging
- Frequency of oscillations at the critical point (onset of slugging)
- Dynamical response to a step change in the valve opening (non-slug regime)
- Steady-state pressure and flow rate values (non-slug regime)
- Maximum and minimum (pressure and flow rate) of the oscillations (slug regime)

The simplified models are also analysed linearly in the frequency domain where we consider the location of unstable poles and important unstable (RHP) zeros in the model. The results presented in this chapter have been partially presented by [34], and [40]. In the present chapter, we compare the new model to the experiments and we extend it to a well-pipeline-riser system. This chapter is organised as follows. In Section 2, we present our new simplified model for pipeline-riser systems. Then, In Section 3, we compare the proposed model and the other simple models to the results from the OLGA simulator and experiments. Finally, in Section 4, we extend this model to well-pipeline-riser systems and compare the extended model to OLGA simulations.

2.2 New simplified four-state model

2.2.1 Mass balance equations for pipeline and riser

For the new simplified model, consider the schematic presentation of the system in Fig. 2.1. The four differential equations in the proposed model are simply the mass conservation law for the gas and liquid phases in the pipeline and riser sections:

$$\frac{dm_{g,p}}{dt} = w_{g,in} - w_{g,rb} \tag{2.1a}$$

$$\frac{dm_{l,p}}{dt} = w_{l,in} - w_{l,rb} \tag{2.1b}$$

$$\frac{dm_{g,r}}{dt} = w_{g,rb} - w_{g,out} \tag{2.1c}$$

$$\frac{dm_{l,r}}{dt} = w_{l,rb} - w_{l,out} \tag{2.1d}$$

The four state variables in the model are

- $m_{g,p}$: mass of gas in pipeline [kg]
- $m_{l,p}$: mass of liquid in pipeline [kg]
- $m_{g,r}$: mass of gas in riser [kg]
- $m_{l,r}$: mass of liquid in riser [kg]

The model is described in detail below and its main parameters are given in Table 2.1. Four tuning parameters, further described below, can be used to fit the model to the experimental or numerical data for given pipeline-riser system.

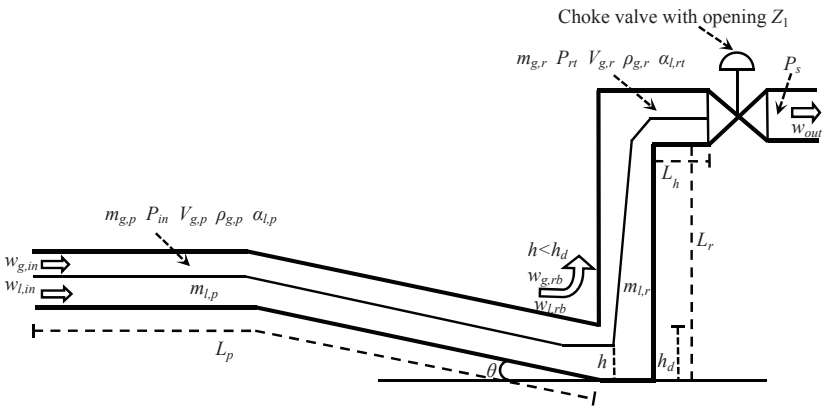

a) Simplified representation of desired flow regime

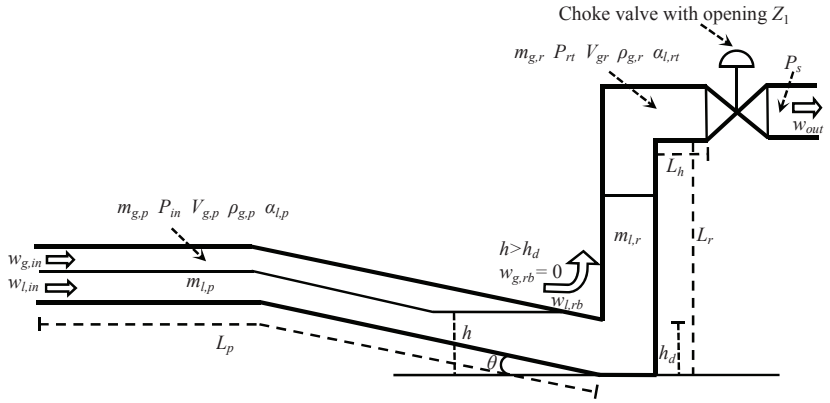

b) Simplified representation of liquid blocking leading to riser slugging

Figure 2.1: Pipeline-riser system with important parameters

- K_h: correction factor for level of liquid in pipeline
- C_{v1}: production choke valve constant
- K_g: coefficient for gas flow through low point
- K_l: coefficient for liquid flow through low point

2.2.2 Inflow conditions

In equations (2.1a) and (2.1b), $w_{g,in}$ and $w_{l,in}$ are the inlet gas and liquid mass flow rates. They are here assumed to be constant, but the inlet

boundary conditions can easily be changed, for example to make the inlet flow pressure-driven.

2.2.3 Outflow conditions

We consider a constant pressure (separator pressure, P_s) as the outlet boundary condition and a simple choke valve equation determines the outflow of the two-phase mixture.

$$w_{out} = C_{v1} f(z_1) \sqrt{\rho_{rt} \max(P_{rt} - P_s, 0)}, \tag{2.2}$$

Here $0 < z_1 < 1$ is the normalized valve opening (we use the 'capital' Z_1 when the valve opening is given in percentage, $0 < Z_1 < 100$) and $f(z_1)$ is the characteristic equation of the valve. In the simulations, a linear valve is used, i.e. $f(z_1) = z_1$, but this should be changed for other valves. $w_{l,out}$ and $w_{g,out}$, the individual outlet mass flow rates of liquid and gas, are calculated as follows,

$$w_{l,out} = \alpha^m_{l,rt} w_{out}, \tag{2.3}$$

$$w_{g,out} = (1 - \alpha^m_{l,rt}) w_{out}. \tag{2.4}$$

Here, $\alpha^m_{l,rt}$, the liquid mass fraction at top of the riser, is given by

$$\alpha^m_{l,rt} = \frac{\alpha_{l,rt}\rho_l}{\alpha_{l,rt}\rho_l + (1 - \alpha_{l,rt})\rho_{g,r}}. \tag{2.5}$$

The density of the two-phase mixture at top of the riser in (2.2) is

$$\rho_{rt} = \alpha_{l,rt}\rho_l + (1 - \alpha_{l,rt})\rho_{g,r}. \tag{2.6}$$

The liquid volume fraction, $\alpha_{l,rt}$ in (2.5) and (2.6), is calculated by equation (2.42).

2.2.4 Pipeline model

We now introduce some important parameters. The liquid volume fraction, α_l, in the pipeline section is given by the liquid mass fraction, α^m_l, and densities of the two phases [7]:

$$\alpha_l = \frac{\alpha^m_l/\rho_l}{\alpha^m_l/\rho_l + (1 - \alpha^m_l)/\rho_g}$$

The average liquid mass fraction in the pipeline section is assumed to be given by the inflow boundary condition:

$$\bar{\alpha}^m_{l,p} = \frac{w_{l,in}}{w_{g,in} + w_{l,in}}$$

The average liquid volume fraction in the pipeline is then

$$\bar{\alpha}_{l,p} = \frac{\bar{\rho}_{g,p} w_{l,in}}{\bar{\rho}_{g,p} w_{l,in} + \rho_l w_{g,in}}. \tag{2.7}$$

The gas density $\bar{\rho}_{gp}$ is calculated based on the nominal pressure (steady-state) in the pipeline by assuming ideal gas,

$$\bar{\rho}_{g,p} = \frac{P_{in,nom} M_g}{R T_p} \tag{2.8}$$

Here, $P_{in,nom}$, which depends itself on $\bar{\alpha}_{l,p}$, is calculated from a steady-state initialization of the overall model. By using (2.8) and constant (nominal) inflow rates, we get $\bar{\alpha}_{l,p}$ in (2.7) as a constant parameter.

The cross section area of the pipeline is

$$A_p = \frac{\pi}{4} D_p^2, \tag{2.9}$$

where D_p is the diameter of the pipeline, then the volume of the pipeline is $V_p = A_p L_p$. When gas and liquid are distributed homogeneously along the pipeline, the mass of liquid in the pipeline is

$$\bar{m}_{l,p} = \rho_l V_p \bar{\alpha}_{l,p}. \tag{2.10}$$

With this assumption, the level of liquid in the pipeline at the low-point is given approximately by $\bar{h} \approx h_d \bar{\alpha}_{l,p}$ where $h_d = D_p / cos(\theta)$ is the pipeline opening at the riser base and θ is the inclination of the pipeline at the low-point. More precisely, we use in the model

$$\bar{h} = K_h h_d \bar{\alpha}_{l,p} \tag{2.11}$$

where K_h is a correction factor around unity which can be used for fine-tuning the model. If the liquid content of the pipeline increases by $\Delta m_{l,p}$, it starts to fill up the pipeline from the low-point. A length of pipeline equal to ΔL will be occupied by only liquid, where

$$\Delta m_{l,p} = m_{l,p} - \bar{m}_{l,p} = \Delta L A_p (1 - \bar{\alpha}_{l,p}) \rho_l$$

and the level of liquid in the pipeline becomes $h = \bar{h} + \Delta L \sin(\theta)$ or

$$h = \bar{h} + \left(\frac{m_{l,p} - \bar{m}_{l,p}}{A_p (1 - \bar{\alpha}_{l,p}) \rho_l} \right) \sin(\theta). \tag{2.12}$$

Thus, the level of liquid in the pipeline, h, can be written as a function of liquid mass in the pipeline $m_{l,p}$ which is a state variable of the model. The rest of the parameters in (2.12) are constants.

The pipeline gas density is

$$\rho_{g,p} = \frac{m_{g,p}}{V_{g,p}}, \tag{2.13}$$

where the volume occupied by gas in the pipeline is

$$V_{g,p} = V_p - m_{l,p}/\rho_l. \tag{2.14}$$

The pressure at the inlet of the pipeline, assuming ideal gas, is

$$P_{in} = \frac{\rho_{g,p} R T_p}{M_g}. \tag{2.15}$$

We consider only the liquid phase when calculating the friction pressure loss in the pipeline [7].

$$\Delta P_{fp} = \frac{\bar{\alpha}_{l,p} \lambda_p \rho_l \bar{U}_{sl,in}^2 L_p}{2 D_p} \tag{2.16}$$

Here, λ_p is the friction factor of the pipeline which an be computed from an explicit approximation of the implicit Colebrook-White equation [26]:

$$\frac{1}{\sqrt{\lambda_p}} = -1.8 \log_{10} \left[\left(\frac{\epsilon/D_p}{3.7} \right)^{1.11} + \frac{6.9}{Re_p} \right] \tag{2.17}$$

Here, the Reynolds number is

$$Re_p = \frac{\rho_l \bar{U}_{sl,in} D_p}{\mu} \tag{2.18}$$

and μ is the viscosity of liquid and $U_{sl,in}$ is the superficial velocity of liquid:

$$\bar{U}_{sl,in} = \frac{4 w_{l,in}}{\pi {D_p}^2 \rho_l} \tag{2.19}$$

2.2.5 Riser model

Total volume of riser:

$$V_r = A_r (L_r + L_h), \tag{2.20}$$

where

$$A_r = \frac{\pi}{4} D_r^2 \tag{2.21}$$

Volume occupied by gas in riser:

$$V_{g,r} = V_r - m_{l,r}/\rho_l \tag{2.22}$$

Density of gas in riser:

$$\rho_{g,r} = \frac{m_{g,r}}{V_{g,r}} \tag{2.23}$$

Pressure at top of riser from ideal gas law:

$$P_{rt} = \frac{\rho_{g,r} R T_r}{M_g} \tag{2.24}$$

Average liquid volume fraction in riser:

$$\bar{\alpha}_{l,r} = \frac{m_{l,r}}{V_r \rho_l} \tag{2.25}$$

Average density of mixture inside riser:

$$\bar{\rho}_{m,r} = \frac{m_{g,r} + m_{l,r}}{V_r} \tag{2.26}$$

Friction loss in riser:

$$\Delta P_{fr} = \frac{\bar{\alpha}_{l,r} \lambda_r \bar{\rho}_{m,r} \bar{U}_m^2 (L_r + L_h)}{2 D_r} \tag{2.27}$$

Friction factor of riser using same correlation as for pipeline:

$$\frac{1}{\sqrt{\lambda_r}} = -1.8 \log_{10} \left[\left(\frac{\epsilon / D_r}{3.7} \right)^{1.11} + \frac{6.9}{Re_r} \right] \tag{2.28}$$

Reynolds number of flow in riser:

$$Re_r = \frac{\bar{\rho}_{m,r} \bar{U}_m D_r}{\mu} \tag{2.29}$$

Average mixture velocity in riser:

$$\bar{U}_m = \bar{U}_{sl,r} + \bar{U}_{sg,r} \tag{2.30}$$

$$\bar{U}_{sl,r} = \frac{w_{l,in}}{\rho_l A_r} \tag{2.31}$$

$$\bar{U}_{sg,r} = \frac{w_{g,in}}{\rho_{g,r} A_r} \tag{2.32}$$

2.2.6 Gas flow model at riser base

As illustrated in Fig. 2.1(b), when the liquid level in the pipeline section exceeds the openings of the pipeline at the riser base ($h > h_d$), the liquid blocks the low-point and the gas flow rate $w_{g,rb}$ at the riser base is zero,

$$w_{g,rb} = 0, \quad h \geq h_d \tag{2.33}$$

When the liquid is not blocking at the low-point ($h < h_d$ in Fig. 2.1(a)), the gas will flow from the volume $V_{g,p}$ to $V_{g,r}$ with a mass rate $w_{g,rb}$ [kg/s] which is assumed to be given by an"orifice equation" (e.g. [73]):

$$w_{g,rb} = K_g A_g \sqrt{\rho_{g,p} \Delta P_g}, \quad h < h_d \tag{2.34}$$

where

$$\Delta P_g = P_{in} - \Delta P_{fp} - P_{rt} - \bar{\rho}_{m,r} g L_r - \Delta P_{fr} \tag{2.35}$$

The free area A_g for gas flow can be calculated precisely using trigonometric functions [76], but for simplicity, a quadratic approximation is used in the new model,

$$A_g = A_p \left(\frac{h_d - h}{h_d} \right)^2, \quad h < h_d \tag{2.36a}$$

$$A_g = 0, \quad h \geq h_d \tag{2.36b}$$

2.2.7 Liquid flow model at riser base

The liquid mass flow rate at the riser base is also described by an orifice equation:

$$w_{l,rb} = K_l A_l \sqrt{\rho_l \Delta P_l}, \tag{2.37}$$

where

$$\Delta P_l = P_{in} - \Delta P_{fp} + \rho_l g h - P_{rt} - \bar{\rho}_{m,r} g L_r - \Delta P_{fr} \tag{2.38}$$

and

$$A_l = A_p - A_g \tag{2.39}$$

2.2.8 Phase distribution model at outlet choke valve

In order to calculate the mass flow rates of the individual phases as given in equations (2.2)-(2.4), the phase distribution at top of the riser must be known. The liquid volume fraction at top of the riser, α_{lt}, which was used in (2.5) and (2.6), can be calculated by the entrainment model proposed by Storkaas [76], but their entrainment equations are complicated. Instead, we use the fact that in a vertical gravity-dominant two-phase pipeline there

is approximately a linear relationship between the pressure and the liquid volume fraction. This has been observed in OLGA simulations. In addition, the pressure gradient is assumed constant along the riser for the desired non-slugging flow regimes, which then gives that the liquid volume fraction gradient is constant, i.e. $\frac{\partial \alpha_{l,r}}{\partial y} = \text{constant}$. It then follows that the average liquid volume fraction in the riser is

$$\bar{\alpha}_{l,r} = \frac{\alpha_{l,rb} + \alpha_{l,rt}}{2} \tag{2.40}$$

Here, $\bar{\alpha}_{l,r}$ is also given by (2.25) and $\alpha_{l,rb}$ is determined by the flow area of the liquid phase at the riser base (low-point):

$$\alpha_{l,rb} = \frac{A_l}{A_p} \tag{2.41}$$

Therefore, the liquid volume fraction at the top of the riser becomes

$$\alpha_{l,rt} = 2\bar{\alpha}_{l,r} - \alpha_{l,rb} = \frac{2m_{l,r}}{V_r \rho_l} - \frac{A_l}{A_p} \tag{2.42}$$

2.3 Comparison of models

2.3.1 OLGA test case and reference model

In order to study the dominant dynamic behavior of a typical, yet simple riser slugging problem, we use the test case for severe slugging in the OLGA simulator. OLGA is a commercial multiphase simulator widely used in the oil industry [5]. The geometry of the system is given in Fig. 2.2. The pipeline diameter is 0.12 m and its length is 4300 m. Starting from the inlet, the first 2000 m of the pipeline is horizontal and the remaining 2300 m is inclined downwards with a 1° angle. This gives a 40.14 m descent and creates a low pint at the end of the pipeline. The riser is a vertical 300 m pipe with a diameter of 0.1 m. A 100 m horizontal section with the same diameter as that of the riser connects the riser to the outlet choke valve. The feed into the system is nominally constant at 9 kg/s, with $w_{l,in} = 8.64$ kg/s (oil) and $w_{g,in} = 0.36$ kg/s (gas). The separator pressure (P_s) after the choke valve, is nominally constant at 50.1 bar. This leaves the choke valve opening Z_1 as the only control degree of freedom (manipulated variable) in the system.

For the present case study, the critical value of the relative valve opening for the transition between a stable non-oscillatory flow regime and riser slugging is $Z_1^* = 5\%$. This is illustrated by the OLGA simulations in Fig. 2.3 which show the inlet pressure, topside pressure and outlet flow rate, with the valve openings of 4% (no slug), 5% (transient) and 6% (riser slugging).

Figure 2.2: Geometry of OLGA pipeline-riser test case

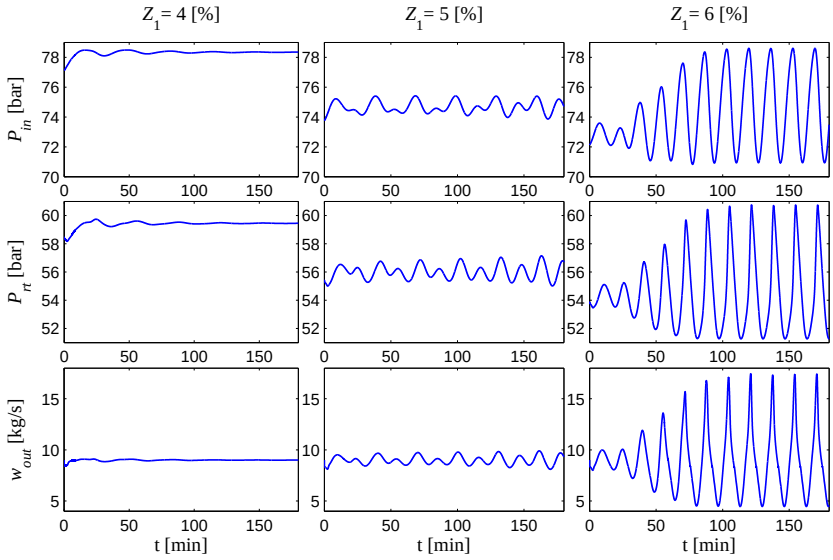

Figure 2.3: Simulations of OLGA test case for different valve openings

2.3.2 Comparison of models with OLGA simulations

The different simplified models were simulated in Matlab and their tuning parameters were adjusted to match the OLGA reference model simulations. This was mostly done by trial and error, but we believe that the obtained tuning parameters are reasonable for all the models. A more systematic approach has been proposed in [14] for tuning the Di Meglio model, but this approach did not work well for the present case study. The results are summarized in Table 2.2 which shows the error (in %) for various parameters. Our most important criteria for the model fitting are critical value of the valve opening (Z_1^*) and the oscillation frequency at this point, which for the present case study, should be 5% and 15.6 [min].

Frequency of oscillations

All models were linearised at the critical operating point $Z_1^* = 5\%$. The period of oscillations at this operating point is related to poles of the linear models. Most of the models give a pair of complex conjugate poles, $s = \pm\omega_c i = \pm 0.0067i$. Note that

$$\omega_c = \frac{2\pi}{T_c}, \quad \frac{2\pi}{15.6[\text{min}]\ 60[\text{s/min}]} = 0.0067\text{s}^{-1}$$

The exceptions are the Eikrem model and the Nydal model that are not able to get the right period time (15.6 [min]) for the critical valve opening, and consequently they result in different poles at $Z_1^* = 5\%$.

Step response

Fig. 2.4 shows the pressure response at the top of the riser to a step change in the valve opening from $Z_1 = 4\%$ to $Z_1 = 4.2\%$ for the OLGA reference model and the new model. Step responses of the OLGA model has one undershoot and one overshoot. The amplitudes of the overshoot and undershoot for different simplified models are given in Table 2.2 in the form of errors from those of the OLGA model. The inverse response (overshoot) is corresponding to the RHP zeros near the imaginary axis which are also given for $Z_1 = 5\%$ in Table 2.2.

Bifurcation diagrams

Fig. 2.5 shows the steady-sate behaviour of the new model (central line) and also the minimum and maximum of the oscillations compared to those of

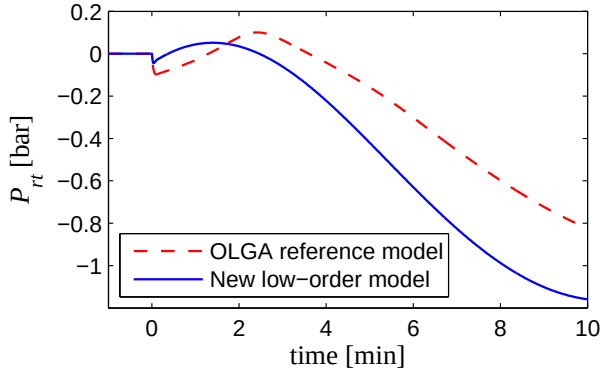

Figure 2.4: Step response of pressure at top of riser

the OLGA model. In order to have a quantitative comparison, deviations of the different simplified models from the OLGA reference model for fully open valve ($Z_1 = 100\%$) are summarised in Table 2.2.

Comparison summary

As seen in Table 2.2, there is a trade-off between model complexity and the number of tuning parameters used to match the actual process data. Very simple models, like the Kaasa model (with seven parameters) and the Di Meglio model (with five parameters), require many parameters to get a good fit. However, finding the parameter values is difficult. The Nydal model and the Eikrem model (with three parameters) are also simple, but they are not able to match the OLGA simulations because of few tuning parameters.

As opposed to the other simplified models, the new model does not require adjusting any physical property of the system, such as volume of gas in the pipeline. The new model (with four parameters) is somewhat complicated, but is able to give a good match with relatively few tuning parameters.

The new model and the De Meglio model have approximately the same accuracy in prediction of the steady-state and also minimum and maximum of slugging pressures and the flow rate, but dynamically the new model is closer to the OLGA simulations. This can be seen by comparing the step response of the top-side pressure.

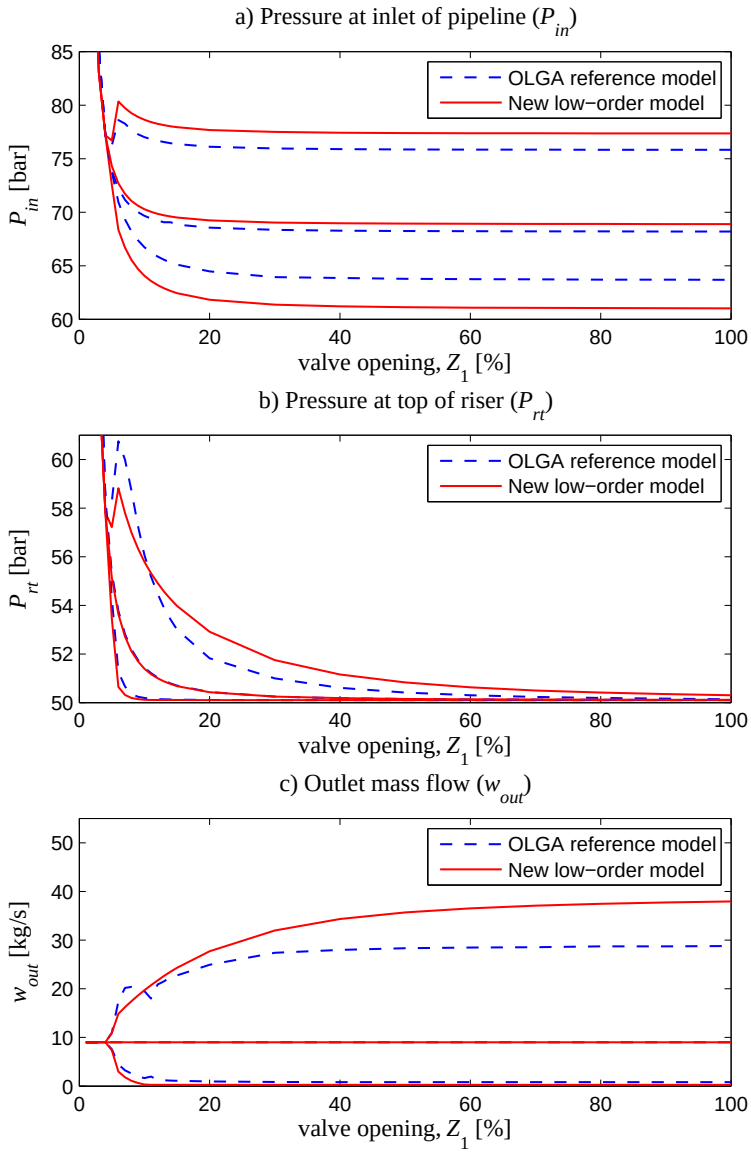

Figure 2.5: Bifurcation diagrams of simplified pipeline-riser model (solid lines) compared OLGA reference model (dashed)

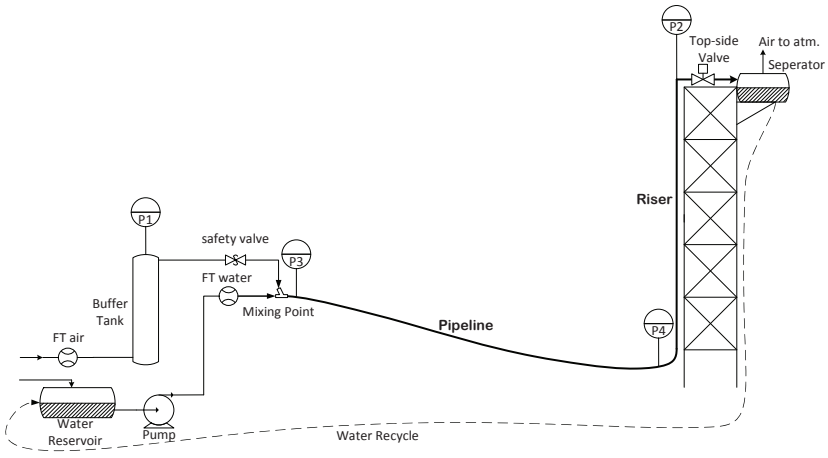

Figure 2.6: Experimental setup

2.3.3 Comparison with experiments

The experiments were performed on a laboratory setup for anti-slug control at the Chemical Engineering Department of NTNU. Fig. 2.6 shows a schematic presentation of the laboratory setup. The pipeline and the riser are made from flexible pipes with 2 cm inner diameter. The length of the pipeline is 4 m, and it is inclined with a 15° angle. The height of the riser is 3 m. A buffer tank is used to simulate the effect of a long pipe with the same volume, such that the total resulting length of pipe would be about 70 m. Other parameters and constants are given in Table 2.3.

The topside choke valve is used as the input for control. The separator pressure after the topside choke valve is nominally constant at atmospheric pressure. The feed into the pipeline is assumed to be at constant flow rates, 4 $litre/min$ of water and 4.5 $litre/min$ of air. With these boundary conditions, the critical valve opening where the system switches from stable (non-slug) to oscillatory (slug) flow is at $Z_1^* = 15\%$.

In addition, we developed a new OLGA case with the same dimensions and boundary conditions as the experimental set-up. The bifurcation diagrams are shown in Fig. 2.7 where simplified model (thin solid lines) is compared to the experiments (bold solid lines) and the OLGA model (dashed lines). In Fig. 2.7, the system has a stable (non-slug) flow when the topside valve opening Z_1 is smaller than 15%, and it switches to slugging flow conditions for $Z_1 > 15\%$.

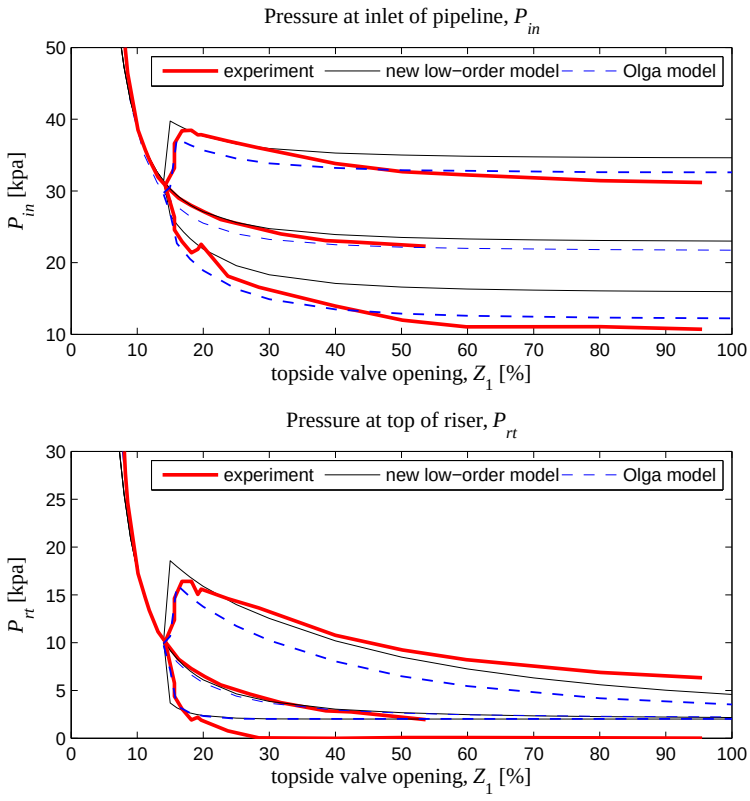

Figure 2.7: Bifurcation diagrams of simplified pipeline-riser model (thin solid lines) compared to experiments (thick solid lines) and OLGA reference model (dashed lines)

2.4 Well-Pipeline-Riser System

In the pipeline-riser model described above constant gas and liquid flow rate were used as inlet boundary conditions. In order to study effect the of pressure-driven inflow, we add an oil well and assume a constant reservoir pressure as the boundary condition (see Fig. 2.8). Moreover, [72] suggests that the origin of severe-slugging instability is at the bottom-hole of the well and that the pressure at this position is the best controlled variable. Considering the oil well dynamic is also helpful to study this possibility theoretically.

2.4.1 Simplified six-state model

We add two state variables, the mass of gas and mass of liquid inside the oil well, to the pipeline-riser system in (2.1a)–(2.1d) to obtain a six-state model. The two additional state equations are as follows.

$$\frac{dm_{g,w}}{dt} = \left(\frac{gor}{gor+1}\right) w_r - w_{g,wh}, \tag{2.43}$$

$$\frac{dm_{l,w}}{dt} = \left(\frac{1}{gor+1}\right) w_r - w_{l,wh}, \tag{2.44}$$

where gor is the average mass ratio of gas and liquid produced from the reservoir, which is assumed to be a known parameter of the well. $w_{g,wh}$ and $w_{l,wh}$ are the flow rates of gas and liquid at the well-head. The production rate w_r from the reservoir to the well is assumed to be described by a linear relationship.

$$w_r = PI \max(0, P_{res} - P_{bh}), \tag{2.45}$$

where PI is the productivity index of the well, P_{res} is the reservoir pressure, which can be assumed constant in a short period of time (e.g. few months), and P_{bh} is the bottom-hole pressure of the well,

$$P_{bh} = P_{wh} + \bar{\rho}_{m,w} g L_w + \Delta P_{fw}. \tag{2.46}$$

Here ΔP_{fw} is the pressure loss due to friction in the well, which is assumed to be given as

$$\Delta P_{fw} = \frac{\bar{\alpha}_{l,w} \lambda_w \bar{\rho}_l \bar{U}^2_{sl,w} L_w}{2 D_w}. \tag{2.47}$$

Furthermore, we have average liquid volume fraction inside well:

$$\bar{\alpha}_{l,w} = \frac{m_{l,w}}{V_w \rho_l} \tag{2.48}$$

Friction factor of well using same correlation as for pipeline [26]:

$$\frac{1}{\sqrt{\lambda_w}} = -1.8 \log_{10} \left[\left(\frac{\epsilon/D_w}{3.7} \right)^{1.11} + \frac{6.9}{Re_w} \right] \tag{2.49}$$

Reynolds number for flow in well:

$$Re_w = \frac{\rho_l \bar{U}_{sl,w} D_w}{\mu} \tag{2.50}$$

Average superficial velocity of liquid in well:

$$\bar{U}_{sl,w} = \frac{4\bar{w}_{nom}}{\pi {D_w}^2 \rho_l} \tag{2.51}$$

where $\bar{w}_{nom}$ is a priori know nominal flow rate of the well. The other important variables in the well model consist of the average density of the two-phase mixture

$$\bar{\rho}_{m,w} = \frac{m_{g,w} + m_{l,w}}{V_w}, \tag{2.52}$$

the density of the gas phase

$$\rho_{g,w} = \frac{m_{g,w}}{V_w - m_{l,w}/\rho_l}, \tag{2.53}$$

and the pressure at the well-head, assuming ideal gas

$$P_{wh} = \frac{m_{g,w} R T_{wh}}{M_g (V_w - m_{l,w}/\rho_l)}. \tag{2.54}$$

In order to calculate the volume fractions at the top of the well, we use the same assumptions as for the phase fraction of the riser in Section 2.2.8.

$$\alpha_{l,wt} = 2\bar{\alpha}_{l,w} - \alpha_{l,wb} \tag{2.55}$$

In this case, because of the high pressure at the bottom-hole, the fluid from the reservoir is saturated [3] and liquid volume fraction at the bottom is $\alpha_{l,wb} = 1$. The gas mass fraction at top of the well is then

$$\alpha^m_{g,wt} = \frac{(1 - \alpha_{l,wt})\rho_{g,w}}{\alpha_{l,wt}\rho_l + (1 - \alpha_{l,wt})\rho_{g,w}}. \tag{2.56}$$

Density of mixture at top of the well:

$$\rho_{wt} = \alpha_{l,wt}\rho_l + (1 - \alpha_{l,wt})\rho_{g,w}. \tag{2.57}$$

Valve equation for subsea choke valve:

$$w_{wh} = C_{v3} z_3 \sqrt{\rho_{wt} \max(P_{wh} - P_{in}, 0)}, \tag{2.58}$$

where P_{in} is the pressure at the inlet of the pipeline which is given by equation (2.15) in the pipeline-riser model, Section 2.2. The flow rates of gas and liquid phases from the well-head are as follows.

$$w_{g,wh} = w_{wh} \alpha_{g,wt}^m \tag{2.59}$$

$$w_{l,wh} = w_{wh} (1 - \alpha_{g,wt}^m) \tag{2.60}$$

Flow rates of gas and liquid phases into the pipeline are respectively

$$w_{g,in} = w_{g,wh} + d_1, \tag{2.61}$$

$$w_{l,in} = w_{l,wh} + d_2, \tag{2.62}$$

where d_1 and d_2 can be assumed as disturbances from the other oil wells in the network.

2.4.2 Comparison to OLGA model

In the OLGA reference model introduced in Section 2.3.1, constant inflow rates were assumed. We modifed the OLGA reference model by connecting an oil well to the inlet of the pipeline as shown in Fig. 2.8. The oil well is vertical, has a depth of 3000 m and the same inner diameter as for the pipeline 0.12 m. The reservoir pressure is constant at 230 bar. Other parameters related to the pipeline and the riser are same as for the OLGA reference model.

The well-pipeline-riser model includes an additional tuning parameter C_{v3}, the valve constant of the subsea choke valve. Hence, we have five tuning parameters in the simple well-pipeline-riser model. Numerical values for all parameters are given in Table 2.1. The resulting bifurcation diagrams of the simple model are compared to the modified OLGA model in Fig. 2.9. The simple model could predict the steady-state and the bifurcation point with a good accuracy. Fig. 2.9.b shows that the inlet mass flow is increasing by opening the topside choke valve. This is because of pressure-driven nature of the flow.

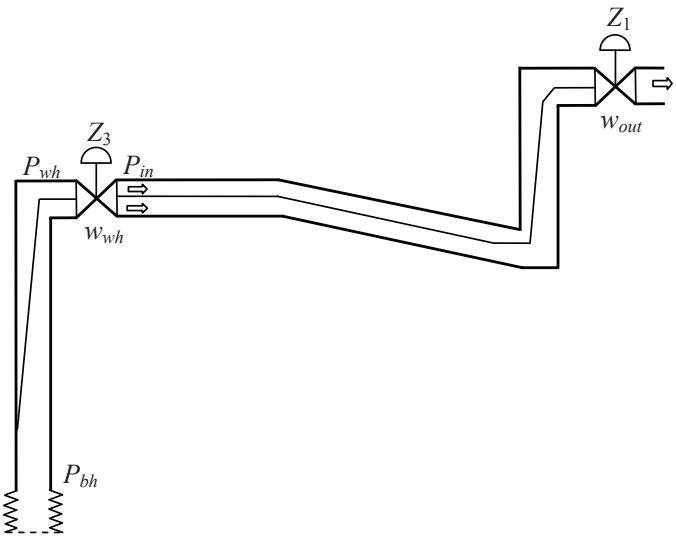

Figure 2.8: Schematic presentation of well-pipeline-riser system

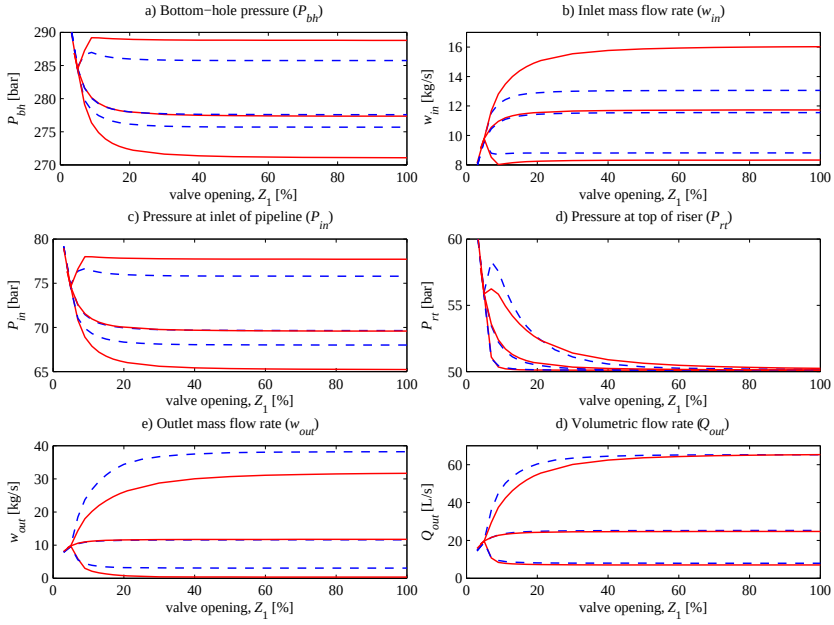

Figure 2.9: Bifurcation diagrams of simplified well-pipeline-riser model (solid lines) compared to OLGA reference model (dashed lines)

2.5 Summary

We have proposed a simplified dynamic model for severe-slugging flow in pipeline-riser systems. The new model and five other models from the literature have been compared with a test case in the OLGA simulator. Furthermore, we verified the new model experimentally. The new model cmpares well with the OLGA simulations and the experiments.

We conclude that the proposed model maintains a good fit for steady-state and dynamics; therefore it will be used in our future works for controllability analysis and controller design. Also, the De Meglio model is quite simple and easy to use, and it can be considered as an alternative.

Finally, we extended the four-state model to a well-pipeline-riser system by adding two states. The extended model was compared well to an OLGA test case. The Matlab codes for the models are available at home page of Sigurd Skogestad.

Table 2.1: Parameters of pipeline-riser and well-pipeline-riser systems

Symb.	Description	Values	Units
R	universal gas constant	8314	$J/(kmol.K)$
g	gravity	9.81	m/s^2
μ	viscosity	1.426×10^{-4}	$Pa.s$
ρ_l	liquid density	832.2	kg/m^3
M_g	gas molecular weight	20	gr
P_{res}	reservoir pressure	320	bar
PI	productivity index	2.75e-6	$kg/(s.Pa)$
$\bar{w}_{nom}$	nominal mass flow from reservoir	9	kg/s
gor	mass gas oil ratio	0.0417	–
T_w	well temperature	369	K
V_w	well volume	33.93	m^3
D_w	well diameter	0.12	m
L_w	well depth	3000	m
T_p	pipeline temperature	337	K
V_p	pipeline volume	48.63	m^3
D_p	pipeline diameter	0.12	m
L_p	pipeline length	4300	m
T_r	riser temperature	298.3	K
V_r	riser volume	3.14	m^3
D_r	riser diameter	0.1	m
L_r	riser length	300	m
L_h	length of horizontal section	100	m
P_s	separator pressure	50.1	bar
K_h	level correction factor	0.7	–
K_g	orifice of gas flow at low-point	3.49×10^{-2}	–
K_l	orifice of liquid flow at low-point	2.81×10^{-1}	–
C_{v1}	production choke constant	1.16×10^{-2}	–
C_{v3}	wellhead choke valve constant	3.30×10^{-3}	–

Table 2.2: Comparison of different simplified models to OLGA reference model

Parameters	**OLGA Model**	**Storkaas Model**	**Eikrem Model**	**Kaasa Model**	**Nydal Model**	**Di Meglio Model**	**New Model**
State equations	Many	3 diff. 1 alg.	4 diff.	3 diff.	4 diff.	4 diff.	4 diff.
Complexity	Complicated	Average	Simple	Very simple	Average	Simple	Average
Tuning parameters	Many	5	3	7	3	5	4
RHP zeros of P_{rt} at $Z = 5\%$	—	0.0146	0.006 + 0.005i 0.006 – 0.005i	—	0.0046	0.019 + 0.034i 0.019 – 0.034i	0.0413 0.0126
Values from OLGA simulator		**Error of the simplified models with respect to OLGA**					
Critical valve opening	5%	0 (0%)	0 (0%)	0 (0%)	0 (0%)	0 (0%)	0 (0%)
Period [min] at $Z = 5\%$	15.6	0 (0%)	26.15 (168%)	0 (0%)	15.97 (102%)	0 (0%)	0 (0%)
Step response of P_{rt}							
undershoot	-0.098	0.10 (99%)	0.08 (78%)		0.12 (89%)	0.07 (68%)	0.05 (54%)
overshoot	0.198	0.16 (80%)	0.18 (89%)	—	0.10 (50%)	0.17 (84%)	0.10 (51%)
at t=10 min	-0.824	0.43 (53%)	0.62 (75%)		0.25 (30%)	0.47 (58%)	0.33 (41%)
Steady-state							
P_{in} [bar]	68.22	1.9 (2.7%)	4.4 (6.46%)	—	1.77 (2.6%)	0.70 (1%)	0.69 (1%)
P_{rb} [bar]	66.76	—	—	0.02 (0.04%)	—	—	—
P_{rt} [bar]	50.10	0.01 (0.02%)	0.01 (.02%)	—	0.01 (.02%)	0.01 (0.02%)	0.01 (.02%)
w_{out} [kg/s]	9.00	0 (0%)	0 (0%)	—	2.90 (32%)	0 (0%)	0 (0%)
Minimum							
P_{in} [bar]	63.50	2.7 (4.3%)	9 (14.2%)	—	8.3 (13%)	2.6 (4.1%)	2.7 (4.2%)
P_{rb} [bar]	62.08	—	—	2.57 (4.1%)	—	—	—
P_{rt} [bar]	50.09	4e-4 (8e-4%)	5e-4 (9e-4%)	—	0.41 (0.82%)	0.003 (.006%)	4e-4 (8e-4%)
w_{out} [kg/s]	0.791	0.55 (69%)	0.14 (17%)	—	0.79 (100%)	3.3 (405%)	0.55 (68%)
Maximum							
P_{in} [bar]	75.83	1.4 (1.8%)	1.89 (2.5%)	—	1.00 (1.3%)	1.3 (1.7%)	1.50 (2.0%)
P_{rb} [bar]	74.55	—	—	0.55 (.075%)	—	—	—
P_{rt} [bar]	50.14	1.5 (3%)	0.95 (1.9%)	—	1.09 (2.2%)	0.71 (0.35%)	0.33 (0.16%)
w_{out} [kg/s]	31.18	80 (278%)	57 (200%)	—	13.3 (43%)	22 (77%)	9.10 (32.0%)

Table 2.3: Parameters of small-scale experimental setup

Symb.	Description	Values	Units
μ	viscosity	1.426×10^{-4}	$Pa.s$
ρ_l	liquid density	832.2	kg/m^3
M_g	gas molecular weight	18	gr
T_p	pipeline temperature	288	K
V_p	pipeline volume	0.0219	m^3
D_p	pipeline diameter	0.02	m
L_p	pipeline length	69.71	m
T_r	riser temperature	288	K
V_r	riser volume	0.001	m^3
D_r	riser diameter	0.02	m
L_r	riser length	3	m
L_h	length of horizontal section	0.2	m
P_s	separator pressure	0.013	bar
K_h	level correction factor	1	–
K_g	orifice of gas flow at low-point	2.07×10^{-2}	–
K_l	orifice of liquid flow at low-point	1.57×10^{-1}	–
C_{v1}	production choke constant	2.21×10^{-4}	–

Chapter 3

CONTROLLED VARIABLE SELECTION

The focus of this chapter is to design simple, yet robust structures for anti-slug control systems (stabilizing control). Control structure design is to identify suitable controlled variables and manipulated variables and their pairings for control. To this end, we perform a controllability analysis of the system with different available measurements and alternative manipulated variables.

The controllability is often evaluated by considering the minimum achievable peaks of individual closed-loop transfer functions (e.g the sensitivity S of complementary sensitivity T). These bounds are independent of the controller design and they are physical properties of the plant (process). Controlled variables, or a combinations of these, that result in small peaks are preferable. We extend the controllability analysis to a mixed sensitivity $\mathcal{H}_\infty$ optimization problem, and we introduce the γ-value as a single measure of controllability. The aim is to unify different and sometimes conflicting controllability measures.

However, our controllability analysis is based on linear systems. Nevertheles, although the nature of severe-slugging, and also the simplified model used in this work, is highly nonlinear, we found that the controllability analysis gives useful information about the fundamental limitations.

Two case studies have been considered. First, a controllability analysis is performed for a well-pipeline-riser system using a 6-state model. Then, the casing-heading instability of gas-lifted oil wells is considered. The results provided in this chapter have been presented in [39], [40].

3.1 Controllability: Theoretical Background

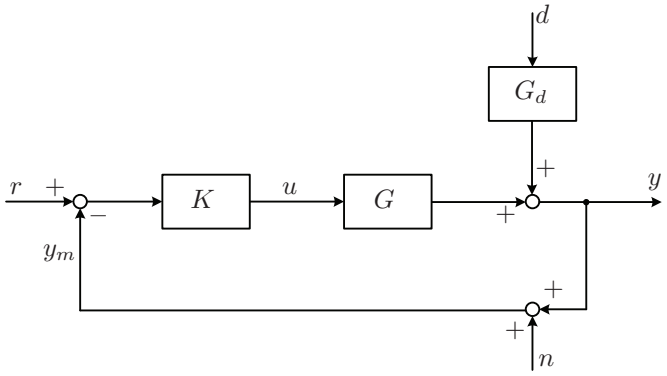

Figure 3.1: Feedback control loop

The conventional state controllability of Kalman [50] is not our interest in this work; instead the more practical concept of input-output controllability as defined in [74] is used.

Definition 1: **(Input-output) controllability** *is the ability to achieve acceptable control performance; that is, to keep outputs (y) within specified bounds or displacement from their references (r), in spite of unknown but bounded variations, such as disturbances (d) and plant changes (including uncertainty), using available inputs (u) and available measurements (y_m and d_m).*

The controllability analysis is performed at unstable operating points, with the valve opening Z_1 at 10% and 20%.

3.1.1 Closed-loop transfer functions

We consider a linear process model in the form $y = G(s)u + G_d(s)d$ with a feedback controller $u = K(s)(r-y-n)$ where d represents disturbances and n is the measurement noise (Figure 3.1). The resulting closed-loop response is

$$y = Tr + SG_d d - Tn, \tag{3.1}$$

or

$$e = r - y = Sr - SG_d d + Tn, \tag{3.2}$$

where $S = (I + GK)^{-1}$ and $T = GK(I + GK)^{-1} = I - S$ represent the sensitivity and the complementary sensitivity functions, respectively.

For an input disturbance, we have $G_d = G$, so the transfer function SG is related to the effect of input disturbances on the control error $r - y$. The

control input for the closed-loop system is

$$u = KS(r - G_d d - n). \tag{3.3}$$

Therefore, we see that the transfer function KS is very important when evaluating input usage (u). One should notice that the closed-loop transfer functions S, T, KS and SG can also be regarded as the measures of robustness against different types of uncertainty [77]. These transfer functions should be as small as possible to achieve better robustness properties of the control system. For instance, the sensitivity transfer function S is also the sensitivity to inverse relative uncertainty, which is a good representation of uncertainty in the pole locations [74]. In summary, the magnetude of the closed-loop transfer functions S, T, KS, SG, KSG_d and SG_d provide information regarding both achievable performance and robustness.

By "peak" we mean the maximum value of the frequency response or $\mathcal{H}_\infty$ norm, $\|M\|_\infty = \max_\omega \|M(j\omega)\|$. The minimum acheiavable peaks are denoted $M_{M,min} = \min_K \|M\|_\infty$ (e.g. $M_{S,min} = \min_K \|S\|_\infty$ and $M_{T,min} = \min_K \|T\|_\infty$). The bounds presented in the following are independent of the controller K, and they are the physical properties of the process itself. The bounds are, however, dependent on a systematic and correct scaling of the variables as explained later.

3.1.2 Lower bound on S and T

The lowest achievable peak of the sensitivity function, $M_{S,min}$, is determined by the distance between the unstable (RHP) poles (p_i) and zeros (z_i) of the process. For SISO systems, we have the following bound for any unstable (RHP) zero z [74]:

$$M_{S,min} = \prod_{i=1}^{N_p} \frac{|z + p_i|}{|z - p_i|}. \tag{3.4}$$

We note that the bound increases rapidly as the unstable zero z gets close to an unstable pole p_i. The bound is tight for a plant with a single RHP zero. The lowest achievable peak of the complementary sensitivity function is similarly bounded

$$M_{T,min} = \prod_{j=1}^{N_z} \frac{|z_j + p|}{|z_j - p|} . |e^{p\theta}| \tag{3.5}$$

and we also have a penalizing term $e^{p\theta}$ for the time delay θ. In (3.5) z_j denotes the N_z RHP-zeros of $G(s)$ and θ denotes the time delay of $G(s)$.

The bound in (3.5) is tight for plants with a single RHP pole. Ofcourse, the achievable peak of S also increases for an unstable plant with time delay, because of the identity constraint $S + T = I$, which implies that $|M_{S,min}| \geq |M_{T,min}| + 1$, but we do not have a tight bound for $M_{S,nmin}$ when threre is a time delay. For MIMO systems with no time delays, the following general tight bounds apply for any number of RHP-poles and RHP-zeros [8]:

$$M_{S,min} = M_{T,min} = \sqrt{1 + \overline{\sigma}^2(Q_p^{-1/2} Q_{zp} Q_z^{-1/2})}, \tag{3.6}$$

Here, the elements of the matrices Q_z, Q_p and Q_{zp} are given by [8]

$$[Q_z]_{ij} = \frac{y_{z,i}^H y_{z,j}}{z_i + \overline{z}_j}, \; [Q_p]_{ij} = \frac{y_{p,i}^H y_{p,j}}{\overline{p}_i + p_j}, \; [Q_{zp}]_{ij} = \frac{y_{z,i}^H y_{p,j}}{z_i - p_j} \tag{3.7}$$

The vectors $y_{z,i}$ and $y_{p,i}$ are the (unit) output direction vectors of the zero z_i and pole p_i, respectively.

3.1.3 Lower bound on KS

The transfer function KS gives the effect of the measurement noise n and output disturbances on the plant input u. For SISO systems, its lowest achievable peak can be calculated from the ([27], [28])

$$M_{KS,min} = |G_s(p)^{-1}|, \tag{3.8}$$

where G_s is the stable version of G with the RHP-poles of G mirrored into the LHP. The bound is tight (with equality) for an plant with one real unstable pole p. For MIMO plants with any number of unstable poles p_i, a tight bound is [22]

$$M_{KS,min} = 1/\underline{\sigma}_H(\mathcal{U}(G)^*), \tag{3.9}$$

where $\underline{\sigma}_H$ is the smallest Hankel singular value and $\mathcal{U}(G)^*$ is the mirror image of the antistable part of G. For a stable plant there is no lower bound.

3.1.4 Lower bounds on SG and SG_d

The transfer function SG should to be small to reduce the effect of input disturbances on the control error, and also for robustness against pole uncertainty. SG_d is related to the effect of a general disturbance. The two following bounds apply for an unstable zero z in G [74]:

$$M_{SG,min} = |G_{ms}(z)| \prod_{i=1}^{N_p} \frac{|z + p_i|}{|z - p_i|}, \tag{3.10}$$

$$M_{SG_d,min} = |G_{d,ms}(z)| \prod_{i=1}^{N_p} \frac{|z+p_i|}{|z-p_i|}, \tag{3.11}$$

Here, G_{ms} and $G_{d,ms}$ are the "minimum-phase, stable version" of the transfer functions G and G_d, respectively, with both RHP-poles and RHP-zeros mirrored into LHP. These bounds are tight for a single unstable zero z, but since they are valid for any RHP-zero z, they are also usefull for systems with multiple unstable zeros [77].

3.1.5 Lower bound on KSG_d

The bound in (3.9) can be generalized [74]

$$M_{KSG_d,min} = 1/\underline{\sigma}_H(\mathcal{U}(G_{d,ms}^{-1}G)^*). \tag{3.12}$$

where $\mathcal{U}(G_{d,ms}^{-1}G)^*$ is the mirror image of the anti-stable part of $G_{d,ms}^{-1}G$. This bound is tight for multiple and complex unstable poles p_i. Note that any unstable modes in G_d must be contained in G such that they are stabilizable with feedback control. A simpler bound is obtianed by using equation (3.8) for any unstable pole p:

$$M_{KSG_d,min} = |G_s^{-1}(p)|.|G_{d,ms}(p)|. \tag{3.13}$$

This bound is tight only for SISO systems with one real unstable pole p [27], [74].

3.1.6 Pole vectors

The output pole vector $y_{p,i}$ for a process with state-space representation (A, B, C, D) is defined as [29]

$$y_{p,i} = Ct_i, \tag{3.14}$$

where t_i is the right (normalized) eigenvector associated with p_i ($At_i = p_i t_i$). Based on minimum input usage for stabilization, it can be suggested that the measurements with the largest element in the output pole vector should be used for stabilizing control [29]. In the same way, for input selection, the input that has the largest element in the input pole vector $u_{p,i} = B^H q_i$, where q_i that is the left eigenvector of A ($q_i^H A = p_i q_i^H$) should be used. One limitation on the use of pole vectors is that the relationship between the magnitude of the input usage and the magnitude of the pole vectors elements only hold for a plant with a single unstable pole p. In our system, there is a pair of complex conjugate unstable poles p_i, but pole vectors still give useful information about the measurement selection [77].

3.1.7 Mixed sensitivity controllability analysis

The above controllability measures were also considered in the previous works [71], [77]. One limitation is that these measures consider only one transfer function at a time, and may give conflicting results. To get a single measure (γ), we consider an $\mathcal{H}_\infty$ problem where we want to bound $\overline{\sigma}(S)$ for performance, $\overline{\sigma}(T)$ for robustness and low sensitivity to noise, and $\overline{\sigma}(KS)$ to penalize large inputs. These requirements may be combined into a stacked $\mathcal{H}_\infty$ problem [74].

$$\min_K \|N(K)\|_\infty, \quad N \triangleq \begin{bmatrix} W_u KS \\ W_T T \\ W_P S \end{bmatrix} \tag{3.15}$$

where W_u, W_T and W_P determine the desired shapes of KS, T and S, respectively. Typically, W_P^{-1} is chosen to be small at low frequencies to achieve good disturbance attenuation (i.e., performance), and W_T^{-1} is chosen to be small outside the control bandwidth, which helps to ensure good stability margin (i.e., robustness). W_u is often chosen as a constant. The solution to this optimization problem gives a stabilizing controller K that satisfies [16], [23]:

$$\begin{aligned} \overline{\sigma}(KS(j\omega)) &\leq \gamma \underline{\sigma}(W_u^{-1}(j\omega)) \\ \overline{\sigma}(T(j\omega)) &\leq \gamma \underline{\sigma}(W_T^{-1}(j\omega)) \\ \overline{\sigma}(S(j\omega)) &\leq \gamma \underline{\sigma}(W_P^{-1}(j\omega)) \end{aligned} \tag{3.16}$$

We want to compare choices for controlled variables (CVs). To have the same cost function in all cases, all the candidate CVs are included in the y_1 part and the particular CV for evaluation is in the y_2 part of the generalized plant in Figure 3.2. The value of γ in equation (3.16) should be as small as possible for good controllability.

3.1.8 Low-frequency performance

Disturbance rejection is not the main objective for stabilizing control, but to avoid the possible destabilizing effect of nonlinearity, the system should not "drift" far away from its nominal operating point. For disturbance rejection without input saturation, we need $|G(j\omega)| \geq |G_d(j\omega)|$ at the frequencies where $|G_d| > 1$. In particular, to achieve low-frequency performance, the steady-state gain of the plant must be large enough [77].

3.1.9 Scaling

One important step before performing a controllability analysis is to scale inputs, outputs and disturbances of the plant. In *Definition 1*, the bound

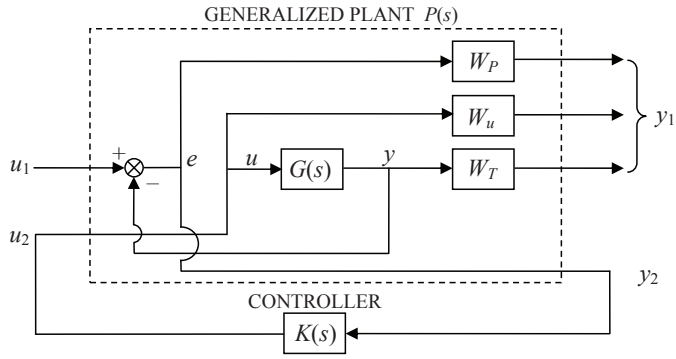

Figure 3.2: Closed-loop system for mixed sensitivity control design

that the controlled variable must be kept within is not the same for different controlled variables. For a correct comparison between candidate controlled variables, each CV must be scaled based on its maximum allowed variations, that the maximum allowed is in the interval [-1,1] for all CVs. We do this by dividing each CV by a scaling factor D_y as given in Table 3.1 and Table 3.3. Disturbances are also scaled to be in the range of [-1,1]. The maximum expected deviations of inflow rates (disturbances) are 10% of the nominal values of $w_{g,in}$ and $w_{l,in}$. This gives the following scaling weights in first case study:

$$D_d = \begin{bmatrix} 1 & 0 \\ 0 & 0.04 \end{bmatrix}$$

The inputs are scaled similarly. The controllability analysis is performed at two operating points ($Z_1 = 10\%$ and $Z_1 = 20\%$); and the maximum possible change of u at the two operating points are therefore $D_u = 0.1$ and $D_u = 0.2$ respectively.

3.2 Well-Pipeline-Riser System

In this Section, we consider the topside valve opening Z_1 as the manipulated variable and we find suitable candidate controlled variables.

3.2.1 Summary of simplified model

First, we considered the pipeline-riser system with constant inflow rates. A PDE-based *two fluid* model with 13 segments was used for the controllability

analysis in [77]. This model resulted in a set of 50 ODEs. In their work, it was concluded that main dynamics of severe slugging in a pipeline-riser system can be captured by a simpler model and we proposed the four-state simplified model given in Section 2.4. Then, we extended this model to a well-pipeline-riser system by adding an oil well as the boundary conditions (Figure 3.3). The oil well dynamics are modelled by two additional state variables, representing the masses of gas and liquid in the well. The state equations of the six-state model are as follows:

$$\frac{dm_{g,w}}{dt} = \left(\frac{gor}{gor+1}\right) w_r - w_{g,wh} \tag{3.17a}$$

$$\frac{dm_{l,w}}{dt} = \left(\frac{1}{gor+1}\right) w_r - w_{l,wh} \tag{3.17b}$$

$$\frac{dm_{g,p}}{dt} = w_{g,in} - w_{g,rb} \tag{3.17c}$$

$$\frac{dm_{l,p}}{dt} = w_{l,in} - w_{l,rb} \tag{3.17d}$$

$$\frac{dm_{g,r}}{dt} = w_{g,rb} - w_{g,out} \tag{3.17e}$$

$$\frac{dm_{l,r}}{dt} = w_{l,rb} - w_{l,out} \tag{3.17f}$$

See Section 2.4 for details of this augmented model. The advantage with this case is that inflow rates are pressure-driven which is closer to practical conditions. In addition, we can consider measurements in the oil well for anti-slug control as suggested in [72]. The OLGA case for the well-pipeline-riser systems introduced in Section 2.4.2 is used a reference for the model fitting. We fit the simplified model to the OLGA case by adjusting five parameters in the model. The parameter values found by trial and error are given in Table 2.1.

3.2.2 Bounds on minimum achievable peaks

Different candidate controlled variables of the well-pipeline-riser system are shown in Figure 3.3. The minimum achievable peaks for selected closed-loop transfer functions are given in Table 3.1 and 3.2 for two operating points $Z_1 = 10\%$ and $Z_1 = 20\%$, receptively. The minimum peaks of T for P_{rt}, ρ_{rt} and $\alpha_{l,t}$ in Table 3.1 are relatively large, and it is expected to be difficult to use these measurements as controlled variables. The large peaks are because of RHP-zeros in transfer functions for these variables.

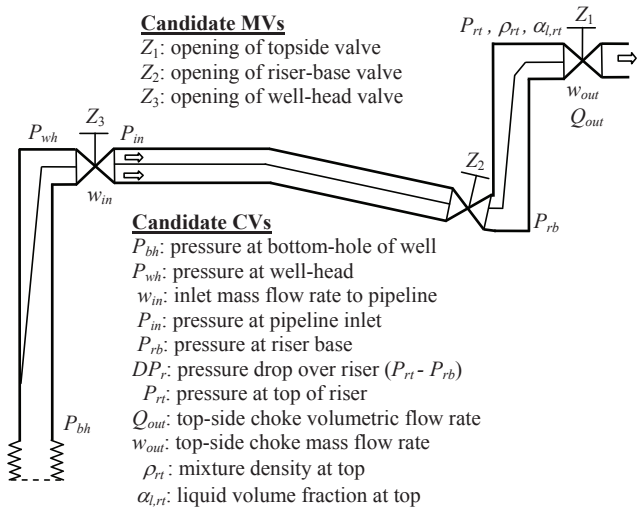

Figure 3.3: Schematic presentation of candidate controlled variables and manipulated variable of well-pipeline-riser system

The RHP-zero dynamics are observed as inverse response in the step test of the system.

The location of RHP-poles of the process and the RHP-zeros for P_{rt} are plotted as a function of the valve opening in Figure 3.4. For $Z_1 = 5\%$ the process is on the limit to intability whith a pair of complex conjugate poles on the Jω-axis. For $Z_1 > 5\%$ the two complex poles are in the RHP, and the process is unstable. For larger valve openings, the unstable RHP-poles and the RHP-zero get very close to each other. From equations (3.4) and (3.5), we see that when the RHP-pole and the RHP-zero are close to each other, the peak of the sensitivity and complementary sensitivity transfer functions are large. This is also seen from Table 3.1 and Table 3.2; the minimum peak for T of P_{rt} is much larger for $Z_1 = 20\%$ than for for $Z_1 = 10\%$.

One of RHP-poles of the system moves far away from the Jω-axis as the valve opening increases. The faster unstable dynamics also make the stabilization more difficult. Another increasing limitation when opening the valve is that gain of the system decreases. These effects can be seen by comparing peack of KS and $G(0)$ for $Z_1 = 10\%$ and $Z_1 = 20\%$. Where smaller gain shows that we need to increase the controller gain to stabilize the process and the higher peak shows that a more aggressive control action is needed for larger valve openings for all CV candidates. It is desired to control the system with a larger valve opening to achieve a higher production

rate, but it is not possible because of fundamental controllability limitations. These findings are in agreement with the results reported by [77] where a more detailed two-fluid model is used. Unlike the pipeline-riser system ([77]), Q_{out} and w_{out} show considerable steady-state gains for the present well-pipeline-riser system which is a result of the pressure-driven nature on the inflows. Therefore, flow rates also can be used in a single loop for the stabilizing control without the drift problem.

The minimum achievable peak of T for DP_r is 1, and no problem in term of controllability is expected. However, the small value of the steady-state gain $G(0)$ implies that the system might drift away from the desired operating point. The controllability data for the combined measurements in Table 3.1 and Table 3.2 show that combining one pressure measurement and one flow rate gives the best result in terms of controllability.

In parctice, there may be time delays in the system, for example, related to the measurements, or valves. From (3.5) the bound on the complementary sensitivity function increase by a factor $e^{p\theta}$. In OLGA simulations, it was observed that the time delay for the measurement from the inlet of the pipeline and the oil well is $\theta = 15$ *sec*. The factor $e^{p\theta}$ becomes 1.19 for $Z_1 = 10\%$ and 1.29 $Z_1 = 20\%$, because the unstable pole p is larger in magnitude for large valve openings (Figure 3.4). The bottom-hole pressure demonstrates the largest steady-state gain and relatively small values for minimum achievable peaks of all closed-loop transfer functions. This means that the pressure at the bottom-hole is an effective controlled variable.

3.2.3 Control structure selection

Next, we consider the mixed sensitivity analysis, which aims to combine important controllability measures into one (γ), where a small value of γ is desired. The resulted γ values given in Table 3.1 and 3.2 contain the information of the other peaks given for each CV. We emphesize role of the γ values by using them as a measure for CV slection. In addition, we show simulation results of the corresonding $\mathcal{H}_\infty$ controller for selected cases. All simulations presented in this paper are based on scaled variables, and the ideal is to keep the controlled variables in the range of [-1,1]. For the well-pipeline-riser case study, we added 10 *sec* time delay at input of the system in all simulations to test robustness of the different control structures.

For $Z_1 = 10\%$, the best single measurement apprears to be P_{bh} ($\gamma = 20.70$). Figure 3.5 shows the simulations using the obtained $\mathcal{H}_\infty$ controller for this case. For the top-side pressure P_{rt} we achieved $\gamma = 35.48$ which shows a poor robustness in Figure 3.5, but the outlet flow Q_{out} ($\gamma = 28.35$)

Table 3.1: Controllability data for well-pipeline-riser case study at operating point $Z_1 = 10\%$

CV	Value	D_y	$G(0)$	Pole vector	M_T	M_{KS}	M_{SG}	$M_{KSG_{d1}}$	$M_{KSG_{d2}}$	$M_{SG_{d1}}$	$M_{SG_{d2}}$	γ
$P_{bh}[bar]$	281.95	1	-3.80	0.0065	1.19	0.62	0	0.24	0.46	0	0	20.70
$P_{wh}[bar]$	68.85	1	-2.76	0.0048	1.19	0.86	0	0.24	0.46	0	0	28.23
$w_{in}[kg/s]$	10.46	1	1.05	0.0037	1.19	1.10	0	0.24	0.46	0	0	31.02
$P_{in}[bar]$	68.66	1	-2.80	0.0049	1.19	0.84	0	0.24	0.46	0	0	27.33
$P_{rb}[bar]$	67.26	1	-3.07	0.0059	1	0.70	0	0.23	0.56	0	0	21.21
$DP_r[bar]$	15.54	1	-0.18	0.0088	1.02	0.47	0.03	0.19	0.46	0.033	0.020	89.07
$P_{rt}[bar]$	51.72	1	-2.89	0.0039	3.17	1.05	5.30	0.17	0.54	0.25	0.66	35.48
$Q_{out}[L/s]$	20.66	2	1.24	0.0115	1	0.36	0	0.24	0.53	0	0	28.35
$w_{out}[kg/s]$	10.46	1	1.05	0.0140	1	0.29	0	0.16	0.57	0	0	31.02
$\rho_{rt}[kg/m^3]$	506.56	50	-0.23	0.0055	3.43	0.74	5.50	0.30	0.84	0.69	1.70	85.47
$\alpha_{l,rt}[-]$	0.58	1	-0.013	0.0004	3.43	11.70	0.35	0.30	0.84	0.044	0.10	–
$P_{in}\&P_{rt}$	–	–	–	–	1	0.65	0	0.22	0.57	0	0	16.72
$P_{bh}\&Q_{out}$	–	–	–	–	1	0.29	0	0.07	0.04	0	0	8.93
$P_{in}\&Q_{out}$	–	–	–	–	1	0.33	0	0.22	0.76	0	0	12.07
$P_{rt}\&Q_{out}$	–	–	–	–	1	0.34	0	0.06	0.04	0	0	12.64
$P_{rt}\&\rho_{rt}$	–	–	–	–	1	0.61	0	0.23	0.72	0	0	22.84

Table 3.2: Controllability data for well-pipeline-riser case study at operating point $Z_1 = 20\%$

CV	Value	D_y	$G(0)$	Pole vector	M_T	M_{KS}	M_{SG}	$M_{KSG_{d1}}$	$M_{KSG_{d2}}$	$M_{SG_{d1}}$	$M_{SG_{d2}}$	γ
$P_{bh}[bar]$	280.25	1	-1.15	0.0045	1.28	3.06	0	0.58	0.95	0	0	–
$P_{wh}[bar]$	67.69	1	-0.83	0.0033	1.28	4.24	0	0.58	0.95	0	0	–
$w_{in}[kg/s]$	10.93	1	0.32	0.0044	1.28	2.69	0	0.58	0.95	0	0	98.3
$P_{in}[bar]$	67.48	1	-0.84	0.0035	1.28	3.89	0	0.58	0.95	0	0	–
$P_{rb}[bar]$	65.98	1	-0.92	0.0060	1	2.12	0	0.58	0.95	0	0	152.3
$DP_r[bar]$	15.43	1	-0.056	0.0087	1.03	1.35	0.02	0.58	0.95	0.034	0.016	104.0
$P_{rt}[bar]$	50.55	1	-0.87	0.0010	12.30	13.63	7.05	0.56	1.44	0.32	0.82	730.5
$Q_{out}[L/s]$	21.79	2	0.37	0.0122	1	1.07	0	0.58	1.20	0	0	67.30
$w_{out}[kg/s]$	10.93	1	0.32	0.0125	1	1.15	0	0.56	1.73	0	0	72.55
$\rho_{rt}[kg/m^3]$	501.63	50	-0.094	0.0012	14.74	15.23	8.74	5.22	10.69	2.76	6.10	–
$\alpha_{l,rt}[-]$	0.58	1	-0.006	0.0000	14.64	238.0	0.55	5.19	10.64	0.17	0.39	–
$P_{in}\&P_{rt}$	–	–	–	–	1	2.53	0	0.93	2.04	0	0	110.7
$P_{bh}\&Q_{out}$	–	–	–	–	1	0.89	0	0.93	1.88	0	0	28.46
$P_{in}\&Q_{out}$	–	–	–	–	1	0.90	0	1.57	3.46	0	0	36.77
$P_{rt}\&Q_{out}$	–	–	–	–	1	0.86	0	0.93	1.88	0	0	39.36
$P_{rt}\&\rho_{rt}$	–	–	–	–	1	0.77	0	2.78	5.00	0	0	–

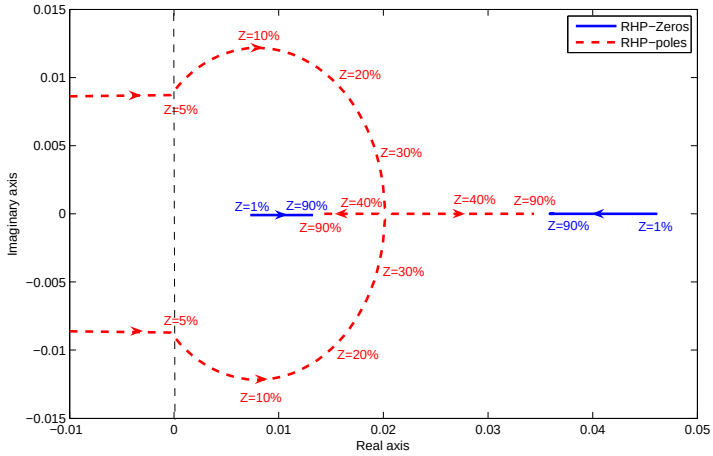

Figure 3.4: Location of RHP-poles and RHP-zeros of top pressure of well-pipeline-riser system for different valve openings

is quite promising in the simulation results in Figure 3.7. We see that the outlet flow can be used for the anti-slug control in theory.

However, it is better to combine measurements, and the combination of one upstream pressure and the outlet flow results in the smallest value for γ. Simulation result with a $\mathcal{H}_\infty$ control ($\gamma = 8.93$) using P_{bh} and Q_{out} as the controlled variables is illustrated in Figure 3.8. Even if the subsea pressure measurements are not available, combing the top-side pressure P_{rt} with the outlet flow Q_{out} gives a statisfactory result ($\gamma = 12.64$). This is shown by the simulation results in Figure 3.9.

Remarks

It should be noted that for combing one flow rate and one pressure, it is impossible to have tight control of both at the same time. If tight pressure control is required, flow rate can not be controlled tightly. Because, when an inflow disturbance comes to the system, it needs to be released to maintain a constant pressure. In this situation, the flow control can only help for robustness of the pressure control. Figure 3.8 and Figure 3.9 show this condition where outlet flow Q_{out} is not controlled tightly. This performance requirement was simulated by considering integral action (i.e. small value for W_P^{-1} at low frequency) for control of the pressure (P_{bh} in Figure 3.8 and P_{rt} in Figure 3.9) and no integral action for Q_{out} (i.e. the weight

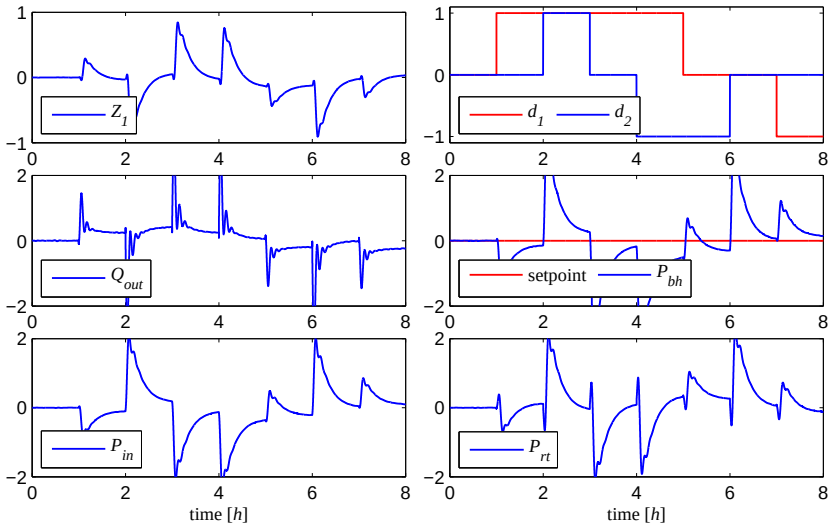

Figure 3.5: $\mathcal{H}_\infty$ control of well-pipeline-riser, $CV = P_{bh}$, $MV = Z_1$

of $W_P^{-1} = 1/M_s$ in which M_s is the desired peak of sensitivity transfer function). Cascade control with the flow control as the inner loop is a simple structure to implement this case in practice. On the other hand, if tight control on the flow rate is required, the pressure fluctuations because of disturbances are unavoidable.

3.3 Gas-Lifted Oil Well

3.3.1 Summary of simplified model

We use a simplified three-state model of the system for the controllability analysis. The model is very similar to the one used in [1], [2], [18], [19], [20]. The state variables are the mass of gas in the annulus ($m_{g,a}$), the mass of gas in the tubing ($m_{g,t}$) and the mass of liquid in the tubing ($m_{l,t}$). The state equations are as follows

$$\frac{dm_{g,a}}{dt} = w_{g,in} - w_{g,inj} \tag{3.18a}$$

$$\frac{dm_{g,t}}{dt} = w_{g,inj} + w_{g,res} - w_{g,out} \tag{3.18b}$$

$$\frac{dm_{l,t}}{dt} = w_{l,res} - w_{l,out} \tag{3.18c}$$

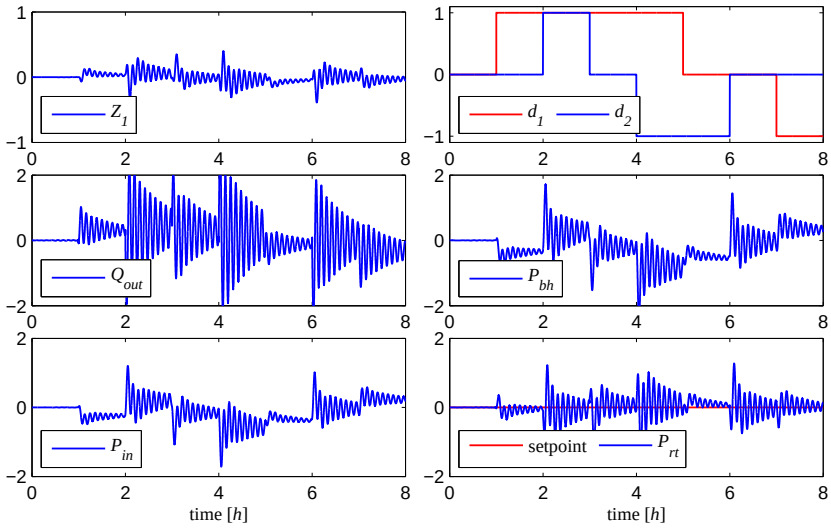

Figure 3.6: $\mathcal{H}_\infty$ control of well-pipeline-riser, $CV = P_{rt}$, $MV = Z_1$

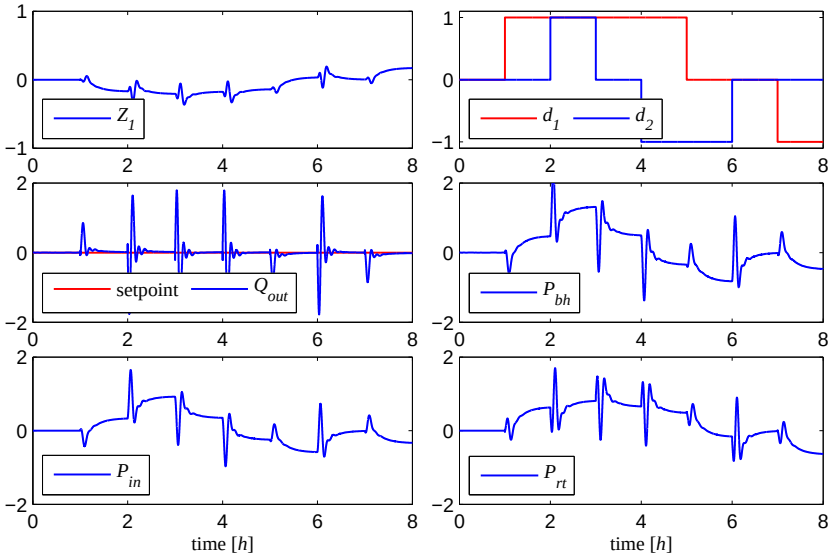

Figure 3.7: $\mathcal{H}_\infty$ control of well-pipeline-riser, $CV = Q_{out}$, $MV = Z_1$

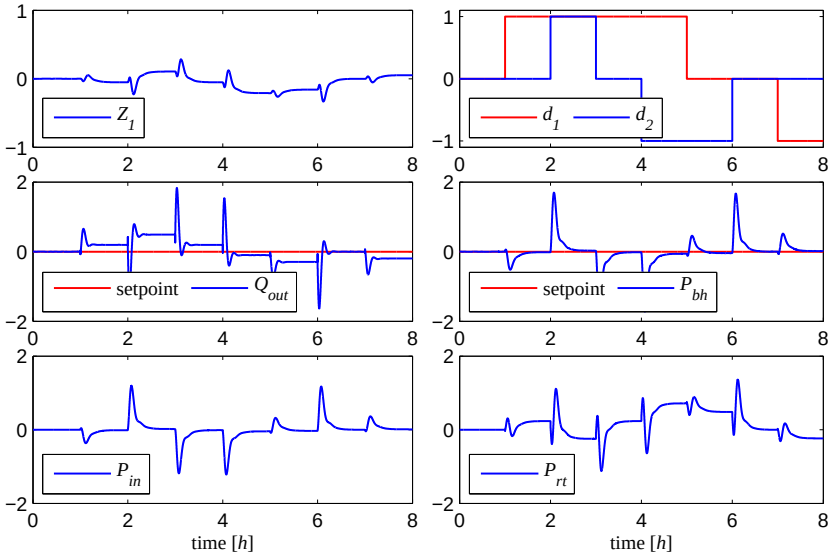

Figure 3.8: $\mathcal{H}_\infty$ control of well-pipeline-riser, $CV = [P_{bh}, Q_{out}]$, $MV = Z_1$

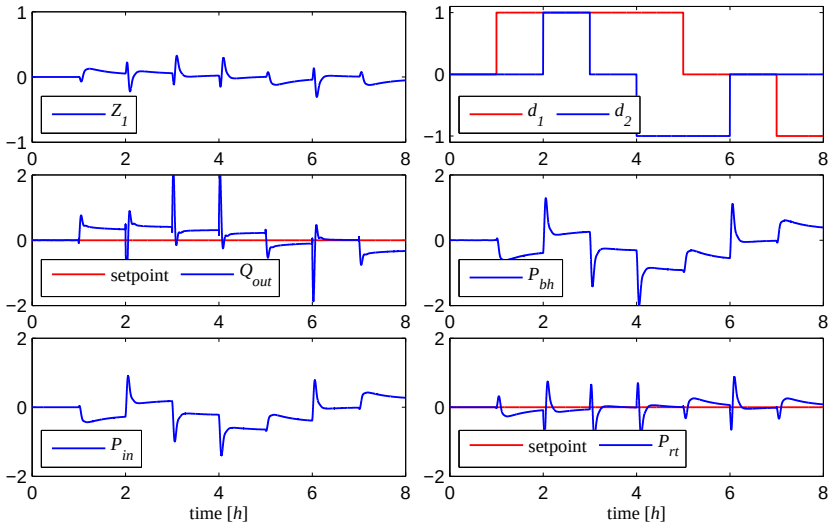

Figure 3.9: $\mathcal{H}_\infty$ control of well-pipeline-riser, $CV = [P_{rt}, Q_{out}]$, $MV = Z_1$

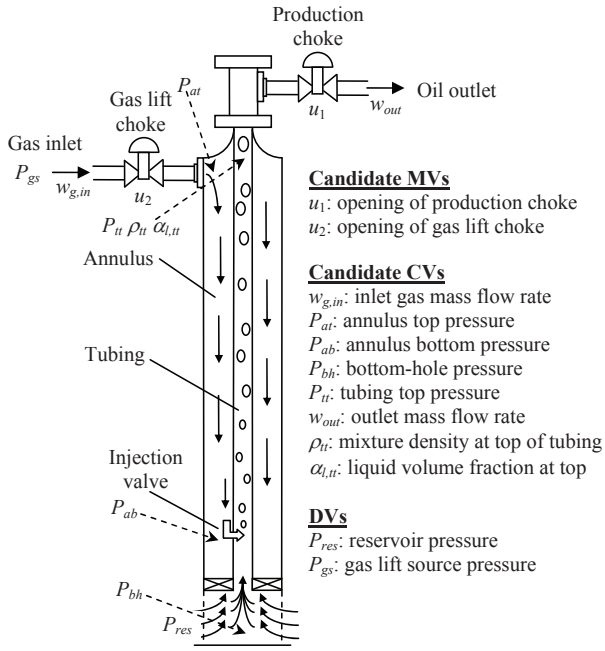

Figure 3.10: Presentation of candidate CVs and MVs of gas-lift oil well

where $w_{g,in}$ is the mass flow rate of inlet gas to the annulus and $w_{g,inj}$ is the mass of injected gas from the annulus into the tubing. $w_{g,res}$ and $w_{l,res}$ are gas and liquid mass flow rates from the reservoir to the tubing. $w_{g,out}$ and $w_{l,out}$ are the mass flow rates of gas and oil outlet from the tubing, respectively. These flow rates are calculated by additional equations given in Appendix A. The simplified model was fitted to a test case implemented in the OLGA simulator. Constants and parameters used in the model are given in Table A.1.

3.3.2 Bounds on minimum achievable peaks

Figure 3.10 shows different candidate controlled variables and the two alternative manipulated variables of the gas-lifted oil well. We identify suitable CVs for this case by using a similar controllability analysis as for the well-pipeline-riser system. The minimum achievable peaks for different closed-loop transfer functions for the gas-lifted oil well case are given in Tables 3.3, 3.4 and 3.5. Location of RHP-poles of the system and RHP-zeros of P_{tt} for $u_2 = 0.4$ and as a function of the production choke valve opening u_1 are

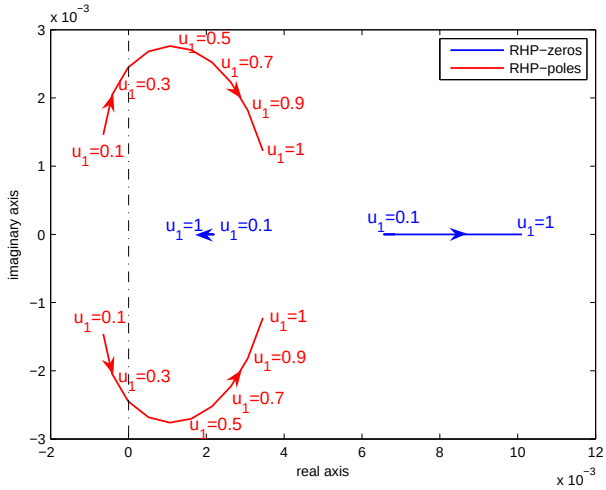

Figure 3.11: Location of RHP-poles of system and RHP-zeros of tubing top pressure for $u_2 = 0.4$ and different values of u_1

shown in Figure 3.11. The critical valve opening for transition from stable to unstable operation is $u_1 = 0.3$. Two poles of the system move to the RHP and the system becomes unstable for $u_1 > 0.3$; this is in agreement with the stability map in Figure 3.12. The controllability results when using the production choke valve u_1 as the manipulated variable are very similar to well-pipeline-riser in the previous Section. P_{tt}, $\rho_{mix,t}$ and $\alpha_{L,t}$ are not suitable controlled variables in a single loop, because of RHP-zero dynamics. P_{tt} shows two RHP-zeros for all u_1 values (Figure 3.11). One of the RHP-zeros does not move so much and it is always close to pole locations. As the production valve opening u_1 increases, RHP-poles get closer to the smaller (important) RHP-zero. The large peak of the complementary sensitivity does not occur when P_{tt} combines with other measurements in Table 3.3, because the system becomes non-square and zeros disappear.

The bottom-hole pressure P_{bh} shows the best controllability properties. It has the largest element in the output pole vector that makes it suitable for stabilization of the unstable system. P_{bh} also has the largest steady-state gain $G(0)$ and the smallest values for all of the closed-loop transfer functions. In the second place, the pressure at the bottom of the annulus P_{ab} shows good controllability properties. The third good candidate is the pressure at top of the annulus, P_{at}.

We performed a similar controllability analysis for using u_2 as the single

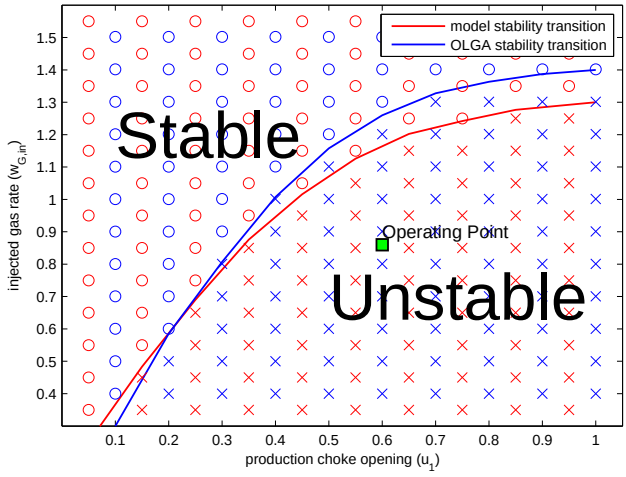

Figure 3.12: Stability transition of system, blue markers for OLGA and red markers for simplified model

manipulating variable of the gas-lifted oil well (Table 3.4), but the results using u_2 were not satisfactory.

3.3.3 Control structure selection

Based on the γ values provided in Table 3.3, 3.4 and 3.5, we can make recommendation about the control structure. First, we consider using the production choke valve u_1 as the manipulated variables. For a SISO control structure, the bottom-hole pressure P_{bh} is the best CV from our results ($\gamma = 3.6$). This is in accordance with previous works [20], [1]. P_{bh} usually is not directly measurable, but as suggested by [20] and [1], it can be estimated using an observer.

In simulations related to gas-lifted oil well case study, we added 20 *sec* time delay at input of the system in all simulations to test robustness of the different control structures. Simulation result of using P_{bh} as the single CV is shown in Fig 3.13. Simulation results of using $P_{tt}(\gamma = 19.16)$ and $P_{at}(\gamma = 14.85)$, shown in Fig 3.14 and Fig 3.15, respectively, indicate poor performance when they are used for SISO control.

Using two controlled variables and one manipulated variable, it is impossible to get tight control on the both controlled variables at the same time. Similar to a cascade controller, we can have tight control with a constant set-point only on one of controlled variables. We calculated γ_1 when

Table 3.3: Controllability data for gas-lift oil well using u_1 as manipulated variable

CV	Value	D_y	$G(0)$	Pole vector	M_T	M_{KS}	M_{SG}	$M_{KSG_{d1}}$	$M_{KSG_{d2}}$	$M_{SG_{d1}}$	$M_{SG_{d2}}$	γ_1	γ_2
$w_{gin}[kg/s]$	0.86	0.05	0.76	0.0004	1.00	3.04	0.00	0.23	1.987	0.00	0.00	89.55	–
$P_{at}[bar]$	81.16	1	5.22	0.0031	1.00	0.44	0.00	0.23	0.10	0.00	0.00	14.85	–
$P_{tt}[bar]$	20.89	1	5.72	0.0028	3.06	0.38	10.49	0.25	0.11	0.69	0.42	19.16	–
$P_{ab}[bar]$	90.35	1	5.81	0.0034	1.00	0.40	0.00	0.23	0.10	0.00	0.00	13.54	–
$P_{bh}[bar]$	88.56	1	6.95	0.0089	1.00	0.11	0.00	0.23	0.09	0.00	0.00	3.60	–
$w_{out}[kg/s]$	18.51	2	0.88	0.0024	1.00	0.49	0.00	0.30	0.11	0.00	0.00	19.35	–
$\rho_{tt}[kg/m^3]$	186.96	20	1.61	0.0013	3.11	1.24	3.77	0.56	0.29	0.71	0.38	38.08	–
$\alpha_{l,tt}[-]$	0.23	0.23	0.17	0.0001	3.11	10.83	0.43	0.57	0.30	0.08	0.04	289.88	–
P_{ab} w_{out}	–	–	–	0.0034	1.00	0.26	0.00	0.13	0.05	0.00	0.00	8.89	19.35
P_{ab} ρ_{tt}	–	–	–	0.0034	1.00	0.36	0.00	0.20	0.08	0.00	0.00	12.20	13.17
P_{ab} $w_{g,in}$	–	–	–	0.0034	1.00	0.40	0.00	0.12	0.10	0.00	0.00	13.42	22.13
P_{at} P_{bh}	–	–	–	0.0089	1.00	0.11	0.00	0.12	0.05	0.00	0.00	4.52	3.45
P_{at} P_{tt}	–	–	–	0.0031	1.00	0.26	0.00	0.12	0.05	0.00	0.00	8.65	11.58
P_{at} w_{out}	–	–	–	0.0031	1.00	0.27	0.00	0.13	0.05	0.00	0.00	9.17	19.35
P_{at} ρ_{tt}	–	–	–	0.0031	1.00	0.39	0.00	0.20	0.08	0.00	0.00	13.12	13.96
P_{at} $w_{g,in}$	–	–	–	0.0031	1.00	0.44	0.00	0.12	0.10	0.00	0.00	14.70	22.13
P_{bh} w_{out}	–	–	–	0.0089	1.00	0.10	0.00	0.13	0.05	0.00	0.00	3.39	19.35
P_{bh} ρ_{tt}	–	–	–	0.0089	1.00	0.11	0.00	0.20	0.09	0.00	0.00	3.53	10.96
P_{bh} $w_{g,in}$	–	–	–	0.0089	1.00	0.11	0.00	0.12	0.10	0.00	0.00	3.60	22.13
P_{tt} P_{bh}	–	–	–	0.0089	1.00	0.10	0.00	0.12	0.05	0.00	0.00	7.25	3.39
P_{tt} w_{out}	–	–	–	0.0028	1.00	0.30	0.00	0.14	0.06	0.00	0.00	15.41	19.35
P_{tt} ρ_{tt}	–	–	–	0.0028	1.00	0.34	0.00	0.21	0.10	0.00	0.00	16.97	12.23
P_{tt} $w_{g,in}$	–	–	–	0.0028	1.00	0.37	0.00	0.12	0.12	0.00	0.00	18.64	22.13
w_{out} $w_{g,in}$	–	–	–	0.0024	1.00	0.47	0.00	0.13	0.12	0.00	0.00	19.35	22.13

Table 3.4: Controllability data for gas-lift oil well using u_2 as manipulated variable

CV	Value	D_y	$G(0)$	Pole vector	M_T	M_{KS}	M_{SG}	$M_{KSG_{d1}}$	$M_{KSG_{d2}}$	$M_{SG_{d1}}$	$M_{SG_{d2}}$	γ_1	γ_2
$w_{gin}[kg/s]$	0.86	0.1	8.85	0.0002	29.30	3.21	186.46	0.22	1.45	0.96	6.75	153.71	—
$P_{at}[bar]$	81.16	1	3.32	0.0031	1.75	0.23	6.43	0.22	0.08	1.31	0.23	21.80	—
$P_{tt}[bar]$	20.89	1	5.60	0.0028	3.04	0.38	12.03	0.22	0.10	0.74	0.44	29.64	—
$P_{ab}[bar]$	90.35	1	3.70	0.0034	1.75	0.21	7.16	0.22	0.08	1.46	0.26	20.60	—
$P_{bh}[bar]$	88.56	1	19.36	0.0089	2.77	0.11	36.98	0.22	0.10	2.88	1.34	14.68	—
$w_{out}[kg/s]$	18.51	2	2.83	0.0024	3.01	0.43	10.06	0.25	0.10	0.79	0.36	32.17	—
$\rho_{tt}[kg/m^3]$	186.96	20	3.17	0.0013	4.77	0.65	12.09	0.35	0.18	0.83	0.44	48.22	—
$\alpha_{l,tt}[-]$	0.23	0	0.38	0.0001	4.76	5.58	1.45	0.36	0.19	0.10	0.05	402.73	—
P_{ab} ρ_{tt}	–	–	–	0.0034	1.00	0.18	0.00	0.16	0.08	0.00	0.00	18.83	16.28
P_{ab} $w_{g,in}$	–	–	–	0.0034	1.00	0.21	0.00	0.11	0.08	0.00	0.00	20.47	20.35
P_{ab} w_{out}	–	–	–	0.0034	1.00	0.17	0.00	0.12	0.05	0.00	0.00	18.14	14.82
P_{bh} ρ_{tt}	–	–	–	0.0089	1.00	0.10	0.00	0.16	0.08	0.00	0.00	14.29	13.97
P_{bh} $w_{g,in}$	–	–	–	0.0089	1.00	0.11	0.00	0.11	0.10	0.00	0.00	14.65	10.58
P_{bh} w_{out}	–	–	–	0.0089	1.00	0.10	0.00	0.12	0.05	0.00	0.00	14.11	13.74
P_{tt} P_{bh}	–	–	–	0.0089	1.00	0.10	0.00	0.12	0.05	0.00	0.00	9.44	14.10
P_{tt} ρ_{tt}	–	–	–	0.0028	1.00	0.30	0.00	0.16	0.08	0.00	0.00	24.02	21.89
P_{tt} $w_{g,in}$	–	–	–	0.0028	1.00	0.37	0.00	0.11	0.11	0.00	0.00	28.70	33.24
P_{tt} w_{out}	–	–	–	0.0028	1.00	0.28	0.00	0.13	0.05	0.00	0.00	22.61	20.94
w_{out} $w_{g,in}$	–	–	–	0.0024	1.00	0.43	0.00	0.12	0.11	0.00	0.00	30.75	37.15

Table 3.5: Controllability data for gas-lift oil well using u_1 and u_2 as manipulated variables (MIMO controller)

CV	Pole vector	M_T	M_{KS}	M_{SG}	$M_{KSG_{d1}}$	$M_{KSG_{d2}}$	$M_{SG_{d1}}$	$M_{SG_{d2}}$	γ_1	γ_2	γ_3
P_{ab} w_{out}	0.0034	1.00	0.12	0.00	0.08	0.03	0.00	0.00	7.55	13.20	15.31
P_{ab} ρ_{tt}	0.0034	1.50	0.14	2.00	0.11	0.05	0.34	0.12	10.39	12.16	16.53
P_{ab} $w_{g,in}$	0.0034	1.00	0.16	0.00	0.09	0.07	0.00	0.00	11.43	10.98	12.40
P_{at} P_{bh}	0.0089	1.00	0.07	0.00	0.08	0.03	0.00	0.00	3.94	3.20	14.47
P_{at} P_{tt}	0.0031	1.59	0.13	11.00	0.08	0.03	0.96	0.62	7.36	7.76	8.16
P_{at} w_{out}	0.0031	1.00	0.13	0.00	0.08	0.03	0.00	0.00	7.83	12.30	15.33
P_{at} ρ_{tt}	0.0031	1.52	0.15	1.87	0.11	0.05	0.32	0.11	11.23	12.89	16.74
P_{at} $w_{g,in}$	0.0031	1.00	0.18	0.00	0.09	0.07	0.00	0.00	12.59	12.20	13.63
P_{bh} w_{out}	0.0089	1.00	0.07	0.00	0.08	0.04	0.00	0.00	3.15	13.30	75.80
P_{bh} ρ_{tt}	0.0089	1.02	0.07	7.71	0.11	0.06	1.05	0.52	3.28	10.07	32.09
P_{bh} $w_{g,in}$	0.0089	1.00	0.07	0.00	0.09	0.09	0.00	0.00	3.35	3.20	3.58
P_{tt} P_{bh}	0.0089	1.20	0.07	16.73	0.08	0.04	1.04	0.64	5.19	3.15	5.22
P_{tt} w_{out}	0.0028	2.05	0.19	0.00	0.09	0.04	1.04	0.64	11.37	13.30	12.33
P_{tt} ρ_{tt}	0.0028	2.15	0.20	19.48	0.12	0.06	1.69	0.95	12.18	11.35	13.09
P_{tt} $w_{g,in}$	0.0028	2.69	0.25	19.38	0.09	0.09	1.14	1.09	14.15	8.78	16.56
w_{out} $w_{g,in}$	0.0024	1.00	0.30	0.00	0.10	0.09	0.00	0.00	13.30	11.32	21.55

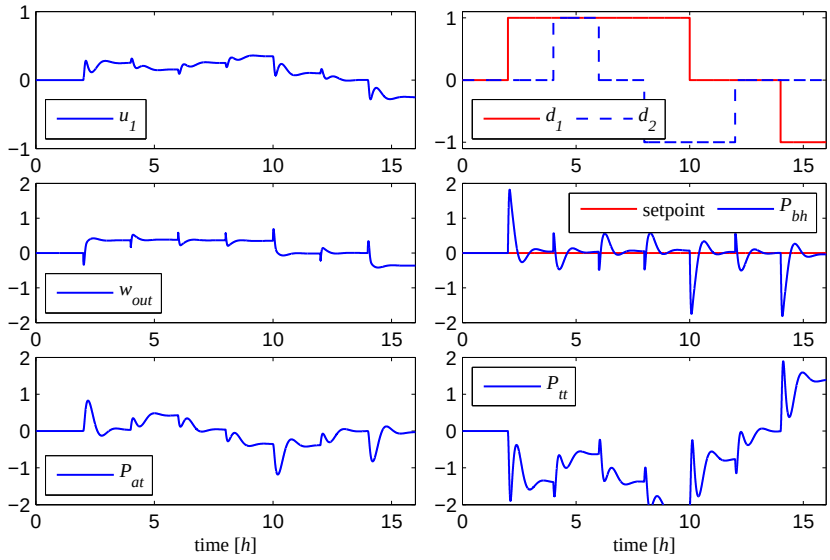

Figure 3.13: $\mathcal{H}_\infty$ control of gas-lift, $CV = P_{bh}$, $MV = u_1$

tight control was required on the first controlled variable of the pair, and γ_2 when tight control was on the second one in the pair.

Looking at cases with two controlled variables and u_1 as the manipulated variable in Table 3.3, all cases including P_{bh} with tight control on P_{bh} result in small γ values. However, there is no significant improvement in γ values compared to using the single controlled variable P_{bh}; simulation result of combing P_{bh} and w_{out} with $\gamma_1 = 3.39$ is shown in Figure 3.16. If P_{bh} is not available as directly measuremed either estimated, the next suitable CV is combination of P_{at} and P_{tt} (two top-side pressures) with $\gamma_1 = 13.12$. The simulation result for this case is given in Figure 3.17.

Table 3.4 shows controllability data for the gas-lift choke valve u_2 as the single manipulated variables where relatively large peak of T and large γ values for all CVs signals that u_2 is not an effective manipulated variable. Combination of P_{bh} and P_{tt} gives the smallest γ value in Table 3.4. Simulation results of the $\mathcal{H}_\infty$ controller for this case with $\gamma_2 = 9.44$ is shown in Figure 3.18. We conclude that the gas-lift choke valve is not a suitable manipulated variable for the stabilizing control.

Using two manipulated variables, it is possible to have tight control on both CVs when combiling two measurements; γ_3 values in Table 3.5 were calculated for this condition. γ_1 and γ_2 in Table 3.5 can be compared to

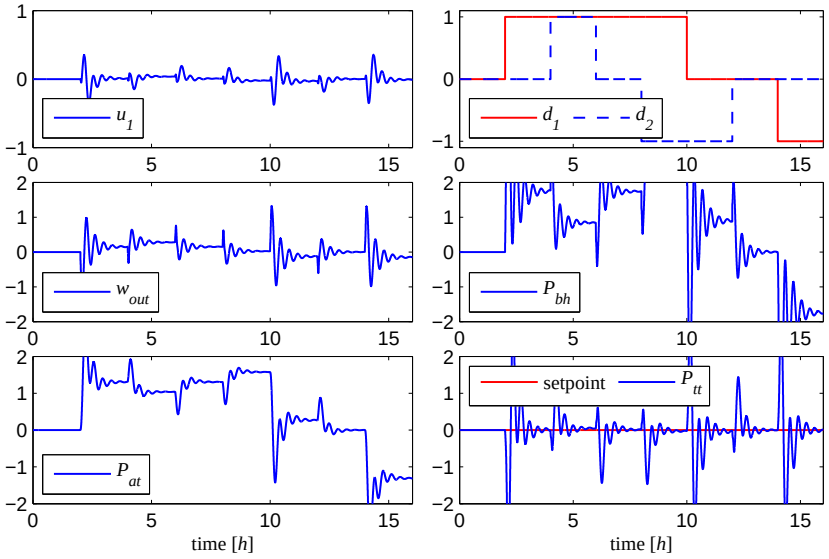

Figure 3.14: $\mathcal{H}_\infty$ control of gas-lift, $CV = P_{tt}$, $MV = u_1$

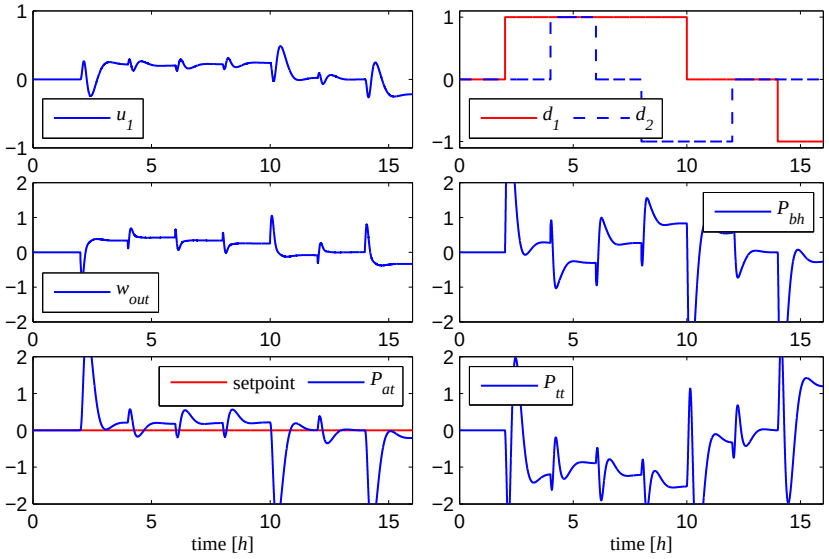

Figure 3.15: $\mathcal{H}_\infty$ control of gas-lift, $CV = P_{at}$, $MV = u_1$

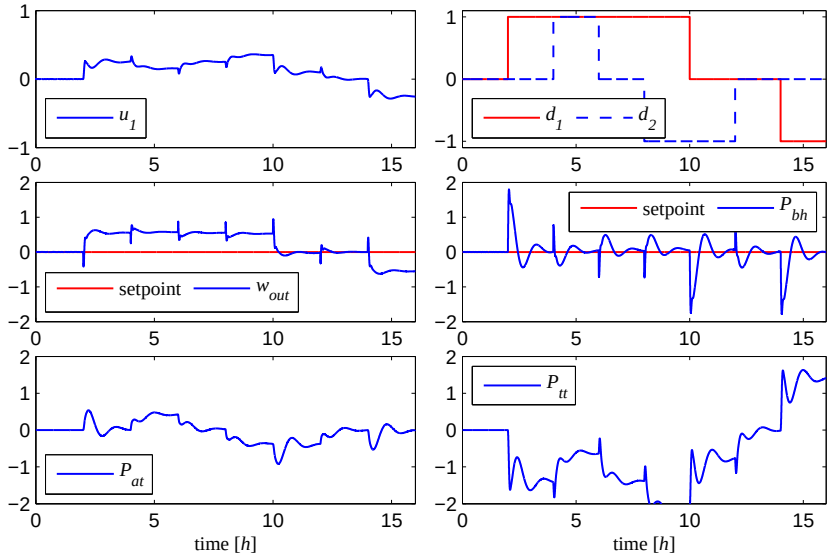

Figure 3.16: $\mathcal{H}_\infty$ control of gas-lift, $CV = [P_{bh}, w_{out}]$, $MV = u_1$

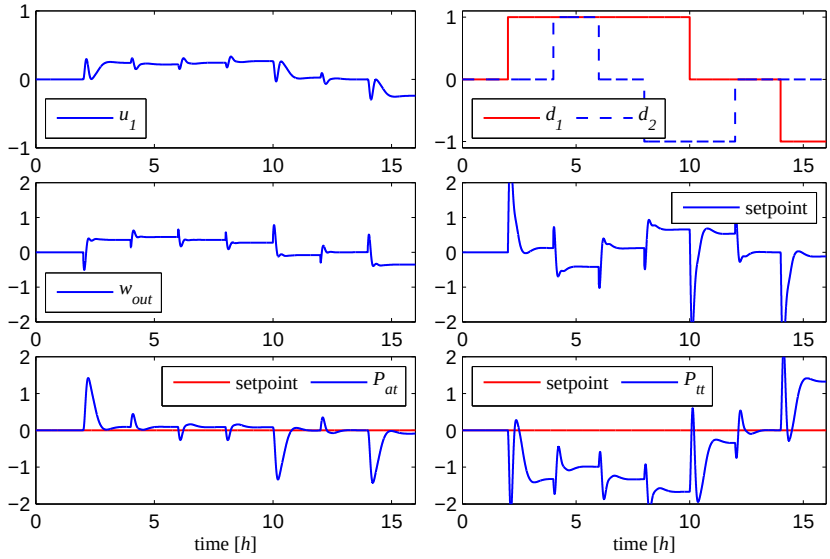

Figure 3.17: $\mathcal{H}_\infty$ control of gas-lift, $CV = [P_{at}, P_{tt}]$, $MV = u_1$

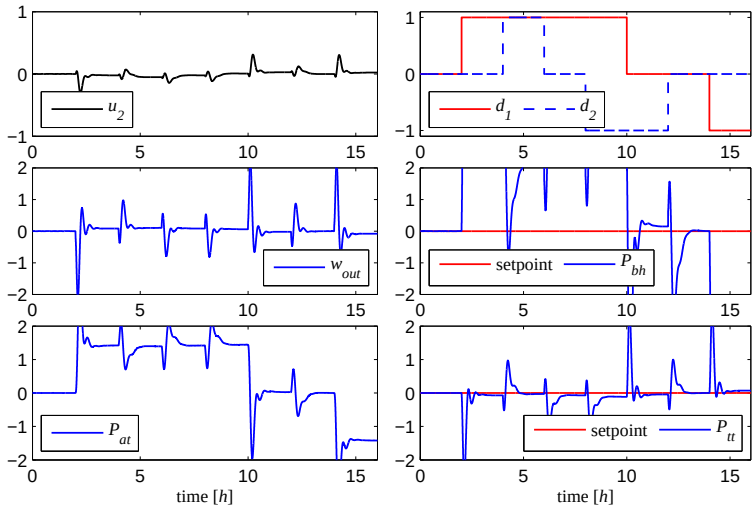

Figure 3.18: $\mathcal{H}_\infty$ control of gas-lift, $CV = [P_{bh}, P_{tt}]$, $MV = u_2$

those in Table 3.3, but the cost function related to the $\mathcal{H}_\infty$ problem for calculating the γ_3 values is different.

Looking at Table 3.5, the pairs with P_{bh} show small γ values, but compared to the γ values in Table 3.3, there is no substantial improvement. The simulation result of using the two top-side pressure measurement, P_{at} and P_{tt}, using two manipulated variables is shown in Figure 3.19.

The pressures at top can be easily measured with good accuracy and a control structure using their combination (Figure 3.17) is recommended. However, by comparing simulation results in Figure 3.17 and Figure 3.19, one should notice that adding the secondary manipulated variable does not enhance the control performance.

Remarks

The choice of the suitable control structure is dependant on proper scaling of the controlled variables. For example for the gas-lift case, first we chose a small scaling factor for the mass flow rate and we wanted to control it in a tight bound. As a result, gain of the system with this output increased and the control structures using the flow rate resulted in better performance compared to those using the pressures.

In order to control the flow rate in a tight range, we must be able to measure it accurately. However, this is unlikely for two-phase flow in

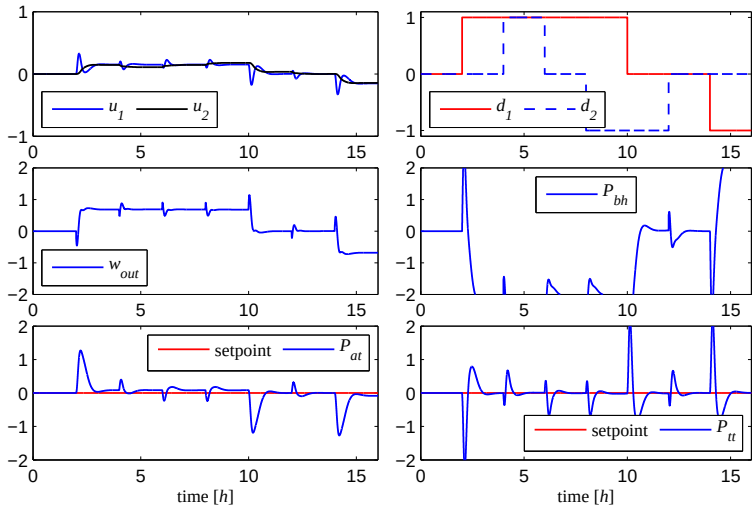

Figure 3.19: $\mathcal{H}_\infty$ control of gas-lift $CV = [P_{at}, P_{tt}]$, $MV = [u_1, u_2]$

practice. Therefore, we chose a wider scaling factor for the flow rate. On the other hand, pressure can be measured more reliably, thus a small scaling factor was used for pressures. Consequently, the control structures using pressure measurements are shown to be superior for the gas-lift case study.

3.4 Summary

We perfomed the controllability analysis for two case studies, a well-pipeline-riser system and a gis-lifted oil well. Suitable CVs for stabilizng control were identified from the analysis. First, minimum achievable peaks of the different closed-loop transfer functions with each of the candidate CVs and their combinations were calculated. Next, performance, robustness and input usage requirements were integrated in a mixed-sensitivity control problem. From this, a new single measure (γ) was introduced to quantify the quality of alternative control structures.

The bottom-hole pressure and the riser-base pressure are the best CVs for SISO control of the well-pipeline-riser system. Because of the pressure driven nature of the oulet flow in this case, the flow measurement shows a larger steady-state gain and consequently a better performance, compared to the pipeline-riser case in [77]. Therefore, having an accurate measurement of the outlet flow rate of the choke valve, it can be used in a SISO control scheme for stabilization.

Combing one pressure measurement from the subsea with the outlet flow rate gives the best result for the well-pipeline-riser system. If the subsea pressure measurements are not available, combining the top pressure and the flow rate gives a satisfactory result too. If the flow measurement is not available, the top pressure combined with the density is able to stabilize the system in theory. However, the measurements P_{rt} and ρ_{rt} and $\alpha_{l,rt}$ are not suitable CVs for a SISO control

For the gas-lifted oil well, the bottom-hole pressure is the best controlled variable. Nevertheless, this variable often is not directly measurable. A control structure using combination of two topside pressures from the annulus and the tubing was found to be effective to prevent the casing-heading instability. This can be implemented as a cascade control or the two topside pressures can be used by an observer to estimate the state variables for a state feedback control.

The production choke valve is the main manipulated variable for the gas-lift well. However, we found that the adding the secondary manipulated variable (gas-lift choke) does not improve stabilization of the gas-lifted oil wells significantly.

Further, it was found that accuracy of the measureing devices (sensors) must be taken into account in order to scalde different outputs of a system correctly.

Chapter 4

MANIPULATED VARIABLE SELECTION

A top-side choke valve is usually used as the manipulated variable for anti-slug control of multi-phase risers at offshore oil-fields. With new advances in the subsea technology, it is now possible to move top-side facilities to the sea floor. The two main contributions in this chapter are to consider an alternative location for the control valve and to consider how to deal with nonlinearity. This research involved controllability analysis based on a simplified model fitted to experiments, simulations using the OLGA simulator, as well as an experimental study. It was concluded that a control valve close to the riser-base is very suitable for anti-slug control, and its operation range is the same as the top-side valve. However, a subsea choke valve placed at the well-head can not be used for preventing the riser-slugging. The results provided in this chapter have been presented in [41].

4.1 Introduction

The oscillatory flow condition in offshore multi-phase pipelines is undesirable and an effective solution is needed to suppress it [25]. Active control of the topside choke valve is the recommended solution to maintain a non-oscillatory flow regime [71]. It also allows for larger valve openings and consequently higher production rate [60], [62]. The control system used for this purpose is called anti-slug control. This control system uses measurements such as pressure, flow rate or fluid density as the controlled variables and a choke valve located at the top-side platform is the usual manipulated variable.

By new advances in the mid-stream technologies, the subsea engineering is an integral part of the oil production. The subsea separation and the subsea compression are now standardized technologies used in practice, and moving all the facilities to the sea floor is the ongoing trend. However, having all facilities at the subsea, the produced oil and gas are needed to be transported to the sea level which involves using risers.

If we need to use the top-side choke valve for purposes other than the stabilizing control (e.g. safety and shut-down), a subsea solution for anti-slug control could be attractive. In order to explore possibilities of doing anti-slug control integrated with the subsea technology, we consider anti-slug control using subsea control valves in this chapter.

To use such a solution, we first need to consider if manipulating a subsea choke can prevent the riser slugging, and then where the control valve must be located for an effective stabilizing control. Next, one must look into input-output pairing to choose the best controlled variable in terms of robustness and performance of the control loop.

We compare different manipulated variables (inputs, MVs) and controlled variables (outputs, CVs) in terms of robustness and performance for stabilizing control. This controllability analysis is done based on a simplified model of the system. We have extended the four-state simplified model in [34] to include two subsea choke valves, one at the wellhead and one close to the riser-base. The simplified model is fitted to both the OLGA model and experiments. Moreover, results from the controllability analysis are verified by simulations using the OLGA simulator as well as experiments.

The system is highly nonlinear and the gain of the system decreases drastically as we open the valve. In the closed-loop system we want to keep the loop gain approximately constant for different operating points. Therefore, we need to increase the controller gain for large valve openings (lower pressure set-points).

4.2 Pipeline-Riser System

4.2.1 Experimental setup

The experiments were performed on a laboratory setup for anti-slug control at the Chemical Engineering Department at NTNU. Fig. 4.1 shows a schematic presentation of the laboratory setup. The pipeline and riser in the L-shaped setup are made from flexible pipes with 2 cm inner diameter. The length of the pipeline is 3 m, inclined downward with a 15° angle, and the height of the riser is 3 m. A buffer tank for gas is used to simulate the

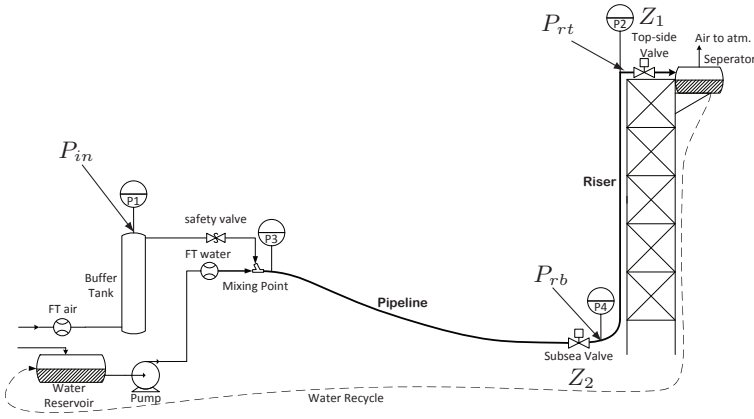

Figure 4.1: Schematic diagram of experimental setup

effect of a long pipe with the same volume, such that the total resulting length of the pipe would be about 70 m. There are two valves that may be used for control puposes; a topside valve and a subsea valve located close to the riser base (see Fig. 4.1).

The feed into the pipeline is at constant flow rates; 4 $litre/min$ of water and 4.5 $litre/min$ of air. The separator pressure after the topside choke valve is nominally constant at the atmospheric pressure. With these boundary conditions, the system switches from stable to unstable operation at $Z_1 = 15\%$ opening of the top-side valve when the subsea choke valve is fully ($Z_2100\%$) open. To stabilize the system using manual choking of the riser-base subsea valve, we need to close this valve to less than $Z_2 = 8\%$.

4.2.2 OLGA model

First, we simulated the experimental rig in the OLGA simulator using the same dimensions, and even including the buffer tank. The results for this are not included, because we found them to be quite similar to our extended OLGA model which includes an hypothetical oil well and its related wellhead valve. Figure 4.2 shows a schematic of the final model that was used in this work. The oil well is vertical with height of 20 m, inner diameter of 0.02 m, and the reservoir pressure is fixed at 3.45 bar. We choose these parameters such that inflow conditions would be similar to the experimental setup. The other dimensions and parameters are chosen very similar to the experimental setup.

In the final model with the oil well, we replaced the buffer tank by a 220 m horizontal pipe, much longer than our estimate of 70 m, to get the

same slug frequency as the experiments. In the experimental setup, the buffer tank contains only the gas phase while in the OLGA model, similar to practical conditions, more than half of the pipeline volume is occupied by liquid. To adjust the slug frequency, the volume occupied by the gas phase in the pipeline is important. The period of oscillations was $T = 68$ *sec*.

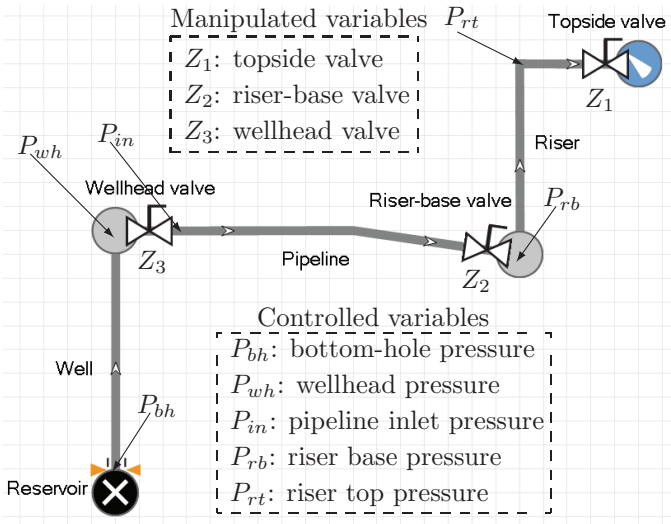

Figure 4.2: OLGA case for well-pipeline-riser system

4.2.3 Simplified model

A four-state simplified model for severe-slugging flow in pipeline-riser systems was presented in [34]. We have extended this model to include two subsea valves; one at the well-head and one near the riser base. The oil well dynamics are modelled by an additional state variable representing the total fluid mass in the well. The state variables of the augmented system model are as these:

- m_{tw}: mass of total fluid in well [kg]
- m_{gp}: mass of gas in pipeline [kg]
- m_{lp}: mass of liquid in pipeline [kg]
- m_{gr}: mass of gas in riser [kg]
- m_{lr}: mass of liquid in riser [kg]

The state equations are the mass conservation laws,

$$\dot{m}_{tw} = w_{res} - w_{wh} \tag{4.1a}$$

$$\dot{m}_{gp} = w_{g,in} - w_{g,rb} \tag{4.1b}$$

$$\dot{m}_{lp} = w_{l,in} - w_{l,rb} \tag{4.1c}$$

$$\dot{m}_{gr} = w_{g,rb} - w_{g,out} \tag{4.1d}$$

$$\dot{m}_{lr} = w_{l,rb} - w_{l,out} \tag{4.1e}$$

where,

- w_{res}: mass flow from reservoir to well [kg/s]
- w_{wh}: mass flow from wellhead to pipeline [kg/s]
- $w_{g,rb}$: mass flow of gas at riser base [kg/s]
- $w_{l,rb}$: mass flow of liquid at riser base [kg/s]
- $w_{g,out}$: outlet gas mass flow [kg/s]
- $w_{l,out}$: outlet liquid mass flow [kg/s]

These flow rates are calculated by valve type equations as given in [54]. The simple model was fitted to the experiments by adjusting the following six parameters:

- K_a: correction factor for average gas fraction in well
- K_{wh}: wellhead choke valve constant
- K_h: correction factor for level of liquid in pipeline
- K_{pc}: production choke valve constant
- K_g: coefficient for gas flow through low point
- K_l: coefficient for liquid flow through low point

We refer to [34] and [54] for more details. The bifurcations diagrams, describing the steady-state behaviour of the system as a function of the valve opening and the transition from stability to instability, are used to compare the simplified model with experiments and the OLGA model [77]. Fig. 4.3 and Fig. 4.4 show the bifurcation diagrams for the topside valve and the

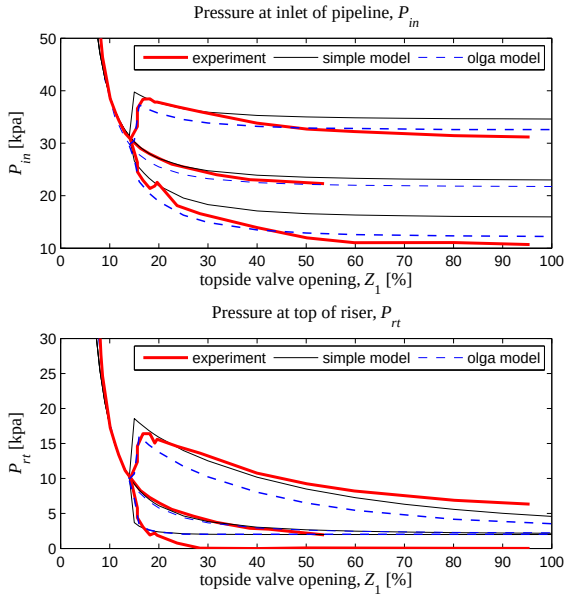

Figure 4.3: Bifurcation diagrams for Z_1 (two other valves fully open)

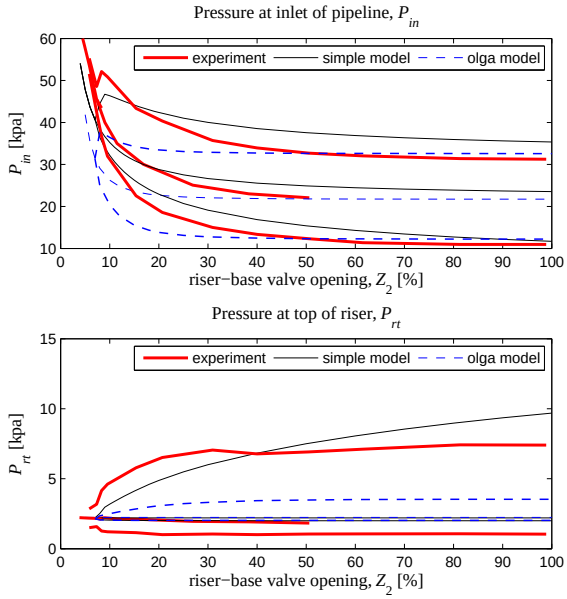

Figure 4.4: Bifurcation diagrams for Z_2 (two other valves fully open)

subsea valve, respectively. The simplified model (thin solid lines) is compared to the experiments (red solid lines) and the OLGA model (dashed lines). In Fig. 4.3, the system has a stable (non-slug) flow when the topside valve opening Z_1 is smaller than $Z_1^* = 15\%$, and it switches to slugging flow conditions for $Z_1 > 15\%$. We see three lines for slugging conditions. They are minimum and maximum pressure of the oscillations for slugging and the non-slug flow pressure. The non-slug flow regime is unstable for $Z_1 > 15\%$, but it can be stabilized by using feedback control.

The corresponding bifurcation diagram for the riser-base valve is shown in Fig. 4.4. The OLGA model could not capture both steady-state and the critical valve opening ($Z_2^* = 8\%$) at the same time for the riser-base valve; it was only possible to get the critical valve opening correct by adjusting the Coefficient of Discharge of this valve. On the other hand, in the simplified model, we have more free parameters and we could fit the simplified model closer to the experiments (Fig. 4.4).

4.3 Controllability Analysis

A controllability analysis should reveal limitations on the achievable performance of a given input(s) and output(s) combination [74]. A controllability analysis was used in Section 3.2 to find suitable controlled variables for anti-slug control when using the top-side choke valve as the manipulated variable. In this Section, we use a similar controllability analysis to compare the three alternative manipulated variables of the system (three control valves).

We compare minimum achievable peaks of three closed-loop transfer functions (S, KS and SG), the output pole vectors and the steady-state gain as given in Tables 4.1, 4.2 and 4.3. It is desirable with a large steady-state gain $|G(0)|$, a large output pole vector and small values for the peaks of the closed-loop transfer function (M_S, M_{KS} and M_{SG}).

The results for the top-side valve (Table 4.1) are similar to what was presented in Section 3.2. The four subsea pressures are all suitable candidates, but the topside pressure (P_{rt}) is not a good controlled variable because of a large peak on S.

The controllability analysis for the riser-base subsea control valve (Table 4.2) shows that the pressure measurements upstream of this valve (P_{bh}, P_{wh} and P_{in}) are good candidate controlled variables. The measurements downstream this valve (P_{rb}, P_{rt} and w_{out}) have small steady-state gains and are not suitable.

The controllability analysis for the wellhead control valve (Table 4.3)

Table 4.1: Controllability data for top-side choke valve $Z_1 = 40\%$

CV	Value	$G(0)$	Pole vector	M_S	M_{KS}	M_{SG}
P_{bh} $[kpa]$	174.12	-1.26	12.09	1.00	2.69	0.00
P_{wh} $[kPa]$	38.96	-1.48	13.17	1.00	2.47	0.00
P_{in} $[kpa]$	24.02	-1.99	15.02	1.00	2.17	0.00
P_{rb} $[kpa]$	21.37	-2.08	23.41	1.00	1.39	0.00
P_{rt} $[kpa]$	3.07	-2.09	8.28	7.00	3.93	5.19
w_{out} $[l/min]$	4.17	0.08	13.47	1.00	2.42	0.00

Table 4.2: Controllability data for riser-base choke valve $Z_2 = 40\%$

CV	Value	$G(0)$	Pole vector	M_S	M_{KS}	M_{SG}
P_{bh} $[kpa]$	164.26	-3.24	17.19	1.00	1.11	0.00
P_{wh} $[kpa]$	28.86	-3.31	17.53	1.00	1.09	0.00
P_{in} $[kpa]$	26.85	-3.47	18.30	1.00	1.05	0.00
P_{rb} $[kpa]$	22.82	0.18	28.66	1.30	0.67	0.94
P_{rt} $[kpa]$	2.25	0.02	2.08	1.00	9.23	0.00
w_{out} $[l/min]$	4.76	0.19	15.76	1.00	1.22	0.00

Table 4.3: Controllability data for well-head choke valve $Z_3 = 40\%$

CV	Value	$G(0)$	Pole vector	M_S	M_{KS}	M_{SG}
P_{bh} $[kpa]$	170.37	-2.78	15.52	4.80	1.73	13.92
P_{wh} $[kpa]$	27.67	-2.01	15.72	3.78	1.70	8.23
P_{in} $[kpa]$	26.37	0.49	16.26	1.00	1.65	0.00
P_{rb} $[kpa]$	20.46	0.03	29.35	1.01	0.91	0.06
P_{rt} $[kpa]$	2.30	0.02	1.65	1.60	16.28	0.07
w_{out} $[l/min]$	4.40	0.17	11.17	1.81	2.40	0.64

Table 4.4: Proportional gains used for different pressure set-points

Experiments		OLGA Simulations	
P_{set} $[kPa]$	K_c	P_{set} $[kPa]$	K_c
25.0	15	24.8	0.2
24.0	20	23.9	0.4
23.5	25	23.2	0.6
23.0	30	22.7	0.8
22.5	40	22.5	1.0
22.0	50	22.2	1.2
21.7	60	22.0	1.4
21.5	70	21.8	1.8
21.3	80		
21.0	90		

shows that none of the candidate controlled variables are very promising. The two pressure measurements upstream this valve have good steady-state gains, but have very large peaks for the sensitivity function. Among the four measurements downstream of this valve, the best is the pressure at inlet of the pipeline (P_{in}). It has relatively high steady-state gain and the peaks of the sensitivities are not large. We will therefore investigate this candidate controlled variable further in the simulations.

4.4 Experimental Results

The middle line in the bifurcations diagrams (Figure 4.3 and Figure 4.4) represents the desired non-slug flow. The slope of this line ($\frac{\partial y}{\partial u} = \frac{\partial P}{\partial Z}$) represents the process gain, and we note that the gain decreases in magnitude and approaches zero as the valve opening increases. In order to stabilize the system with larger valve openings (lower pressure set-points) we need to increase the controller gain. We used a simple PI controller implemented in LabView in the experiments. The integral time ($T_i = 120\ s$) was kept constant in the two experiments, and values of K_c for different pressure set-pints are given in Table 4.4. These values for the proportional gain were found by trial and error. Developing a procedure for tuning the controller parameters considering nonlinearity of the system is subject of the next chapter.

The same set of set-point dependant controller gains (Table 4.4) were used for all experiments, both with the topside and the subsea riser-base valve. The results are shown in Figure 4.5 and Figure 4.6, respectively. For

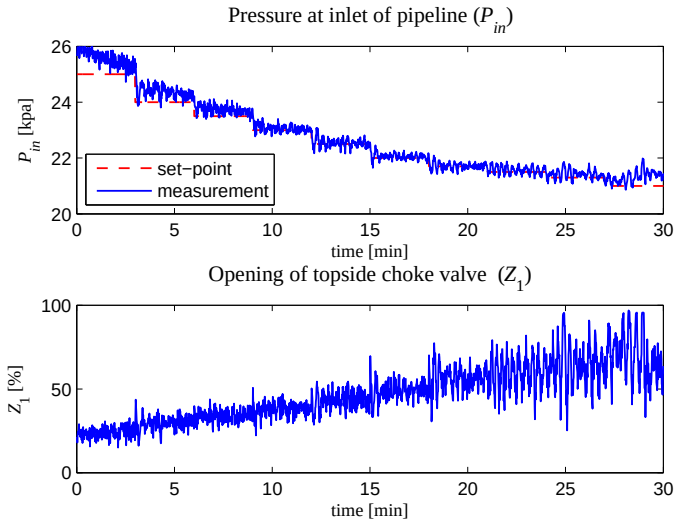

Figure 4.5: Experiment with MV = Z_1 and CV = P_{in}

the both valve locations we could stabilize the system without saturating the valve down to a set-point of 21.5 kPa. The average valve opening with this set-point is 63% for the top-side valve and 59% for the subsea valve.

4.5 OLGA Simulation Results

As for the experiments, a simple PI controller was used in the OLGA simulations with tunings obtained by trial and error. Tuning values for different pressure set-points are given in Table 4.4. Simulation results of control using the top-side choke valve (Figure 4.7) are shown in Figure 4.8 and the results using the riser-base control valve (Figure 4.9) are shown in Figure 4.10. The maximum achievable valve opening can be used as a measure of the benefit achieved from the anti-slug control. However, if two control valves have different sizes or Coefficients of Discharge, they produce different amounts of pressure drop for the same valve opening. Therefore, the minimum pressure set-point is used as a better measure, as it was used also by [62], especially when comparing two different valves. As shown in Figure 4.8 and Figure 4.10, in the OLGA Simulations, both the control valves can stabilize the system down to the same pressure set-point of 22 kPa. The valve opening with this set-point for the top-side valve is 42%, and for the subsea valve, it is 21%.

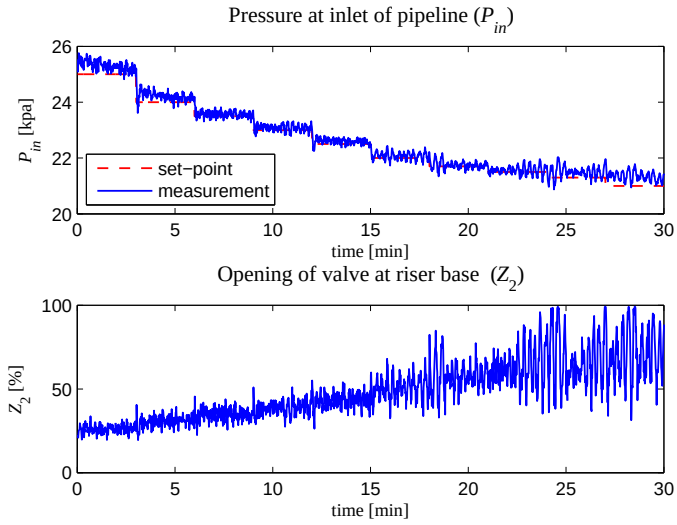

Figure 4.6: Experiment with MV = Z_2 and CV = P_{in}

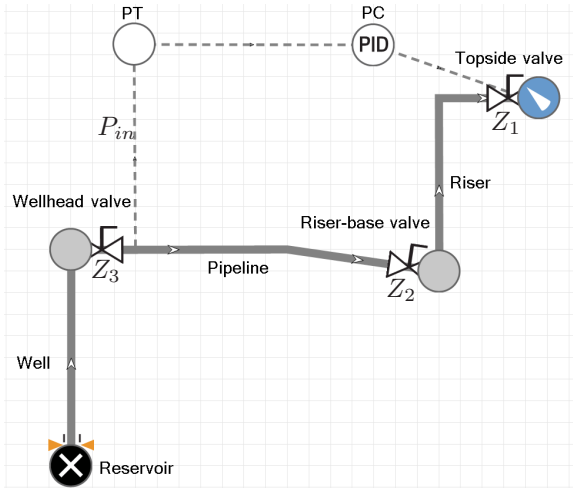

Figure 4.7: Control structure with MV = Z_1 and CV = P_{in}

In the OLGA simulations in Figure 4.8 and Figure 4.10, we use an oil well as the boundary condition such that the inflow rates are pressure driven. Indeed, one can notice from Figure 4.8 and Figure 4.10 that when we decrease the pressure set-point, the inlet mass flow rate from the oil well increases. Thus, in addition to the pressure set-point, we can see the benefit of the stabilizing control by looking at the inflow rates. The final

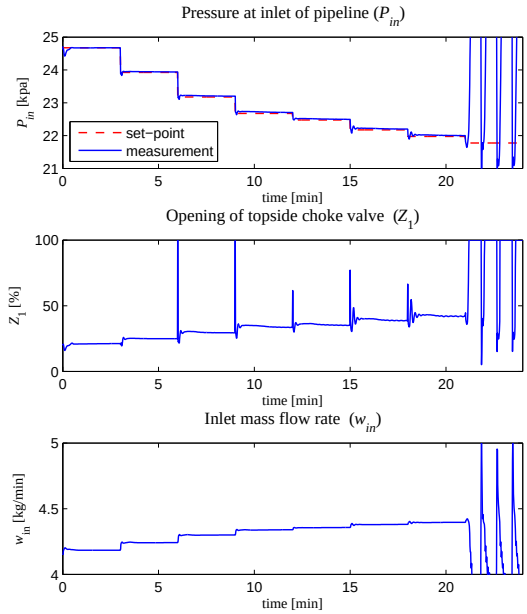

Figure 4.8: OLGA simulation with MV = Z_1 and CV = P_{in}

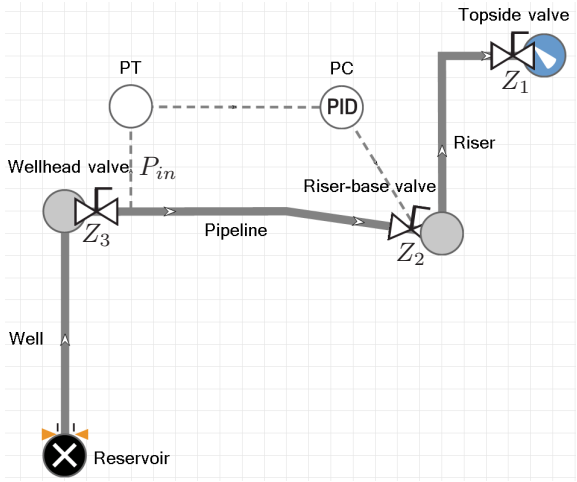

Figure 4.9: Control structure with MV = Z_2 and CV = P_{in}

production rate achieved by using both the control valves is the same value of 4.4 *kg/min*.

Next, we consider using the wellhead valve (Figure 4.11). From the con-

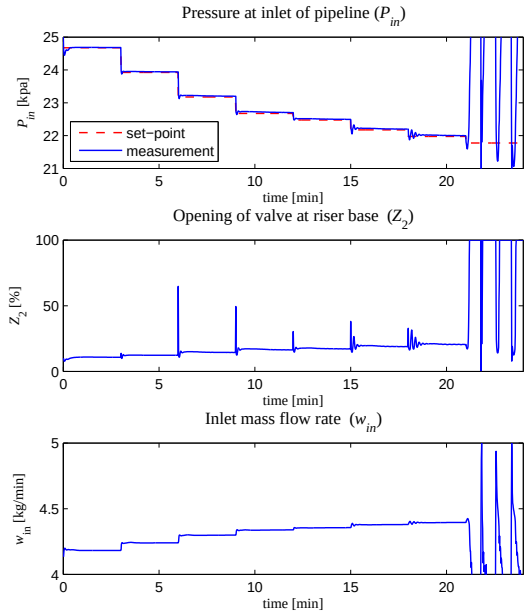

Figure 4.10: OLGA simulation with MV = Z_2 and CV = P_{in}

trollability analysis in the previous section, we predicted that control of the bottom-hole pressure (P_{bh}) and well-head pressure (P_{wh}) using the valve at the well-head (Z_3) is difficult because of large peaks of the sensitivity transfer function. Indeed, it was not possible to control these two variables by manipulating the wellhead valve in the OLGA simulations. On the other hand, the steady-state gain of the inlet pressure (P_{in}) is larger than for the other measurements downstream of the wellhead and it does not show any high peak. The simulation results in Figure 4.12 and Figure 4.13 show that the inlet pressure can be regulated, but it causes the valve to close, thus it shuts down the production. In Figure 4.12, we increase the set-point, but it does not have much effect and flow rate decreases again after a while. Because of small steady-state gain, by increasing the set-point the valve opening does not change considerably. We decrease the set-point in Figure 4.13. Since the lower set-point is infeasible, the valve closes completely but the pressure can not track the given set-point. In summary, the wellhead valve cannot be used for anti-slug control.

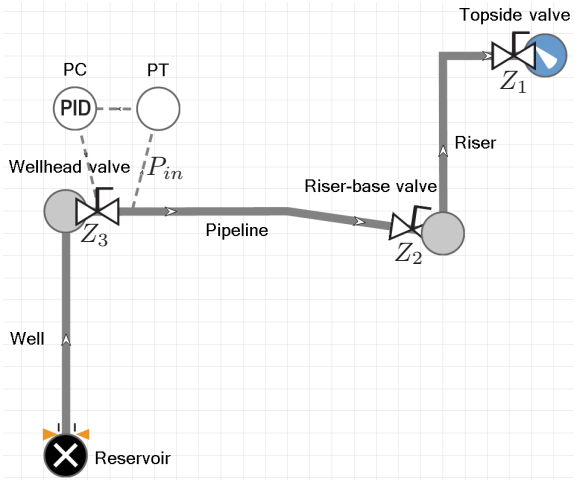

Figure 4.11: Control structure with MV = Z_3 and CV = P_{in}

4.6 Discussion

In addition to the controllability analysis, there are some physical reasons for the wellhead valve could not be used to stabilize the system. One intuitive reason is that the riser-slugging instability is because of dynamics between the pipeline (volume of gas) and the riser (weight of liquid). Therefore, manipulating a valve at the inlet does not have any effect on this and cannot stabilize the unstable dynamics.

Considering the simulations in Fig. 4.12 and Fig. 4.13 using the wellhead valve, the valve tends to close down. The reason for this is that the closed-loop system is internally unstable. In this situation, the riser becomes full of the liquid and only some gas bubbles will go out of the riser. The weight of a column of the liquid in the riser maintains the pressure regulation without a considerable flow out of the riser.

4.7 Summary

There is a good agreement between the OLGA model, simplified model and the experiments in bifurcations diagrams for the topside valve. We could fit the simple model closer to the experiments compared to the OLGA model for the subsea valve. Furthermore, the controllability analysis results based on the simplified model are consistent with the simulations and experiments.

The control valve close to the riser-base is very suitable for anti-slug control, and the resulted benefit in terms of the production rate is same

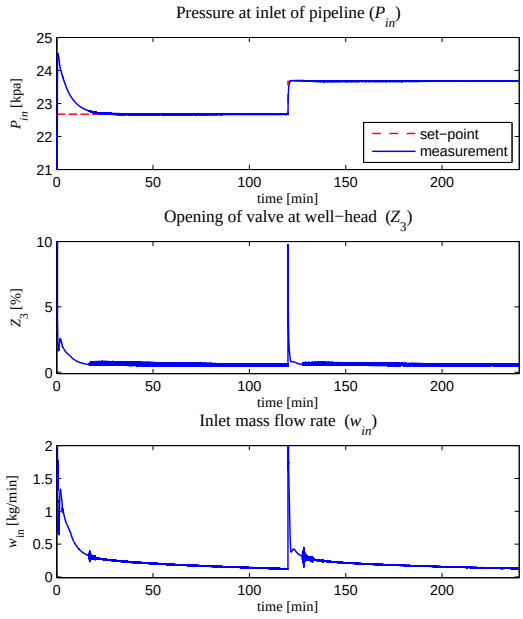

Figure 4.12: OLGA simulation with MV = Z_3 and CV = P_{in}

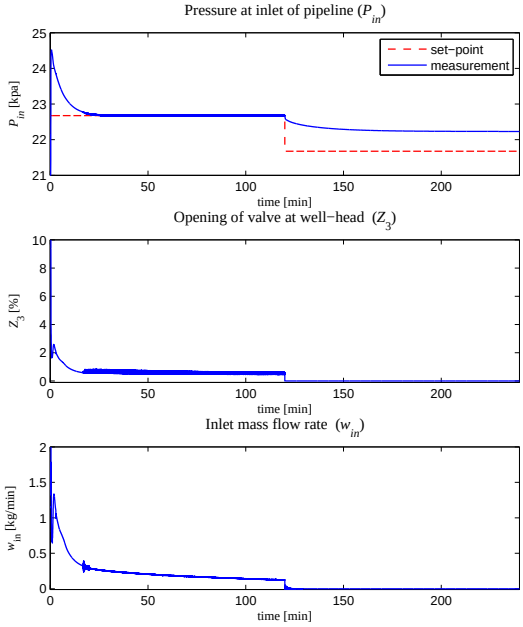

Figure 4.13: OLGA simulation with MV = Z_3 and CV = P_{in}

as using the top-side valve. However, a subsea choke valve placed at the wellhead can not be used for preventing the riser-slugging. This valve closes down and decreases the production rate drastically.

We could stabilize the system in the OLGA simulations and experiments up to very large valve openings by considering nonlinearity of the system and gain-scheduling of the proportional gain for a PI controller.

Chapter 5

LINEAR CONTROL SOLUTIONS

The anti-slug control requires operation around an open-loop unstable operating point. One solution is to use a robust controller based on a mechanistic model, for this purpose, we consider $\mathcal{H}_\infty$ control. As an alternative, we design an IMC (Internal Model Control) controller from a model identified by a closed-loop step test. We obtain a second order IMC controller that can be implemented as a PID controller with a low-pass filter on its derivative action. As the third solution, we consider using PI-control, which is the preferred choice in the industry. However, appropriate tuning is required for robustness against plant changes and large inflow disturbances. We obtain the PI-controler tuning from asymptotes of the proposed IMC controller. The proposed model identification and control solutions were verified experimentally on two different test rigs. Furthermore, we showed that robustness and performance of the IMC-PID can match a $\mathcal{H}_\infty$ controller. However, the prosed IMC-PID is easier to tune compared to $\mathcal{H}_\infty$ control. The results provided in this chapter are submitted for presentation in [35].

5.1 Robust Control Based on Mechanistic Model

Here, we linearize the four-state mechanistic model presented in Section 2.2 by calculating Jacobian matrices. Then, we design the $\mathcal{H}_\infty$ controller based on the linear model. We use two approaches to obtain the robust controller, $\mathcal{H}_\infty$ mixed-sensitivity design and $\mathcal{H}_\infty$ loop-shaping design.

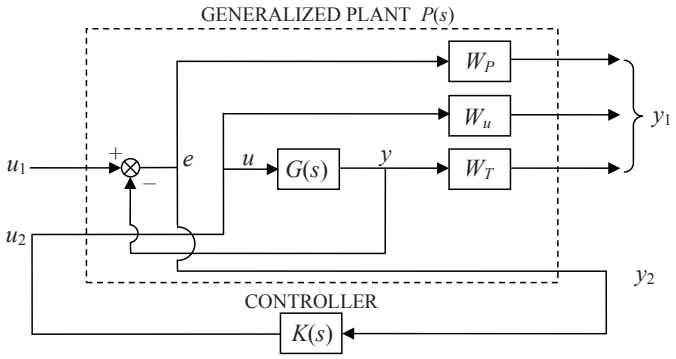

Figure 5.1: Closed-loop system for mixed sensitivity control design

5.1.1 $\mathcal{H}_\infty$ mixed-sensitivity design

We consider an $\mathcal{H}_\infty$ problem where we want to bound $\overline{\sigma}(S)$ for performance, $\overline{\sigma}(T)$ for robustness and low sensitivity to noise, and $\overline{\sigma}(KS)$ to penalize large inputs. These requirements may be combined into a stacked $\mathcal{H}_\infty$ problem [74].

$$\min_K \|N(K)\|_\infty, \quad N \triangleq \begin{bmatrix} W_u KS \\ W_T T \\ W_P S \end{bmatrix} \tag{5.1}$$

where W_u, W_T and W_P determine the desired shapes of KS, T and S, respectively. Typically, W_P^{-1} is chosen to be small at low frequencies to achieve good disturbance attenuation (i.e., performance), and W_T^{-1} is chosen to be small outside the control bandwidth, which helps to ensure good stability margin (i.e., robustness). W_u is often chosen as a constant. The solution to this optimization problem gives a stabilizing controller K that satisfies [16], [23]:

$$\begin{aligned} \overline{\sigma}(KS(j\omega)) &\leq \gamma \underline{\sigma}(W_u^{-1}(j\omega)) \\ \overline{\sigma}(T(j\omega)) &\leq \gamma \underline{\sigma}(W_T^{-1}(j\omega)) \\ \overline{\sigma}(S(j\omega)) &\leq \gamma \underline{\sigma}(W_P^{-1}(j\omega)) \end{aligned} \tag{5.2}$$

We assume four outputs for the model (P_{in}, P_{rt}, w_{out} and Q_{out}); all the four outputs are in the y_1 part and the particular output for feedback P_{in} is in the y_2 part of the generalized plant in Figure 5.1. The value of γ in equation (5.2) should be as small as possible for good controllability. However, it depends on the design specifications W_u, W_T and W_P.

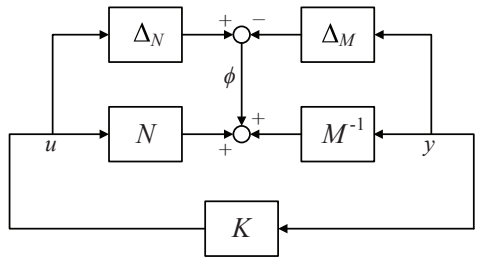

Figure 5.2: $\mathcal{H}_\infty$ robust stabilization problem

5.1.2 $\mathcal{H}_\infty$ loop-shaping design

We consider the stabilization of the plant G which has a normalized left coprime factorization

$$G = M^{-1}N \tag{5.3}$$

where we have dropped the subscripts from M and N for simplicity. A perturbed plant model G_p can then be written as

$$G_p = (M + \Delta_M)^{-1}(N + \Delta_N) \tag{5.4}$$

where Δ_M and Δ_N are stable unknown transfer functions which represent the uncertainty in the nominal plant model G. The objective of robust stabilization is to stabilize not only the nominal model G, but a family of perturbed plants defined by

$$G_p = \left\{(M + \Delta_M)^{-1}(N + \Delta_N) : \|[\Delta_N \;\; \Delta_M]\|_\infty < \epsilon\right\} \tag{5.5}$$

where $\epsilon > 0$ is then the stability margin [74]. To maximize this stability margin is the problem of robust stabilization of normalized coprime factor plant description as introduced and solved by Glover and McFarlane [24].

For the perturbed feedback system of Figure 5.2, the stability property is robust if and only if the nominal feedback system is stable and

$$\gamma_K \triangleq \left\| \begin{bmatrix} K \\ I \end{bmatrix} (I - GK)^{-1} M^{-1} \right\|_\infty \leq \frac{1}{\epsilon} \tag{5.6}$$

Notice that γ_K is the $\mathcal{H}_\infty$ norm from ϕ to $\begin{bmatrix} u \\ y \end{bmatrix}$ and $(I - GK)^{-1}$ is the sensivity function for this positive feedback arragmenet. A samll γ_K is corresponding to a large stability margin.

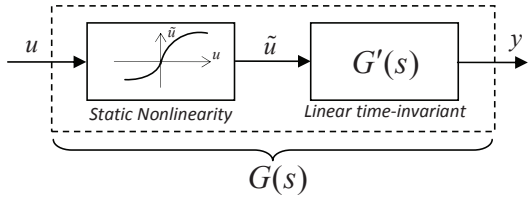

Figure 5.3: Block diagram for Hammerstein model

5.2 IMC Based On Identified Model

5.2.1 Model Identification

We use a Hammerstein model structure (Figure 5.3) to describe the desired unstable operating point (flow regime). The Hammerstein model consists of a series connection of a static nonlinearity (gain K) and a linear time-invariant dynamic system, $G'(s)$. For identification of the unstable dynamics, we need to assume a structure. We first considered a simple unstable first-order plus delay model:

$$G(s) = \frac{Ke^{-\theta s}}{\tau s - 1} = \frac{be^{-\theta s}}{s - a} \tag{5.7}$$

where $a > 0$. If we control this system with a proportional controller with gain K_{c0} (Figure 5.4), the closed-loop transfer function from the set-point (y_s) to the output (y) becomes

$$\frac{y(s)}{y_s(s)} = \frac{K_{c0}G(s)}{1 + K_{c0}G(s)} = \frac{K_{c0}be^{-\theta s}}{s - a + K_{c0}be^{-\theta s}}. \tag{5.8}$$

In order to get a stable closed-loop system, we need $K_{c0}b > a$. The steady-state gain of the closed-loop transfer function is then

$$\frac{\Delta y_\infty}{\Delta y_s} = \frac{K_{c0}b}{K_{c0}b - a} > 1. \tag{5.9}$$

However, the closed-loop experimental step response (see Figure 5.5) shows that the steady-state gain is smaller than one. Therefore, the model form in (5.7) is not a correct choice.

If we linearize the four-state mechanistic model in Section 2.2 around the desired unstable operating point, we get a fourth-order linear model in the form

$$G(s) = \frac{\theta_1(s + \theta_2)(s + \theta_3)}{(s^2 - \theta_4 s + \theta_5)(s^2 + \theta_6 s + \theta_7)}. \tag{5.10}$$

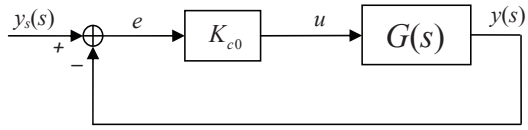

Figure 5.4: Closed-loop system with conventional feedback. In the experimental step test we use $C(s) = K_{c0}$

.

This model contains two unstable poles, two stable poles and two zeros. Seven parameters (θ_i) must be estimated to identify this model. However, if we look at the Hankel Singular Values of the fourth-order model (Figure 5.6), we find that the stable part of the system has little dynamic contribution. This suggests that a model with two unstable poles is sufficient for control design. Using a model truncation (square root method), we obtained a reduced-order model in the form of

$$G(s) = \frac{b_1 s + b_0}{s^2 - a_1 s + a_0}, \tag{5.11}$$

where $a_0 > 0$ and $a_1 > 0$. The model has two unstable poles and four parameters, b_1, b_0, a_1 and a_0, need to be estimated. If we control the unstable process in (5.11) using a proportional controller with gain K_{c0}, the closed-loop transfer function from set-point (y_s) to output (y) becomes

$$\frac{y(s)}{y_s(s)} = \frac{K_{c0}(b_1 s + b_0)}{s^2 + (-a_1 + K_{c0} b_1)s + (a_0 + K_{c0} b_0)}. \tag{5.12}$$

This can be rewritten to the model used in [83]:

$$\frac{y(s)}{y_s(s)} = \frac{K_2(1 + \tau_z s)}{\tau^2 s^2 + 2\zeta\tau s + 1} \tag{5.13}$$

To estimate the four parameters (K_2, τ_z, τ and ζ) in (5.13), we use six data (Δy_p, Δy_u, Δy_∞, Δy_s, t_p and t_u) observed from the closed-loop response (see Figure 5.5). Then, we back-calculate the parameters of the open-loop unstable model in (5.11). Details are given in B.

5.2.2 IMC design for unstable systems

The Internal Model Control (IMC) design procedure is summarized in [58]. The block diagram of the IMC structure is shown in Figure 5.7. Here, $G(s)$

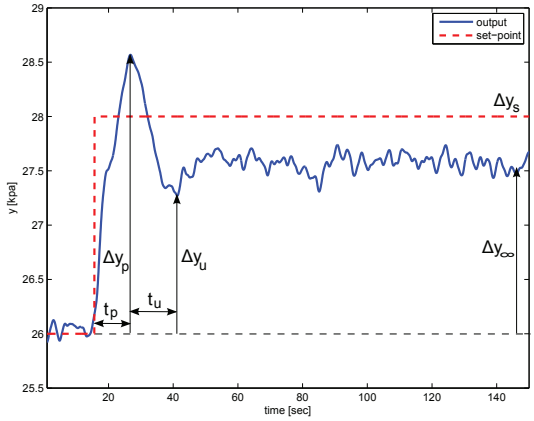

Figure 5.5: Experimental closed-loop step response for system stabilized with proportional control

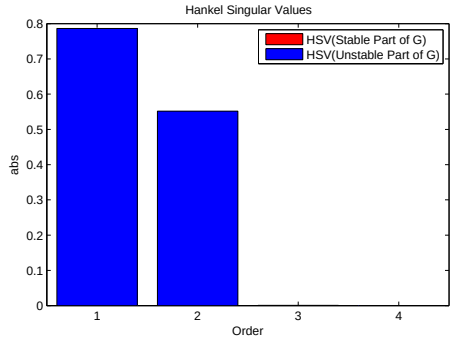

Figure 5.6: Hankel Singular Values of fourth order model

is the nominal model which in general has some mismatch with the real plant $G_p(s)$. $\tilde{Q}(s)$ is the inverse of the minimum phase part of $G(s)$ and $f(s)$ is a low-pass filter for robustness of the closed-loop system.

The IMC configuration in Figure 5.7 cannot be used directly for unstable systems; instead we use the conventional feedback structure in Figure 5.4 with the stabilizing controller

$$C(s) = \frac{\tilde{Q}(s)f(s)}{1 - G(s)\tilde{Q}(s)f(s)}. \tag{5.14}$$

For internal stability, $\tilde{Q}f$ and $(1 - G\tilde{Q}f)$ have to be stable. We use the identified model from the previous section as the plant model:

$$G(s) = \frac{\hat{b}_1 s + \hat{b}_0}{s^2 - \hat{a}_1 s + \hat{a}_0} = \frac{k'(s + \varphi)}{(s - \pi_1)(s - \pi_2)} \tag{5.15}$$

and we get

$$\tilde{Q}(s) = \frac{(1/k')(s - \pi_1)(s - \pi_2)}{s + \varphi} \tag{5.16}$$

We design the filter $f(s)$ as explained in [58]:
k = number of RHP poles + 1 = 3
m = max(number of zeros of $\tilde{Q}(s)$ - number of pole of $\tilde{Q}(s)$,1) = 1 (to make $Q = \tilde{Q}f$ proper)
n = m + k -1 = 3 (filter order)

The filter is in the following from:

$$f(s) = \frac{\alpha_2 s^2 + \alpha_1 s + \alpha_0}{(\lambda s + 1)^3}, \tag{5.17}$$

where λ is an adjustable closed-loop time-constant. We choose $\alpha_0 = 1$ to get integral action and the coefficients α_1 and α_2 are calculated by solving the following system of linear equations:

$$\begin{pmatrix} {\pi_1}^2 & \pi_1 & 1 \\ {\pi_2}^2 & \pi_2 & 1 \end{pmatrix} \begin{pmatrix} \alpha_2 \\ \alpha_1 \\ \alpha_0 \end{pmatrix} = \begin{pmatrix} (\lambda\pi_1 + 1)^3 \\ (\lambda\pi_2 + 1)^3 \end{pmatrix} \tag{5.18}$$

Finally, from (5.14) the feedback version of the IMC controller becomes

$$C(s) = \frac{[\frac{1}{k'\lambda^3}](\alpha_2 s^2 + \alpha_1 s + 1)}{s(s + \varphi)}. \tag{5.19}$$

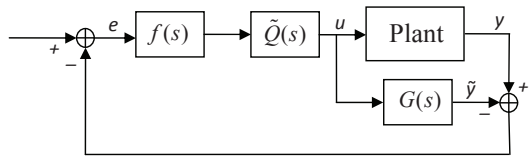

Figure 5.7: Block diagram of Internal Model Control system

5.2.3 PID implementation of IMC controller

Here, we obtain a PIDF tuning from the proposed IMC controller. The IMC controller in (5.19) is a second order transfer function which can be written in form of a PID controller with a low-pass filter.

$$K_{PID}(s) = K_c + \frac{K_i}{s} + \frac{K_d s}{T_f s + 1} \tag{5.20}$$

where

$$T_f = 1/\varphi \tag{5.21}$$

$$K_i = \frac{T_f}{k'\lambda^3} \tag{5.22}$$

$$K_c = K_i\alpha_1 - K_i T_f \tag{5.23}$$

$$K_d = K_i\alpha_2 - K_c T_f \tag{5.24}$$

For the controller work in practice, we require that $K_c < 0$ and $K_d < 0$; and we must choose λ such that these two conditions are satisfied. This was observed in the experiments.

5.3 PI Control

Next, we consider PI control. There are many approaches to get tuning values for PI control. For example, relay-feedback auto-tuning has been used in [61] for PI tuning based on a first-order unstable model. Here, we obtain the PI tuning based on the IMC controller from the previous Section. We consider a PI controller in the following form

$$K_{PI}(s) = K_c\left(1 + \frac{1}{\tau_I s}\right), \tag{5.25}$$

The PIDF controller in (5.20) can be approximated by a PI-controller by considering the high- and low-frequency asymptotes of $C(s)$ in (5.19).

$$K_c = \lim_{s\to\infty} C(s) = \frac{\alpha_2}{k'\lambda^3} \tag{5.26}$$

$$\tau_I = \frac{K_c}{\lim\limits_{s\to 0} sC(s)} = \alpha_2 \varphi \tag{5.27}$$

5.4 Small-Scale Experiments

5.4.1 Experimental setup

Here, we use the small-scale experimental set-up introduced in Section 4.2.1 to test the proposed PI and PID tuning rules.

5.4.2 Experiment 1: IMC-PID controller at Z=20%

The flow regime switches to slugging flow at a valve opening of $Z = 15\%$, hence it is unstable at $Z = 20\%$. We closed the loop with a proportional controller with $K_{c0} = -10$, and changed the set-point by 2 kPa (Figure 5.8). Since the response is noisy, a low-pass filter was used to reduce the noise effect. Then, we use the method described in Section 5.2.1 to identify the closed-loop stable transfer function:

$$\frac{y(s)}{y_s(s)} = \frac{2.317s + 0.8241}{19.91s^2 + 2.279s + 1} \tag{5.28}$$

The identified closed-loop transfer function is shown by the red line in Figure 5.8. From this, we back-calculate to an open-loop unstable process model:

$$G(s) = \frac{-0.012s - 0.0041}{s^2 - 0.0019s + 0.0088} \tag{5.29}$$

We select $\lambda = 10$ s for an IMC design to get the controller:

$$C(s) = \frac{-25.94(s^2 + 0.07s + 0.0033)}{s(s + 0.35)} \tag{5.30}$$

The corresponding PIDF tuning values, as given in Section 5.2.3, are $K_c = -4.44$, $K_i = -0.24$, $K_d = -60.49$ and $T_f = 2.81$ s. Figure 5.9 shows the PIDF controller performance. This controller was tuned for $Z = 20\%$ valve opening, but it can stabilize the system up to $Z = 32\%$ valve opening which shows good gain margin. In addition, we tested its delay margin by adding time delay to the measurement. It was stable with 3 *sec* added time delay.

5.4.3 Experiment 2: PI tuning at Z=20%

Next, we obtain the PI tuning from the IMC controller (5.30) as explained in Section 5.3. The PI tuning parameters are $K_c = -25.95$ and $\tau_I =$

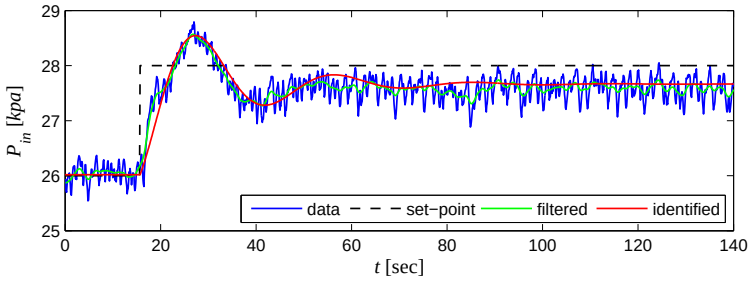

Figure 5.8: Closed-loop step test for experiment 1

107.38 s. Figure 5.10 shows result of experiment using the PI controller. This controller was stable with 2 *sec* time delay.

5.4.4 Experiment 3: IMC-PID controller at Z=30%

We repeated the previous experiment at $Z = 30\%$ valve opening. We closed the loop using a proportional controller with $K_{c0} = -20$ and changed the set-point by 2 kPa (Figure 5.11). Then, we use the method explained in Section 5.2.1 to identify the closed-loop stable transfer function:

$$\frac{y(s)}{y_s(s)} = \frac{2.634s + 0.6635}{13.39s^2 + 2.097s + 1} \tag{5.31}$$

The identified closed-loop transfer function is shown by the red line in Figure 5.11. Then, we back-calculate to an open-loop unstable system:

$$G(s) = \frac{-0.0098s - 0.0025}{s^2 - 0.0401s + 0.0251} \tag{5.32}$$

We select $\lambda = 8\ s$ for an IMC design to get the controller:

$$C(s) = \frac{-42.20(s^2 + 0.052s + 0.0047)}{s(s + 0.251)} \tag{5.33}$$

The corresponding PIDF tuning parameters, as in Section 5.2.3, are $K_c = -5.65$, $K_i = -0.79$, $K_d = -145.15$ and $T_f = 3.97\ s$. Figure 5.12 shows the closed-loop performance of the PIDF controller. This controller was tuned for a $Z = 30\%$ valve openings, but it can stabilize the system up to a valve opening of $Z = 50\%$ which shows that controller has a good gain margin. In addition, we tested its delay margin by adding time delay to the measurement. It was stable with 2 *sec* added time delay.

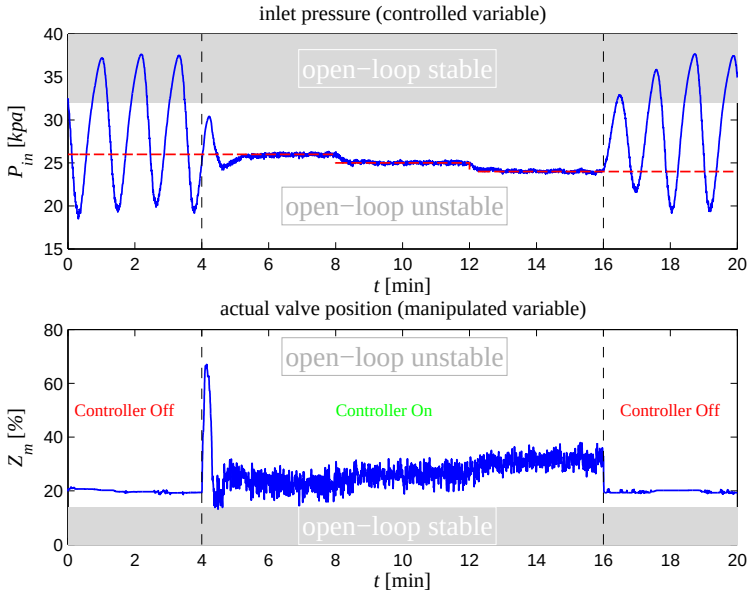

Figure 5.9: Result of IMC-PID controller for experiment 1

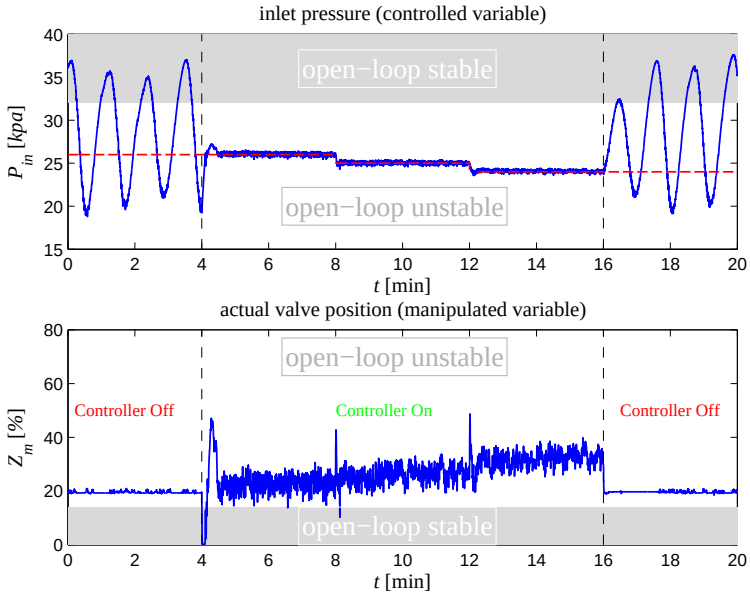

Figure 5.10: Result of PI controller for experiment 2

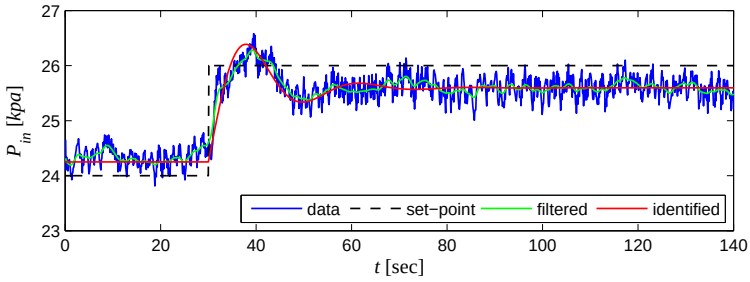

Figure 5.11: Closed-loop step test for experiment 3

5.4.5 Experiment 4: PI tuning at Z=30%

The corresponding PI tuning obtained from the IMC controller in (5.33), as in Section 5.3, are $K_c = -42.20$ and $\tau_I = 53.53$ s. Figure 5.13 shows an experimental run using the PI controller. This controller was only stable with added time delay less than 1 *sec*.

5.4.6 Experiment 5: $\mathcal{H}_\infty$ mixed-sensitivity controller at Z=30%

We design the robust controller using the $\mathcal{H}_\infty$ mixed-sensitivity method at the operating point with $Z = 30\%$ with the following design specifications:

$$W_T(s) = \frac{(s+1)^2}{(0.1s+1)^2}, \tag{5.34}$$

$$W_u = 1/100, \tag{5.35}$$

$$W_{P0} = 1/3, \tag{5.36}$$

$$W_P(s) = \frac{s/M_s + \omega_B}{s + \omega_B A}, \tag{5.37}$$

where $M_s = 3$, $\omega_B = 0.5$ and $A = 0.01$. One should notice that W_{P0} does not apply any integral action and it is considered for the uncontrolled outputs (P_{rt}, w_{out} and Q_{out}) in the y_1 part of the generalized plant. $W_P(s)$ applies an integral action with the bandwidth $\omega_B = 0.5$ on the controlled output P_{in}. With these specifications, $\gamma = 3.86$ is achieved, and we get a 6th-order stabilizing controller. After removing two unimportant states, we have

$$C(s) = \frac{-110.13(s+4.58)(s^2+0.025s+0.0058)}{s(s+0.22)(s^2+6.71s+15.03)}. \tag{5.38}$$

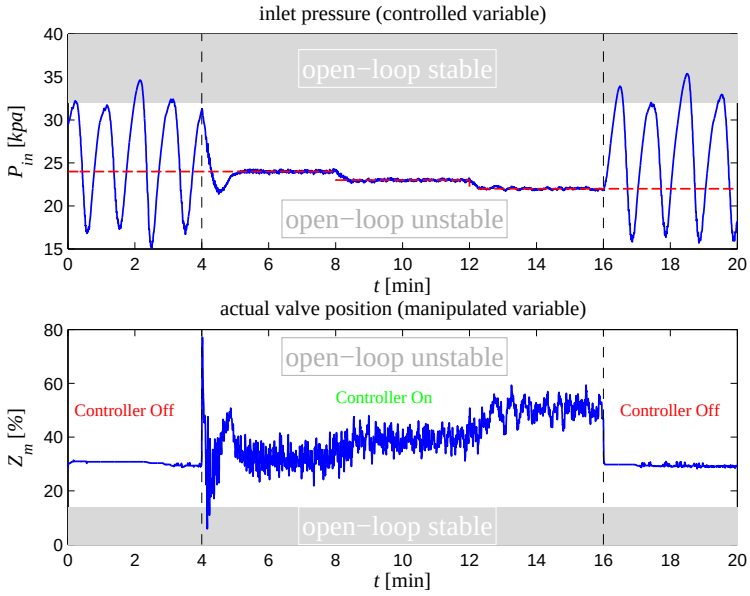

Figure 5.12: Result of IMC-PID controller for experiment 3

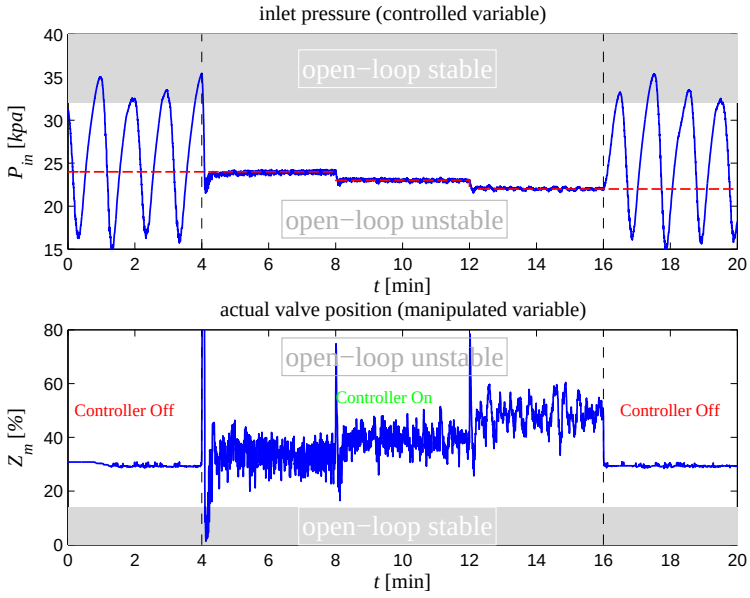

Figure 5.13: Result of PI controller for experiment 4

Table 5.1: Comparison between IMC-PID controller and $\mathcal{H}_\infty$ controllers

	IMC-PID	$\mathcal{H}_\infty$ mixed-sensitivity	$\mathcal{H}_\infty$ loop-shaping
Gain Margin	0.38	0.46	0.29
GM Frequency	0.19	0.18	0.16
Phase Margin	61.68	50.63	64.44
PM Frequency	0.52	0.43	0.64
Delay Margin	2.07	2.07	1.77
$\|S\|_\infty$	1.02	1.17	1.14
$\|T\|_\infty$	1.63	1.86	1.41
$\|KS\|_\infty$	43.17	36.86	55.67
Z_{max}	50%	50%	58%

Figure 5.14 compares the Bode plot of this controller with the IMC-PID controller in (5.33), and Figure 5.15 compares the closed-loop transfer functions of the controllers. Figure 5.16 shows experimental result of using the $\mathcal{H}_\infty$-controller in (5.38); similar to the IMC-PID controller in (5.33), this $\mathcal{H}_\infty$ controller could stabilize the system up to a valve opening of $Z = 50\%$, and it was stable with 2 *sec* added time delay. The margins of the two controllers are compared in Table 5.1. The gain-margin of the IMC-PID is better than that of the the $\mathcal{H}_\infty$ controller.

It must be noted that although specifying suitable weights for the $\mathcal{H}_\infty$ is much more complicated than tuning the IMC-PID using the filter time constant λ, the two controllers can achieve similar performance and robustness.

5.4.7 Experiment 6: $\mathcal{H}_\infty$ loop-shaping controller at Z=30%

We use the IMC-PID controller in (5.33) to get a initially shaped plant for the loop-shaping design. The code listed in Table 9.2 in [74] is used for this design procedure. The lowest achievable value of γ_K in (5.6) for this case is 1.77. The procedure gives a eight-state stabilizing controller. After removing unimportant states, we obtain the following third-order controller.

$$C(s) = \frac{-257.77(s^2 + 0.0046s + 0.0024)}{s(s + 0.26)(s + 4.9)} \tag{5.39}$$

The gain-margin, the phase-margin and peaks for the closed-transfer functions for this controller are compared with the two previous controller in Table 5.1. This controller is faster; it has a better gain-margin and slightly less delay-margin. The larger value for $\|KS\|_\infty$ indicates a more aggressive control signal, but it shows a smaller value for $\|T\|_\infty$. The Bode plot

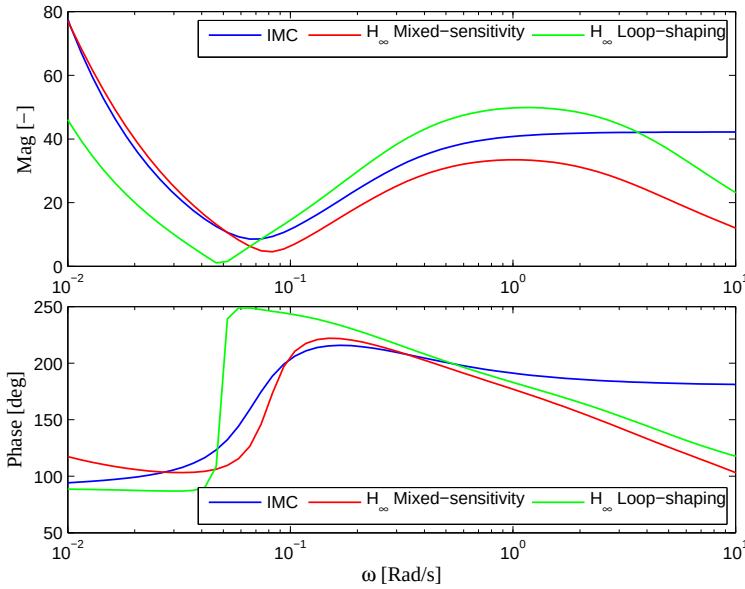

Figure 5.14: Bode plot of $\mathcal{H}_\infty$ controllers compared to IMC controller

of the loop-shaping controller is compared with the two other controller in Figure 5.14, and the closed-loop transfer functions are compared in Figure 5.15.

Figure 5.17 shows experimental result of using the $\mathcal{H}_\infty$ loop-shaping controller. When the controller is switched on, it is very aggressive which was expected from the large $\|KS\|_\infty$. Because of the better gain-margin, it can stabilize the system in a wider range of the valve operation (from a valve opening of $Z = 30\%$ up to $Z = 58\%$). We tested the delay margin by adding extra delay to the measured output; it was stable with 2 *sec* added delay.

5.5 Medium-Scale Experiments

5.5.1 Experimental setup

The tuning procedures were validated also on a medium-scale test rig. This test rig is an S-riser with a height of about 7 *m*. Other dimensions of this experimental set-up are shown in Figure 5.18. This riser is made from stainless steel pipes with inner diameter of 50 *mm*. Similar to the small scale setup, an air buffer thank is installed at inlet to emulate the effect of a long

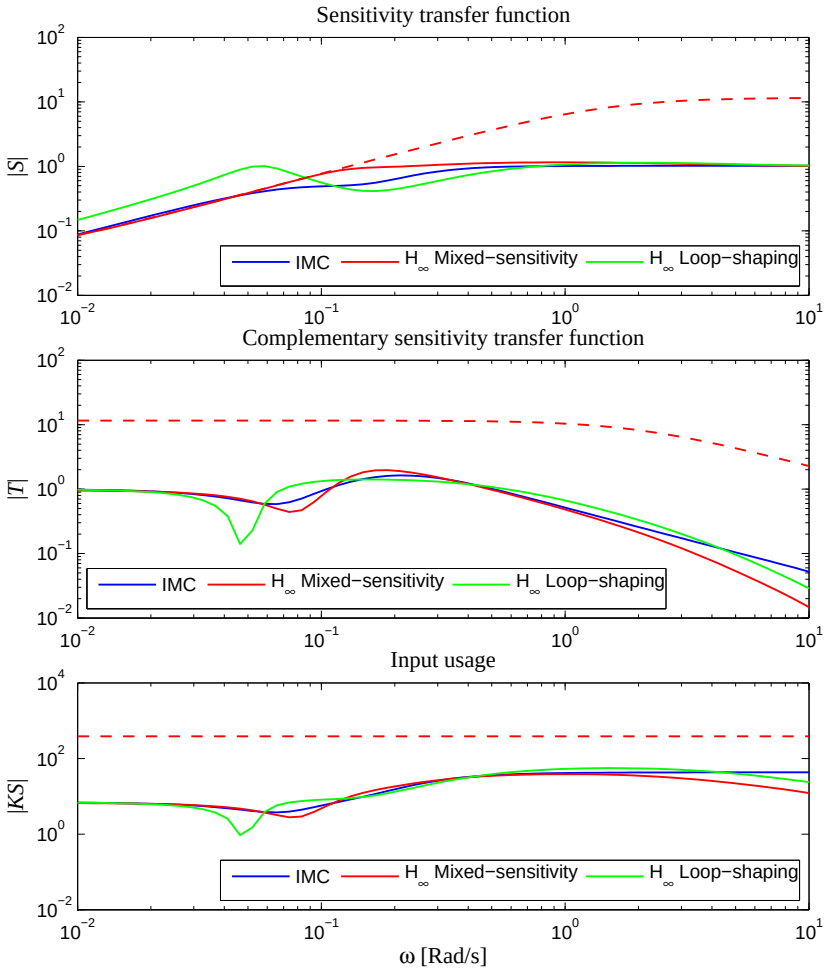

Figure 5.15: Closed-loop transfer functions for $\mathcal{H}_\infty$ Controllers compared to IMC controller

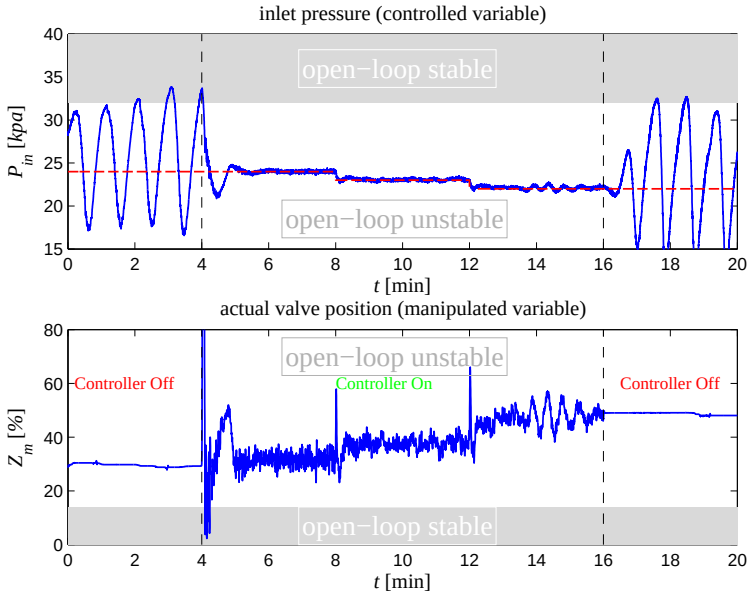

Figure 5.16: Result of mixed-sensitivity $\mathcal{H}_\infty$ controller in experiment 5

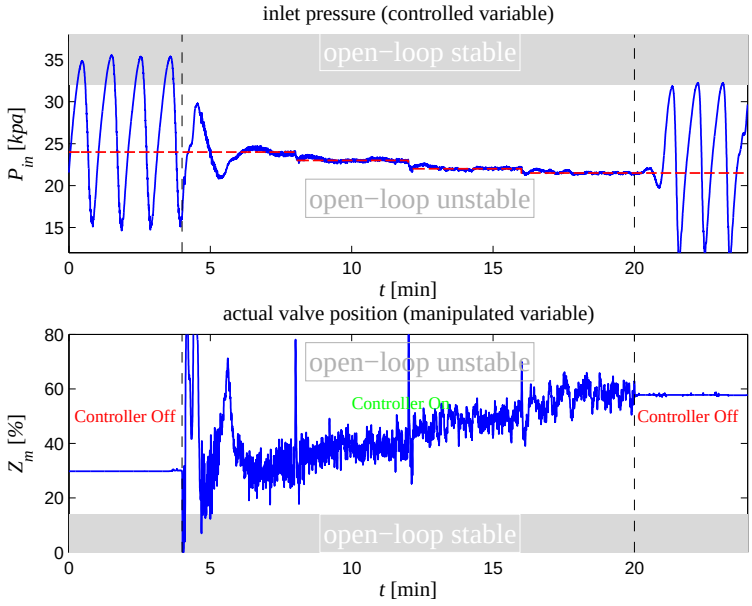

Figure 5.17: Result of loop-shaping $\mathcal{H}_\infty$ controller in experiment 6

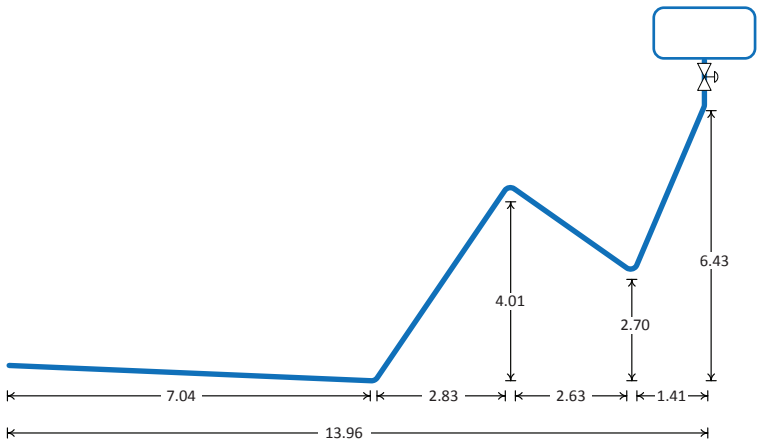

Figure 5.18: Experimental setup for S-riser (all values in *meter*)

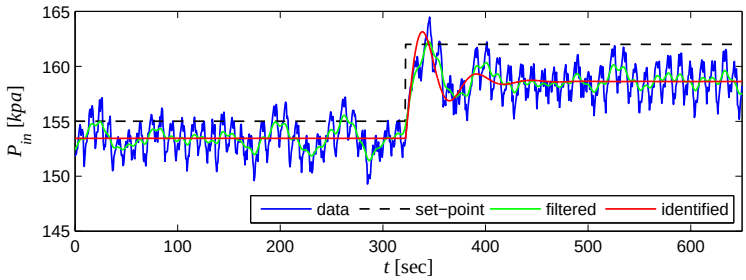

Figure 5.19: Closed-loop step test on medium-scale rig in experiment 7

pipeline with the same volume. The volume of the buffer tank is 200 litres; this is equivalent 101.86 m of pipe. The inlet flow rates to the system are 0.0024 *kg/sec* air and 0.3927 *kg/sec* water. The outlet separator pressure is constant at the atmospheric pressure. With these boundary conditions, the system switches from non-slug to slugging flow conditions at $Z^* = 16\%$ opening of the topside valve.

5.5.2 Experiment 7: IMC-PID controller at Z=18%

Figure 5.19 shows a closed-loop step test performed on the S-riser. A proportional controller with the gain $K_{c0} = -250$ was used for the test. The pressure set-point before the step test was 155 kPa which results in a valve opening of $Z = 18\%$ (region of unstable open-loop operation). We identified

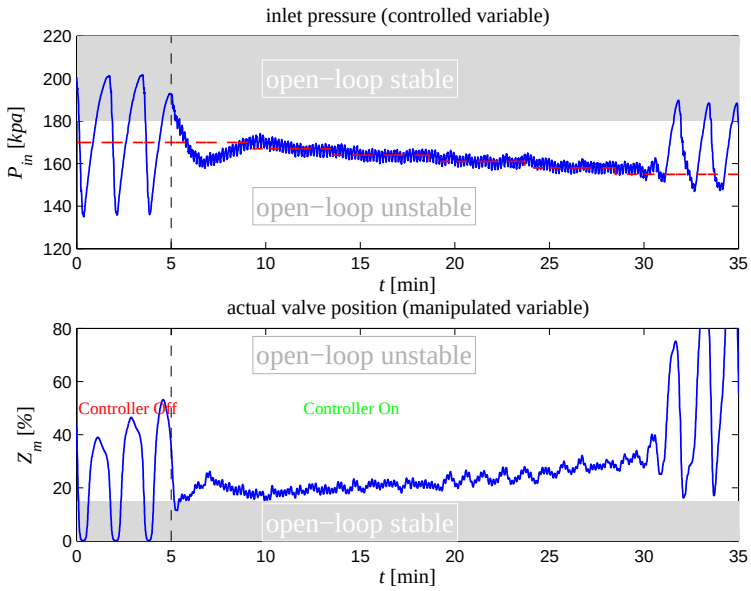

Figure 5.20: Experimental result of IMC-PID controller on medium-scale setup in experiment 7

an unstable model as the following:

$$G(s) = \frac{-5.6 \times 10^{-4}(s + 0.082)}{s^2 - 0.069s + 0.0040} \tag{5.40}$$

By choosing $\lambda = 24.5$, we designed the following IMC controller:

$$C(s) = \frac{-340.75(s^2 + 0.0052s + 0.00036)}{\mathrm{s}(\mathrm{s} + 0.0816)} \tag{5.41}$$

The corresponding PID tuning are $K_c = -3.47$, $K_i = -1.49$, $K_d = -4.13 \times 10^4$ and $T_f = 12.25$. Experimental result of control using this PID tuning is shown in Figure 5.20. In this experiment, we decreased the set-point until the system becomes unstable. This controller was able to control the system up to a $Z = 32\%$ valve opening, which is two time of the critical valve opening $Z^* = 16\%$.

5.5.3 Experiment 8: PI tuning at Z=18%

The PI tuning obtained from the IMC controller in (5.41) are $K_c = -340.75$ and $\tau_I = 229.23$. The experimental result is given in Figure 5.21 where system was stabilized up to $Z = 24\%$.

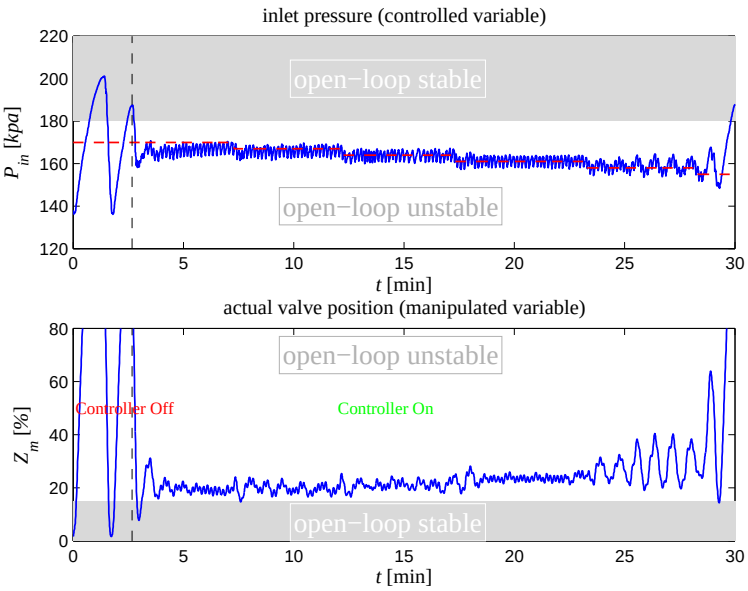

Figure 5.21: Experimental result of PI controller on medium-scale setup in experiment 8

5.6 Summary

A model structure including two unstable poles and one zero was used to identify an unstable model for the desired non-slug flow dynamics which are open-loop unstable. The model parameters were estimated from a closed-loop step test, and the identified model was used for an IMC design. The proposed IMC controller can be implemented as a PID-F controller that results in good gain margin and phase margin. PI tunings were also obtained from the IMC controller. This scheme was tested experimentally on two experimental rigs (the small-scale and the medium-scale S-riser). The performance and the robustness of the IMC-PID controller was very similar to the mixed-sensitivity $\mathcal{H}_\infty$ controller. The two controller can stabilize the system up to the same valve opening ($Z = 50\%$), and they were stable with 2 *sec* extra delay. However, compared to the $\mathcal{H}_\infty$ controller, the IMC-PID is easier to tune and it does not require a mechanistic model.

In addition to the $\mathcal{H}_\infty$ mixed-sensitivity design, the loop-shaping design was tested where the new IMC controller was used to obtain the initially shaped plant. The loop-shaping procedure improves the gain-margin. The final controller is faster and generates an aggressive control action, but it can stabilize the system up to a larger valve opening ($Z = 58\%$).

Chapter 6

NONLINEAR CONTROL SOLUTIONS

Instability and the inverse response behaviour make anti-slug control at offshore oil-fields an interesting control problem where a robust solution considering the nonlinearity of the system is required. Existing anti-slug control systems become unstable after some time, because of inflow disturbances or plant changes. The nonlinearity at different operating conditions is one source of plant changes. In addition, the time delay is another problematic factor for stabilization. The nonlinearity can be counteracted by model-based nonlinear controllers or by gain-scheduling of multiple linear controllers. A summary of the different anti-slug control solutions proposed in previous works is given in Table 6.1.

In this chapter, We test four new control solutions experimentally. First, we use state feedback based on state estimation using nonlinear observers. Second, we apply feedback linearization with measured outputs. Then, we consider a PI controller with adaptive gain correction based on the static

Table 6.1: success of different control solutions in previous works

method \ measurement	topside pressure	subsea pressure	using both pressures	top pressure & flow
PID/$\mathcal{H}_\infty$/LQG [71], [75]	†	☺	☺	☺
Linear observer [37]	†	☺	–	–
Nonlinear observer [37]	☹	†	†	–
Feedback linearization [38]	–	–	☺	–
Back stepping [48]	–	☺	–	–

–: not investigated ☺: works well ☹: not robust †: doesn't work

gain of the system. Finally, we use gain scheduling for IMC (Internal Model Control) based on linear models identified from closed-loop step tests. We compare these four approaches in terms of robustness and operation range, more precisely, we compare delay margin of the controllers and the maximum achievable valve opening for each control solution. The results provided in the chapter have been presented in [37], [38], [35], [36].

6.1 Pipeline-Riser System

6.1.1 Simplified dynamical model

A four-state simplified model for the severe-slugging flow was presented in Section 2.2. The state variables of this model are as:

- m_{gp}: mass of gas in pipeline [kg]
- m_{lp}: mass of liquid in pipeline [kg]
- m_{gr}: mass of gas in riser [kg]
- m_{lr}: mass of liquid in riser [kg]

The four state equations of the model are

$$\dot{m}_{gp} = w_{g,in} - w_g \tag{6.1}$$

$$\dot{m}_{lp} = w_{l,in} - w_l \tag{6.2}$$

$$\dot{m}_{gr} = w_g - \alpha w \tag{6.3}$$

$$\dot{m}_{lr} = w_l - (1-\alpha) w \tag{6.4}$$

Fig. 6.1 shows a schematic presentation of the model. The inflow rates of gas and liquid to the system, $w_{g,in}$ and $w_{l,in}$, are assumed to be constant. The flow rates of gas and liquid from the pipeline to the riser, w_g and w_l, are determined by pressure drop across the riser-base where they are described by virtual valve equations. The outlet mixture flow rate, w, is determined by the opening percentage of the top-side choke valve, u, which is the manipulated variable of the control system. The different flow rates and the gas mass fraction, α, in the equations (6.1)-(6.4) are given by additional model equations presented in Section 2.2.

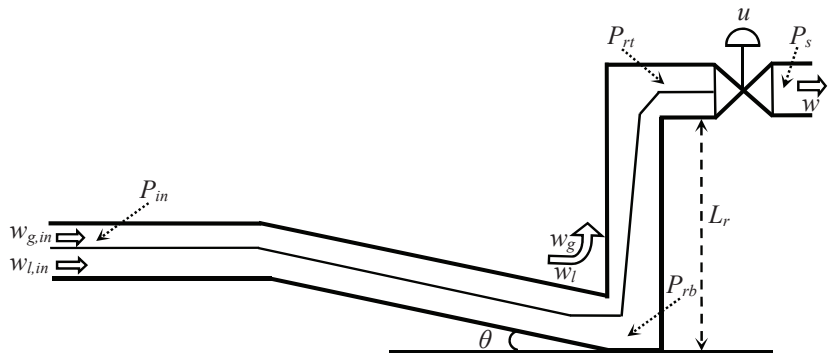

Figure 6.1: Schematic presentation of system

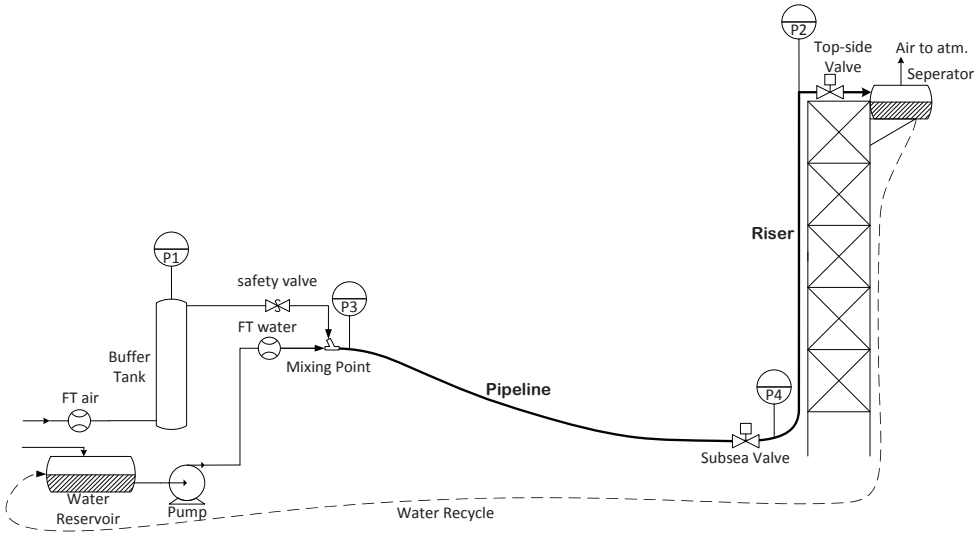

Figure 6.2: Schematic diagram of experimental setup

6.1.2 Experimental setup

The experiments were performed on a laboratory setup for anti-slug control at the Chemical Engineering Department of NTNU. Fig. 6.2 shows a schematic representation of the laboratory setup. The pipeline and the riser are made from flexible pipes with 2 cm inner diameter. The length of the pipeline is 4 m, and it is inclined with a 15° angle. The height of the riser is 3 m. A buffer tank is used to simulate the effect of a long pipe with the same volume, such that the total resulting length of pipe would be about 70 m.

The topside choke valve is used as the input for control. The separator pressure after the topside choke valve is nominally constant at atmospheric pressure. The feed into the pipeline is assumed to be at constant flow rates, 4 $litre/min$ of water and 4.5 $litre/min$ of air. With these boundary conditions, the critical valve opening where the system switches from stable (non-slug) to oscillatory (slug) flow is at $Z^* = 15\%$ for the top-side valve.

Bifurcations diagrams, describing the steady-state and the dynamics of this system, are used to fit the model to the experimental rig ([77]). Fig. 6.3 shows the bifurcation diagrams of the simplified model (solid lines) compared to the those of the experiments (dashed lines). The system has a stable (non-slug) flow when the valve opening Z is smaller than 15%, and it switches to slugging flow conditions for larger valve openings. The minimum and maximum of the oscillations of the slugging together with the steady-state (in the middle) are shown in Fig. 6.3.

The desired steady-state (middle line) in slugging condition ($Z > 15\%$) is unstable, but it can be stabilized by using control. The slope of the steady-state line is the static gain of the system, $G = \partial y/\partial u = \partial P_{in}/\partial Z$. As the valve opening increase this slope decreases, and the gain finally approaches to zero. This makes control of the system with large valve openings very difficult. The controller should keep the loop-gain ($L = KG$, where G is the process gain and K is the controller gain) constant in order to stabilize the system over the whole range of operation.

6.2 State Feedback with Nonlinear Observer

It has been shown that it is difficult to avoid slugging in pipeline-riser systems when using only the top-side pressure measurement [77]. The reason is that the unstable Right Half-Plane (RHP) zeros of the system with this measurement are relatively close to the unstable poles of the system, and consequently the sensitivity transfer function of the system has an unavoid-

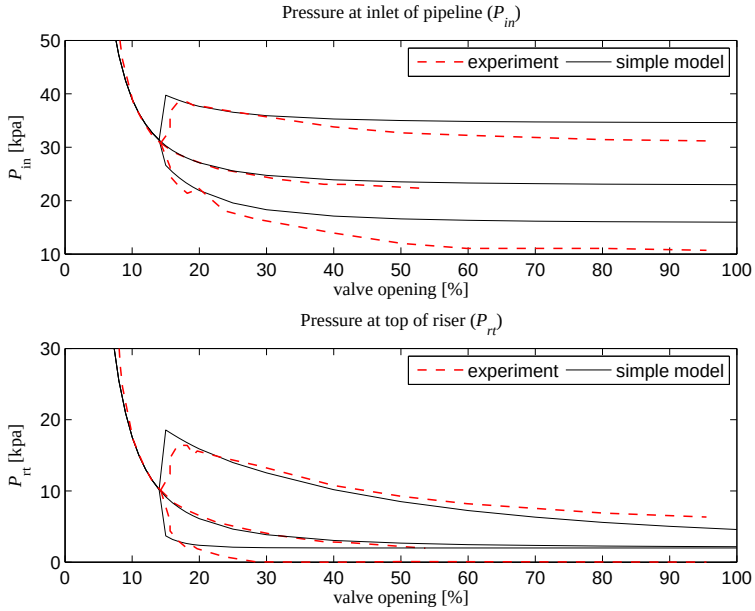

Figure 6.3: Bifurcation diagrams of simplified model (solid) compared to experiments (dashed)

able large peak. On the other hand, the pressure measurement at the subsea is a suitable controlled variable, and a simple PI controller is used in practice [25].

If only the top-side pressure measurement is available, a conventional control solution is to design an observer which uses the top-side pressure measurement to estimate the states of the system including the bottom pressure, and then use these estimates for control. However, the fundamental controllability limitation of unstable zero associated with the top-side pressure can not be bypassed by the observer. Nevertheless, we want to see if this solution is applicable for anti-slug control, and which kind of observer is more suitable.

The Extended Kalman Filter has been previously used for estimating the bottom pressure and other other state variables in gas-lifted oil wells [20]. Moreover, a nonlinear observer based on back-stepping design was proposed for this purpose [2], and it was tested in experiments [18]. The gas-lift system has a similar unstable zero dynamic associated with the tubing pressure, but the tubing pressure in combination of the other top-side measurement has been used in [18], [20].

A nonlinear Luenberger-type observer that uses only the topside pressure to reproduce oscillations of the riser-slugging instability was proposed in [14], and then used for anti-slug control of a pipeline-riser system in experiments [56]. This observer was designed based on a three-state simplified model of the system [13]. It was found that in their case the peak of the sensitivity transfer function of the topside pressure was not large, and it did not impose limitations on the controllability [12]. However, as discussed later, this is true only for small valve openings, and we can not open the valve for large production rates when using the top-side pressure.

We use the four-state simplified model presented in Section 2.2 for the observer and control design in this work. The model is fitted to experimental data by adjusting four parameters, and it shows good agreement with experiments.

Three types of observer using the top-side pressure were tested experimentally. These are a Luenberger-type nonlinear high-gain observer, a standard Unscented Kalman Filter (UKF), and a UKF modified to incorporate the high-gain observer concept [51] which we call "Fast UKF".

The term "High-Gain observer" can cause confusion in some cases. One may say a observer is not high-gain, because the observer gain is a small number (e.g. $K = 0.1$) [56] [15]. However, it depends on which unit is used for the measurement; for example there is a scaling factor of 10^3 between Pa and kPa for pressure. Hence, the speed (convergence rate) of the observer

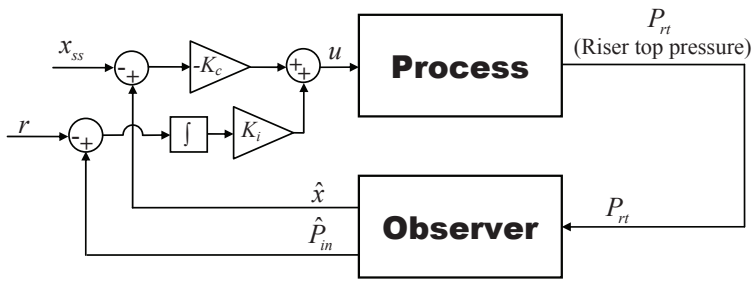

Figure 6.4: Block diagram of closed-loop system

is a better indicator.

As illustrated in Figure 6.4, we want to estimate the state variables of the system by use of an observer and use the estimates for state feedback. The *separation principle* allows us to separate the design into two tasks. First, we design a state feedback controller that stabilizes the system and meets other design specifications. Then an output feedback controller is obtained by replacing the state x by its estimate $\hat{x}$ provided by observers [51]. However, the *separation principle* does not hold in general for nonlinear systems, and we have to test this solution for the anti-slug control by experiments.

6.2.1 State feedback

As shown in Figure 6.4, we apply full state feedback by using the estimated states. In addition, to prevent drift from the operating point, integral action is added by integrating the set-point deviation for the estimated subsea pressure ($\hat{P}_{in}$). The total control action can be expressed as

$$u(t) = -K_c(\hat{x}(t) - x_{ss}) + K_i \int_0^t (\hat{P}_{in}(\tau) - r)d\tau. \tag{6.5}$$

Here, K_c is a linear optimal controller calculated by solving *Riccati equation* and K_i is a relatively small integral gain.

6.2.2 Nonlinear Observers

Unscented Kalman Filter

First, we consider the standard form of the Unscented Kalman Filter (UKF) as explained by [47]. The nonlinear state space system is given as

$$x_k = f(x_{k-1}, u_{k-1}) + v_{k-1}, \tag{6.6a}$$

Table 6.2: Unscented Kalman Filter algorithm

(1) Prediction step:
$\hat{X}_{k-1} = [\hat{x}_{k-1} \quad \dots \quad \hat{x}_{k-1}] + \sqrt{c}\,[\sqrt{P_{k-1}} \quad -\sqrt{P_{k-1}}\,]$
$\hat{X}_k = f(\hat{X}_{k-1}, u_{k-1})$
$\hat{x}_k^- = \hat{X}_k W_m$
$P_k^- = \hat{X}_k W_c [\hat{X}_k]^T + Q_{k-1}$
(2) Update step:
$\hat{X}_k^- = \left[\hat{x}_k^- \quad \dots \quad \hat{x}_k^-\right] + \sqrt{c}\left[\sqrt{P_k^-} \quad -\sqrt{P_k^-}\right]$
$Y_k^- = h(\hat{X}_k^-)$
$\mu_k = Y_k^- W_m$
$S_k = Y_k^- W_m \left[Y_k^-\right]^T + R_k$
$C_k = \hat{X}_k^- W_c \left[Y_k^-\right]^T$
(3) Compute filter gain K_k, updated state mean $\hat{x}_k$ and covariance P_k:
$K_k = C_k S_k^{-1}$
$\hat{x}_k = \hat{x}_k^- + K_k\,[y_k - \mu_k]$
$P_k = P_k^- - K_k S_k K_k^T$

$$y_k = h(x_k, u_k) + w_k, \tag{6.6b}$$

where v_{k-1} is a vector of Gaussian zero-mean process noise with the covariance matrix Q_{k-1}, representing model error and disturbances. w_k is a vector of Gaussian zero-mean measurement noise with the covariance matrix R_k.

We assume that the state vector is a random variable with mean value $\hat{x}_{k-1}$ and the covariance matrix P_{k-1}, undergoing the nonlinear transform of f. The general problem is to find the statistics of this random variable after the nonlinear transform ($\hat{x}_k$). The main idea behind the UKF, unlike the Monte Carlo simulations which need a large number of samples, is that the statistics of a nonlinear transformation can be found with fair accuracy by only a limited number of samples called *sigma points*. The samples in Monte Carlo simulations are chosen randomly, whereas in the UKF algorithm the sigma points are chosen deterministically. Similar to the EKF, the UKF algorithm has a predictor/corrector nature, but we do not need to linearize the model by calculating the Jacobian matrices. The UKF algorithm is summarized in Table 6.2.

We do not discretize the model or the observers, instead we use Matlab (*ode15s* solver) to integrate the model from time $k-1$ to k. Because of small dimensions of the laboratory set-up, the frequency of the unstable dynamics are relatively high, and we need a small sampling time ($T_s = 0.1\ sec$). With the four-state model, we get eight sigma points, and integrating the model eight times needs more computation time than the sampling time. We solved

this problem by using parallel processing in Matlab.

High-Gain Luenberger observer

A high-gain observer, under certain conditions, guarantees that the output feedback controller recovers the performance of the state-feedback controller when the observer gain is sufficiently high. The observer gain is designed so that the observer is robust to uncertainties in modeling the nonlinear functions. The structure of the high-gain observer is similar to the one used in [14]:

$$\begin{aligned}
\dot{\hat{z}}_1 &= f_1(\hat{z}) \\
\dot{\hat{z}}_2 &= f_2(\hat{z}) \\
\dot{\hat{z}}_3 &= f_3(\hat{z}) + \frac{1}{\epsilon}(y - \hat{y}) \\
\dot{\hat{z}}_4 &= f_4(\hat{z})
\end{aligned} \tag{6.7}$$

where

- z_1, mass of gas in pipeline (m_{gp})
- z_2, mass of liquid in pipeline (m_{lp})
- z_3, pressure at top of riser (P_{rt})
- z_4, mass of liquid in riser (m_{lr})

and $\frac{1}{\epsilon}$ is the high gain. Three of the equations (f_1, f_2 and f_4) are the same as the model in equations (6.1), (6.2) and (6.4) in Section 6.1. For the third state equation (f_3), we transform the state into top pressure which is a measurement ($y = z_3$ and $\hat{y} = \hat{z}_3$). We use $z_3 = P_{rt}$, because it is directly related to the mass of gas in the riser (m_{gr}) which is the third state of the model:

$$P_{rt} = \frac{m_{gr} R T_r}{M_G \left(V_r - \frac{m_{lg}}{\rho_l} \right)} \tag{6.8}$$

$$f_3(z) = \frac{dP_{rt}}{dt} \tag{6.9}$$

We get the time derivative of the top-pressure by using partial derivatives:

$$\frac{dP_{rt}}{dt} = \frac{\partial P_{rt}}{\partial m_{gr}} \dot{m}_{gr} + \frac{\partial P_{rt}}{\partial m_{lr}} \dot{m}_{lr} \tag{6.10}$$

where

$$\frac{\partial P_{rt}}{\partial m_{gr}} = \frac{a}{b - m_{lr}} \tag{6.11}$$

$$\frac{\partial P_{rt}}{\partial m_{lr}} = \frac{a m_{gr}}{(b - m_{lr})^2} \tag{6.12}$$

In (6.11) and (6.12), $a = RT_r\rho_l/M_G$ and $b = \rho_l V_r$ are model constants; see Section 2.2 for details of the model.

Fast UKF

One advantage of the Unscented kalman Filter (UKF) over a simple high-gain observer is that the UKF relates the measurements to all the state equations with appropriate gains. Moreover, a Kalman Filter averages out measurement noise, and thus the estimates are less sensitive to noise. However, the standard UKF is not sufficiently robust in closed-loop for our application. In most of the experimental runs, the closed-loop system using the UKF was not able to stabilize the flow. However, by increasing the observer gain, promising results were achieved. Although the observer gain for the UKF can be increased by using a small value for R_k and a large value for Q_{k-1}, there is a limitation with this approach. By looking at the UKF algorithm, the observer gain is

$$K_k = \frac{\hat{X}_k^- W_c \left[Y_k^-\right]^T}{Y_k^- W_m \left[Y_k^-\right]^T + R_k}. \tag{6.13}$$

One notices that the observer gain is highly dependent on the scale of states and measurements. In the case of measuring one of states, the maximum gain in direction of the measured state is 1. Even though the UKF, similar to the linear Kalman Filter, is optimal for estimation errors at steady-state, it can not guarantee robustness of the closed-loop system.

We aim to combine the advantages of the UKF with the robustness properties of a high-gain observer. We implement this idea in a basic and simple way. We use the transformed model, similar to (6.7), instead of the original model in (6.1)-(6.4). It is similar to the high-gain observer, but without the observer term.

$$\begin{aligned} \dot{z}_1 &= f_1(z) \\ \dot{z}_2 &= f_2(z) \\ \dot{z}_3 &= f_3(z) \\ \dot{z}_4 &= f_4(z) \end{aligned} \tag{6.14}$$

These are the model equations, only the third state has been transformed. We do not specify the observer term in the state equations explicitly, neither do we determine the observer gain directly; we let the Unscented Transformation calculate the four elements of the observer gain. The matrix Q_k in the UKF algorithm represents process noises, and larger Q_k leads to a large observer gain. The third state of the model in (6.14) is measured. By choosing suitable values for the elements of Q_k, we can put more weight in the direction of the measured state. We construct Q_k as follows:

$$Q_k = diag(q_{min}, q_{min}, q_{max}, q_{min}) \tag{6.15}$$

where q_{min} and q_{max} are treated as tuning parameters. The UKF algorithm calculates the observer gains in an adaptive manner, and unlike a simple high-gain observer, it gives four elements corresponding to the four states. As suggested in [6], we incorporated the innovation information (Mean Square Error in a moving window) to make R_k and Q_k adaptive as well. This idea was tested in simulations, using OLGA simulator as the real process, also in experiments. We found that the closed-loop system is more robust in experiments when we have R_k and Q_k constant.

Since we are using the UKF algorithm with a measured state ($y = z_3$), the maximum observer gain is 1. To have better control of the observer gain, we scale the states and measurements of the system based on their steady-state values. All the states are normalized to 100, and the measurement is normalized to 1000. This scaling implies that when the UKF gives a gain of 1, we have enforced a factor of 10. However, we present the measurements with their original scales in the experimental results.

6.2.3 Experimental results

Measuring top-side pressure

The experimental result using the high-gain Luenberger observer is shown in Figure 6.5. The same experiment using the Fast UKF is shown in Figure 6.6. Comparing Figures 6.5 and 6.6, we see that the Fast UKF behaves better and, unlike the high-gain observer, does not show any oscillation when the controller is on.

As shown in Figure 6.3, the open-loop system switches from stable to slugging flow for valve openings $Z > 15\%$. We were able to stabilize the system up to $Z = 20\%$ by using nonlinear observers when the top-side pressure without any delay was measured. However, as the valve opening increases, control becomes more difficult [40].

The standard UKF was not able to stabilize the system for most of experimental runs, while the two other observers were successful in all experiment runs with $Z = 20\%$. The result of using the standard UKF, when the system can be stabilized, is similar to Figure 6.6. We do not present the result here due to space limitation.

Measuring subsea pressure

Based on previous controllability analysis [77], [40], it is much easier to stabilize the system using the subsea pressure instead of the top-side pressure. Indeed, we found that the system could be stabilized up to $Z = 40\%$ valve opening by controlling subsea pressure using a simple PI control (Figure 6.7), that is, with no observer.

Next, we considered state feedback control based on observers using the subsea pressure as the only measurement. Surprisingly, it was not possible to stabilize the system when used any of the fast observers (high-gain Luenberger and fast UKF). We constructed observers for the subsea pressure measurement, as done in the previous section, by transforming the first state by choosing $z_1 = P_{in}$.

Figure 6.8 shows the result of open-loop estimation by a Luenberger observer with a large gain ($\epsilon = 10^{-4}$), where the subsea pressure is the measurement used by the observer. The top-side pressure and its related state variables are not correctly estimated, and this seems to be the reason we were not able to stabilize the system. This happens when we increase the gain of the observer for supposedly robustness of the closed-loop system.

On the other hand, we used a linear Kalman Filter with the subsea pressure measurement, and it was possible to stabilize the system up to $Z = 40\%$ valve opening. As shown in Figure 6.9, an aggressive control action is needed to stabilize the system at this operating point.

We also performed closed-loop experiments where we started the experiment in closed-loop to keep the system always around its equilibrium point, and the results were the same; none of the three nonlinear observers worked properly. The Fast UKF was able to stabilize the system, but it was not robust against disturbance in boundary (inflow) conditions. We summarize performance of different observers for state estimation in Table 6.3, and performance of different methods for stabilizing control in Table 6.4.

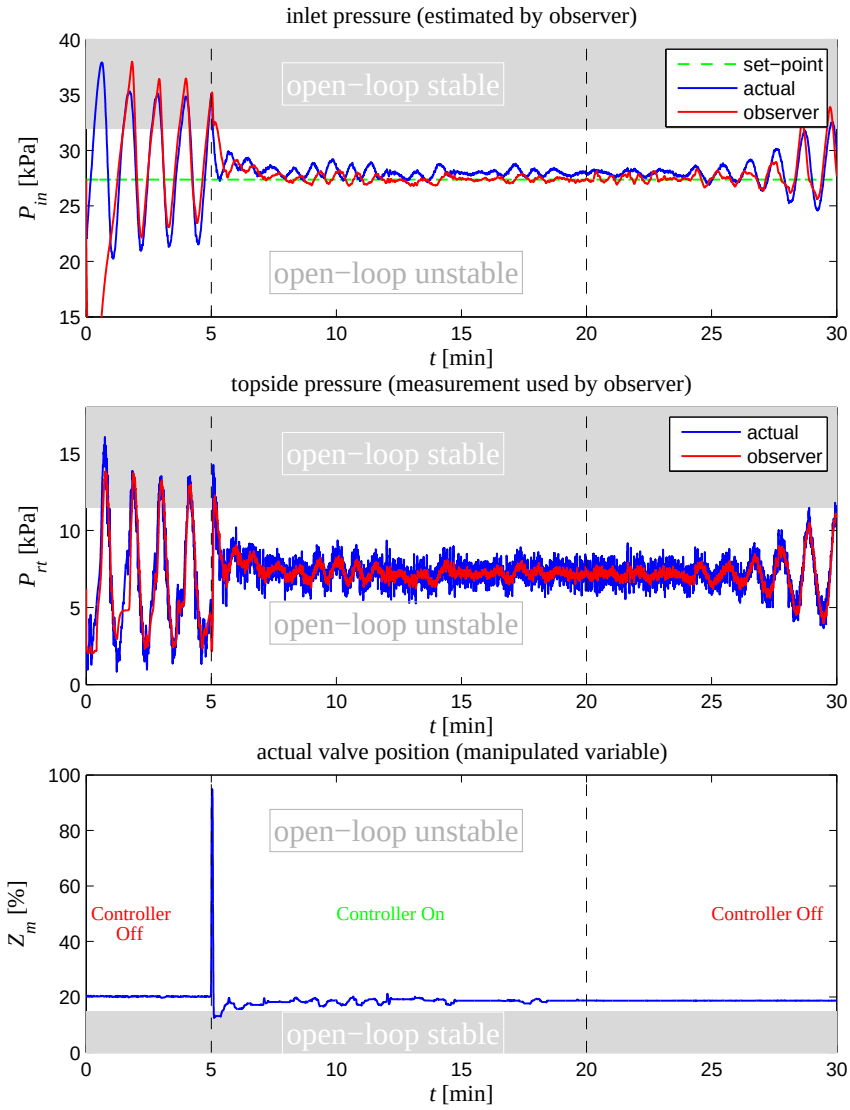

Figure 6.5: Control experiment with top-side pressure (P_{rt}) measurement used by high-gain observer, $Z = 20\%$

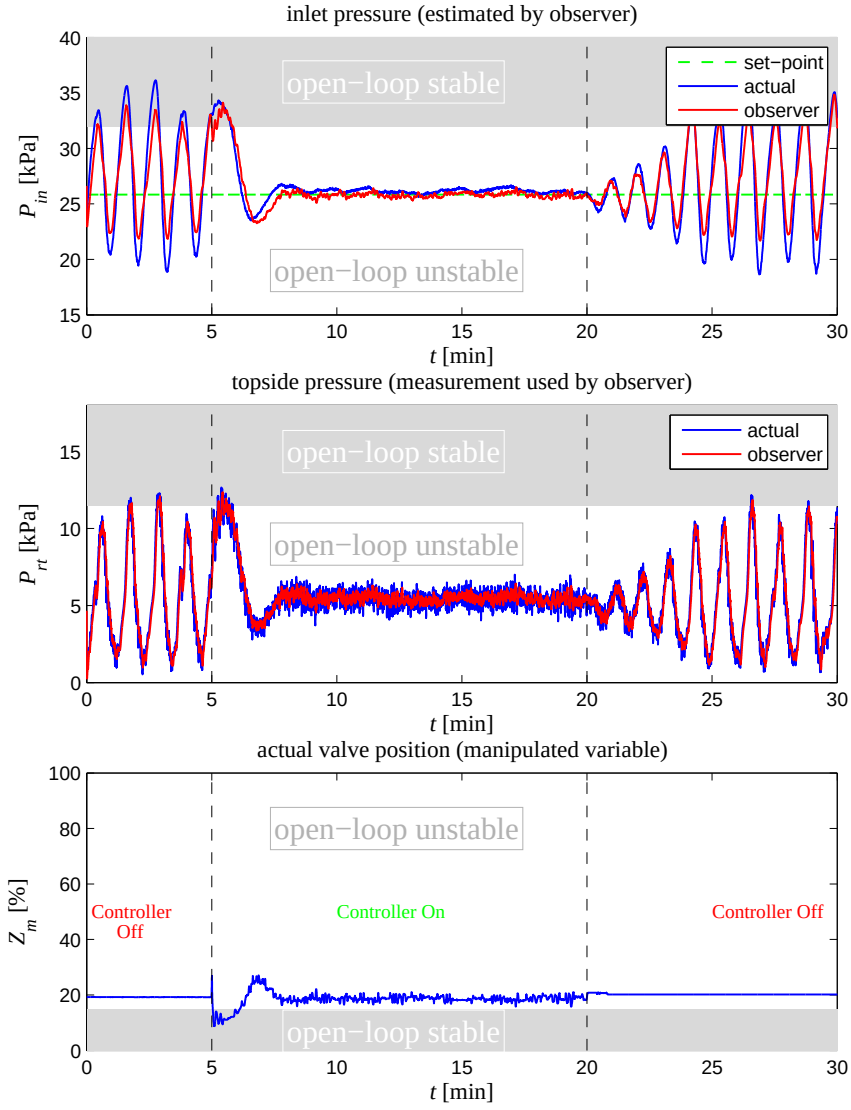

Figure 6.6: Control experiment with top-side pressure (P_{rt}) measurement used by Fast UKF, $Z = 20\%$

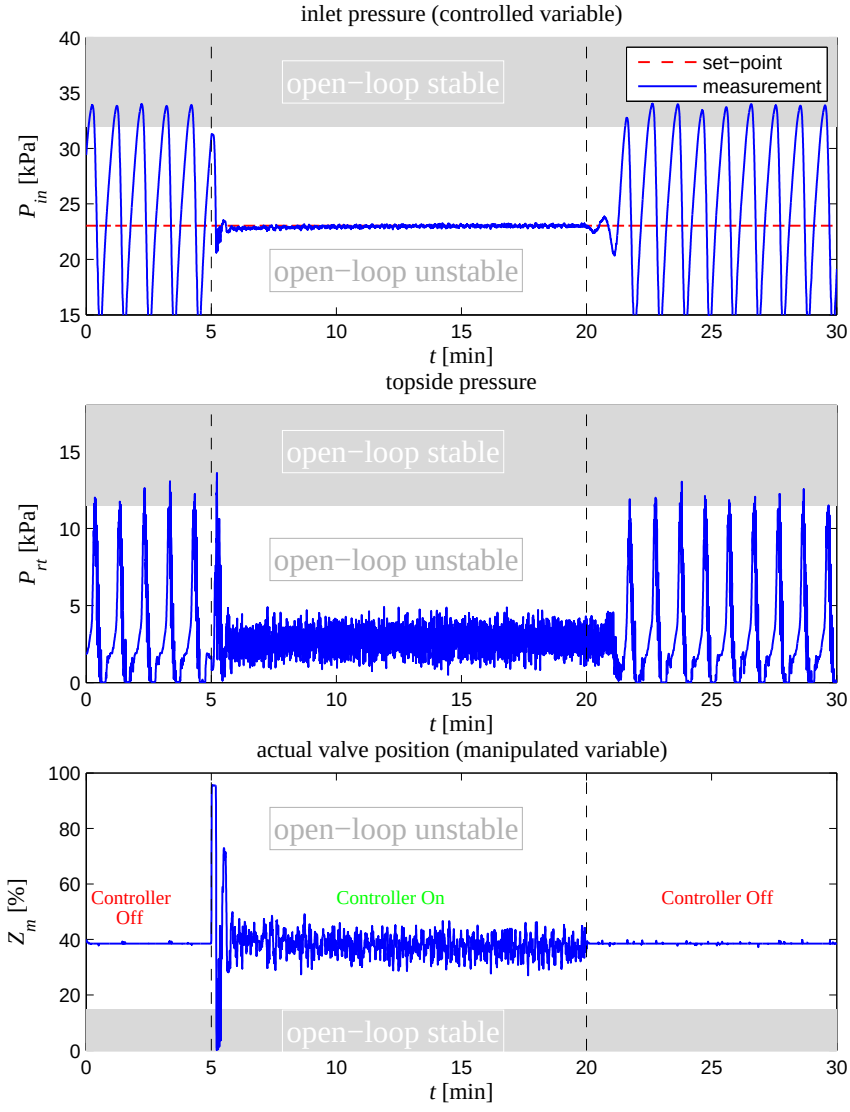

Figure 6.7: Control using subsea pressure measurement (P_{in}) and PI controller ($K_c = -10,\ T_i = 200sec$), $Z = 40\%$

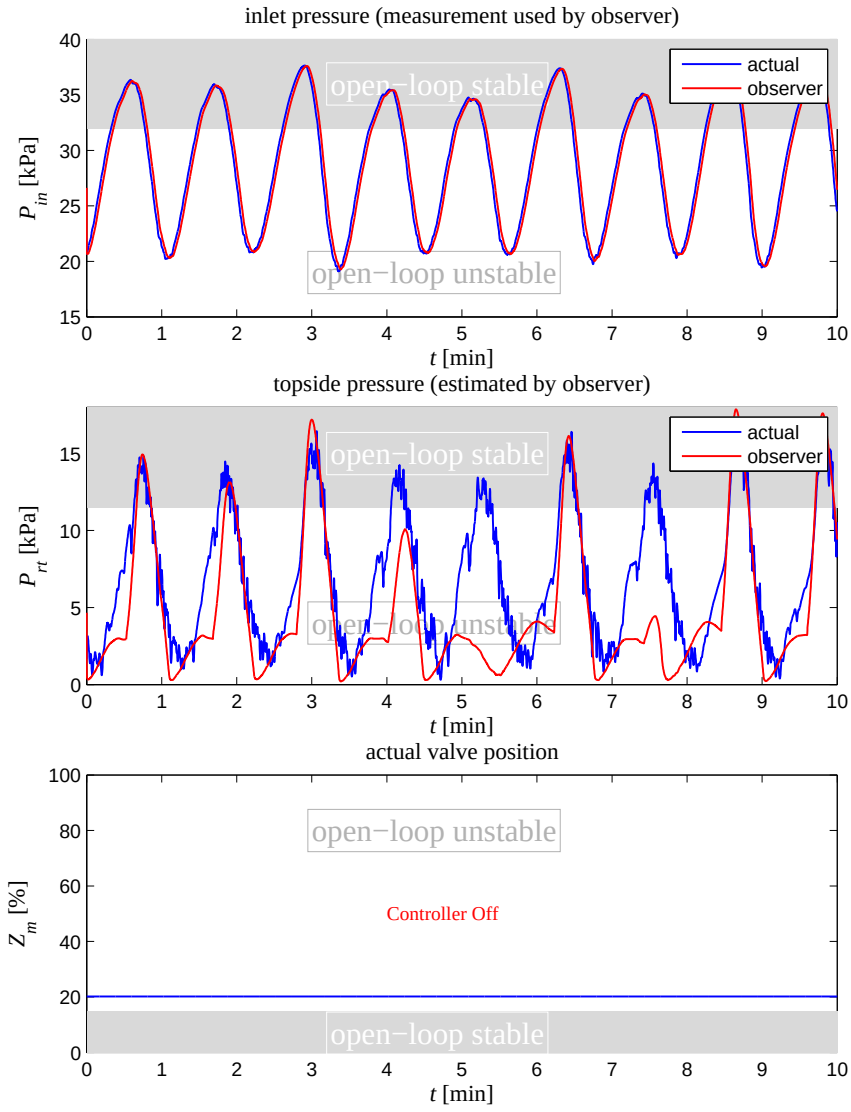

Figure 6.8: Open-loop estimation using High-Gain observer and measuring subsea pressure (P_{in}), $Z = 20\%$

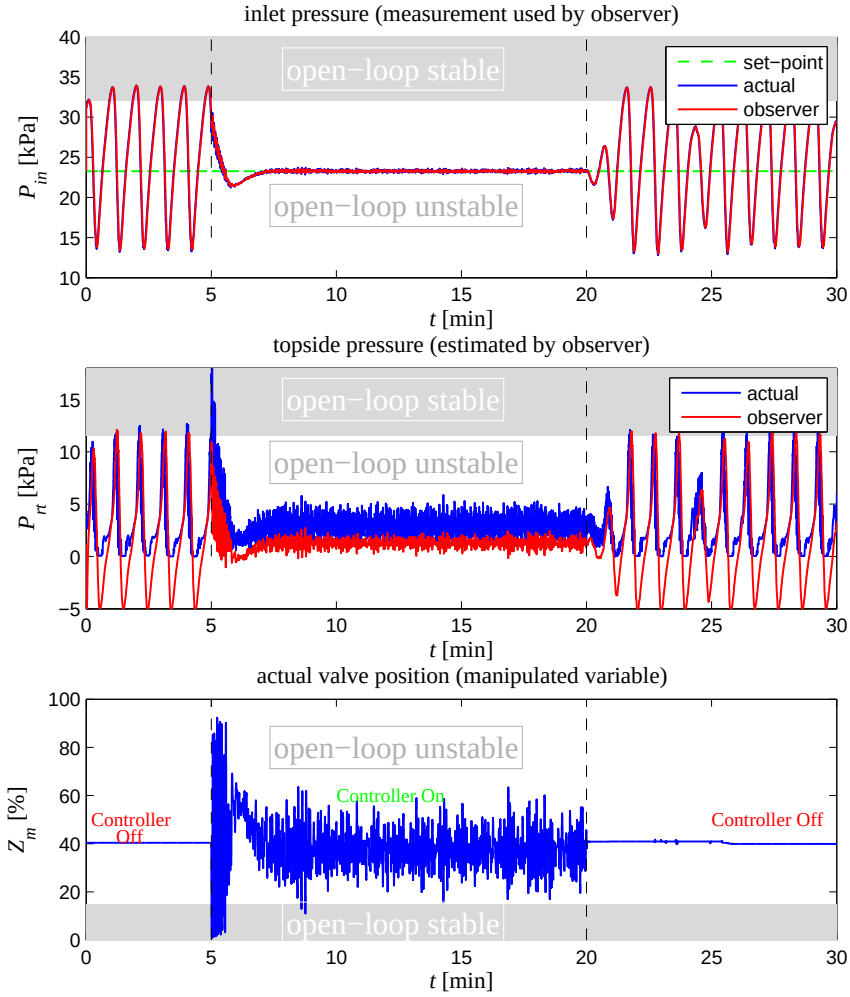

Figure 6.9: Control experiment with subsea pressure measurement (P_{in}) used by linear KF, $Z = 40\%$

6.2.4 Discussion

Measuring top-side pressure (P_{rt})

We failed to control the top-side pressure directly using a PI controller. Different tunings were used without any success. However, we could stabilize the system when we used the top-side pressure measurement to estimate the states using a fast nonlinear observer, and applied a linear state feedback. We make two hypotheses to explain this observation:

- The top-side pressure dynamics is highly nonlinear towards the valve
- The RHP-zero (inverse response) in top pressure dynamics limits the controllability

One or both of these two reasons can be correct. We tried to stabilize the system by using a fast linear observer, but it was not possible. This confirms that the first factor (nonlinearity effect) is important. The nonlinear observer counteracts the nonlinearity of the dynamics and the states are more linear towards the valve.

The unstable zero dynamics combined with unstable poles lead to high peaks of the sensitivity transfer functions and they impose a limitation on the controllability of the system. The minimum achievable peaks of sensitivity and complementary sensitivity transfer functions, denoted $M_{S,min}$ and $M_{T,min}$, respectively, are closely related to the distance between the unstable poles (p_i) and zeros (z_i). Considering SISO systems, for any unstable (RHP) zero z:

$$\|S\|_\infty \geq M_{S,min} = \prod_{i=1}^{N_p} \frac{|z + p_i|}{|z - p_i|}. \tag{6.16}$$

This bound for our system at the operating point $Z = 20\%$ with the top-side pressure as the output is 2.1, which is quite high signals fundamental problem related to stabilization. However, this bound does not consider how much fast control (bandwidth) is needed to stabilize the system. We

Table 6.3: State estimation using different observers

method \ measurement	subsea pressure	top pressure
fast linear observer	working	not working
fast nonlinear observer	not working	working
slow nonlinear observer	working	working

investigated this more closely using a $\mathcal{H}_\infty$ controller for control of the top-side pressure. We need a fast control action, with about 1 *sec* response time, to stabilize the system. When applying a bandwidth of 1 rad/sec in loop shaping specifications of the $\mathcal{H}_\infty$ controller, the peak of the sensitivity transfer function increases to 4. This is called the *water-bed effect*; if we push down the sensitivity transfer function in low frequencies, it will increase in other frequencies [74]. Furthermore, the minimum achievable peak of the sensitivity function increases to 7.0 for $Z = 40\%$. This means that the stabilization with larger valve openings becomes impossible.

Measuring subsea pressure (P_{in})

"Slow" nonlinear observers like the standard UKF can produce estimates of the top-side pressure and its related states when measuring the subsea pressure. However, when increasing the observer gain they fail. In contrary, the fast nonlinear observers work well when measuring the top-side pressure. what is the reason?

The structure of the model for the high-gain observer is in [51] introduced as a chain of integrators with the measured state is at the end of the chain (e.g. measuring the position and estimating velocity in mechanical systems). The high-gain observer behaves like a differentiator and the estimate is more accurate with a higher gain, similar to calculating derivative by finite difference by using smaller step [51].

If we consider the structure of the four-state model [34] with the topside pressure as a measurement, we indeed find a chain of integrators. The mass of gas in the riser, which is closely related to the top-pressure, is the integral of the gas flow rate at the riser-base, which is determined by the subsea pressure. Roughly speaking, the subsea pressure is related to derivative of the top-side pressure, and as a result, fast observer works very well by measuring the top pressure.

Table 6.4: Stabilizing control using different methods

method \ measurement	subsea pressure	top pressure
linear controller (PI, $\mathcal{H}_\infty$)	working	not working
fast linear observer	working	not working
fast nonlinear observer	not working	working
slow nonlinear observer	not robust	not robust
max. valve opening	40%	20%

On the other hand, by measuring the the subsea pressure, we have the opposite situations and we actually need to integrate the measured pressure to find the top-side pressure and the associated state variables. There are two problems arising in estimation by integration. First, for a good estimate we need a larger integration time; this is the reason for success of slow observers in estimation. The second problem is that it is very sensitive to modeling errors and disturbances. When an unknown model change or disturbance happens, the observer continues to integrate the wrong conditions, and finally it will fail as shown in Figure 6.8. In fact, even when we initialize the system in closed-loop to keep it always near the stationary point, it was not robust against disturbances in inflow conditions.

In the case of the linear observer, we assume the correct stationary point and we only deal with the deviations. Consequently, as shown in Figure 6.9, the estimation of the linear observer is less accurate, but it does not fail to stabilize the system.

6.3 Output Linearizing Controller

The *separation principle* does not hold for nonlinear systems in general, and the closed-loop observer/controller is not guaranteed to be stable for all conditions. In the previous Section, we showed that a nonlinear observer fails in closed-loop for the supposedly simple case where the subsea pressure is the measurement. On the other hand, the system could be stabilized only in a limited range ($Z = 20\%$) using a fast nonlinear observer and measuring the topside pressure. Here, we propose a nonlinear model-based controller by feedback linearization [38]. This controller directly uses the pressure at the riser-base (P_{rb}) and the pressure at the top of the riser (P_{rt}) as measurements, without using any observer.

6.3.1 Cascade system structure

In order to simplify the system analysis, we separate it into two subsystems and analyze the individual subsystems and their interconnecting relationships. As illustrated in Fig. 6.10, the input to the "Riser" subsystem (Σ_2) is the choke valve opening, $u = Z$, and the output is the pressure at the riser-base, P_{rb}, which is also the input to the "Pipeline" subsystem (Σ_1).

6.3.2 Stability analysis of cascade system

Apart from the riser-slugging, other phenomena may lead to the flow instability in pipeline-riser systems. The pipeline-riser system may have an

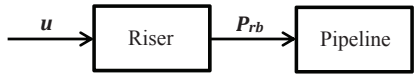

Figure 6.10: Pipeline-riser system as a cascaded connection of two subsystems

unstable oil well as the inlet boundary, also the density-wave instability can happen in long risers. Here, we consider only the riser-slugging instability and we state the following hypothesis about the "Pipeline" subsystem:

Hypothesis 1. If riser-slugging is the destabilizing dynamics of the pipeline-riser system, then the "Pipeline" subsystem with the riser-base pressure, P_{rb}, as its input is"input-to-state stable".

We investigate the input-to-state stability of the pipeline subsystem by a simulation test as shown in Fig. 6.11. The riser-base pressure in this simulation is 19.7 kPa. This pressure is corresponding to 50% opening of the top-side valve for which the pipeline-riser system is unstable. However, the pipeline subsystem separated from the riser is always stable. In addition, the local exponential stability of the Pipeline" subsystem can be verified by looking at eigenvalues. The above hypothesis is reasonably correct, because the riser-base pressure is a recommended candidate controlled variable to stabilize the system [40]. This means when the riser-base pressure has small variations, the whole system becomes stabilized which follows $\mathcal{L}_2$-gain stability from P_{rb} to state variables of the pipeline subsystem.

We can now state the following proposition:
Proposition 1. Let hypothesis 1 hold. If the Riser subsystem becomes globally asymptotically stable under a stabilizing feedback control, then the pipeline-riser system is globally asymptotically stable.

Proof: We use conditions for stability of cascaded systems as stated by *Corollary 10.5.3* in [33]. As shown in Fig. 6.12, if Σ_1 is input-to-state stable (ISS) and origin of Σ_2 is globally asymptotically stable (GAS), then origin of the cascaded system Σ_1 and Σ_2 is globally asymptotically stable (GAS). Therefore, if *Hypothesis 1* holds, the proposition is verified.

□

It is not possible to achieve GAS for the riser subsystem due to controllability limitations and other physical limits of the system. Instead, we show partial stabilization with respect to the output that enters the pipeline subsystem, P_{rb}, on a set $\mathcal{D}$ which is the physical domain of the system.

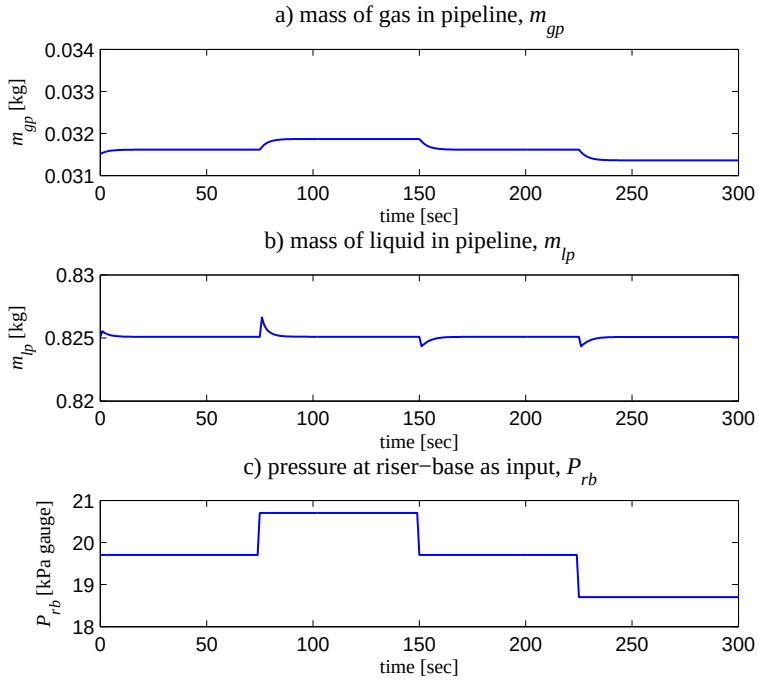

Figure 6.11: Simulation test of pipeline subsystem

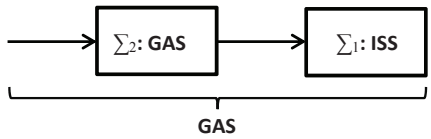

Figure 6.12: Stability of a cascaded system

6.3.3 Stabilizing Feedback Control

We use feedback linearization to design a control law. For simplicity, the outlet mass flow rate, w, is used as a virtual control input. First, we transform the state equations and write a model in 'normal form' based on the two measurements, the pressure at the riser-base (P_{rb}) and the pressure at top of the riser (P_{rt}).

Transforming state equations

Two state variables govern the dynamics of the Riser subsystem (Σ_2). We start with writing the model in the new coordinates $(x_3, x_4) = (m_{gr}, m_{lr} + m_{gr})$. We get the following system:

$$\dot{x}_3 = w_g - \alpha w \tag{6.17}$$

$$\dot{x}_4 = w_g + w_l - w \tag{6.18}$$

The two measurements are $y_1 = P_{rb}$ and $y_2 = P_{rt}$. From the ideal gas law we get

$$y_2 = \frac{a x_3}{b + x_3 - x_4}, \tag{6.19}$$

where $a = RT_r\rho_l/M_G$ and $b = \rho_l V_r$ are model parameters [34]. The pressure drop over the riser is the sum of the hydrostatic head and the friction term:

$$y_1 = y_2 + cx_4 + F_r, \tag{6.20}$$

where $c = gL_r/V_r$ and F_r is the friction in the riser that depends on constant inflow rates and other constant parameters. Differentiating and rearranging the equations gives the system equations in y coordinates.

$$\dot{y}_1 = (w_g + w_l)\left[F(y) + c\right] - \left[F(y) + c\right] w \tag{6.21}$$

$$\dot{y}_2 = (w_g + w_l)F(y) - F(y)w, \tag{6.22}$$

where

$$F(y) = c\left(1 - \frac{y_2}{a}\right)\frac{a\alpha + y_2(1-\alpha)}{bc - (y_1 - y_2 - F_r)}. \tag{6.23}$$

Since $\rho_l > \rho_g$, we have that $a > y_2$. In addition, $bc = \rho_l g L_r$ is the hydrostatic pressure when the riser is full of liquid which is larger than the gravity term in normal operation $(y_1 - y_2 - F_r)$. Thus, the physical domain of the system outputs is defined as follows:

$$\mathcal{D} = \{(y_1, y_2) | y_2 + bc + F_r > y_1 > y_2 > 0\}. \tag{6.24}$$

The numerator in equation (6.23) is always positive, therefore, $F(y) > 0, \forall (y_1, y_2) \in \mathcal{D}$. In addition, it can be shown that $F(y)$ is strictly increasing in y_1 and strictly decreasing in y_2.

The transformation $T : \mathcal{S} \to \mathcal{D},\ y = T(x)$ in (6.19) and (6.20) where $y = (y_1, y_2)^T$, $x = (x_3, x_4)^T$ and

$$T(x) = \begin{bmatrix} \frac{ax_3}{b+x_3-x_4} + cx_4 + F_r \\ \frac{ax_3}{b+x_3-x_4} \end{bmatrix} \tag{6.25}$$

is a diffeomorphism on $\mathcal{S} = \{(x_3, x_4) | x_3 > 0, x_4 - x_3 < b\}$, because both $T(x)$ and $T^{-1}(y)$ exist and are continuously differentiable. $b = \rho_l V_r$ is the mass of a volume of liquid equal to volume of the riser, hence $b > m_{lr} = x_4 - x_3$ in the normal operation of the system where $x_3 > 0$.

For simplicity we will use the following assumption:
Assumption 1. The gas mass fraction in the riser, α, is given by the constant inflow rates of the gas and the liquid:

$$\alpha = \frac{w_{g,in}}{w_{g,in} + w_{l,in}}. \tag{6.26}$$

This particularly holds exactly at steady state, but dynamically it is a simplification.

Partial input-output linearization

With $\xi = y_1 - \bar{y}_1$ (riser-base pressure) and $\eta = y_2 - \bar{y}_2$ (topside pressure), where $\bar{y}_1$ and $\bar{y}_2$ are steady-state values, we can write the system in normal form:

$$\dot{\xi} = (w_g + w_l)\left[F(\xi, \eta) + c\right] - \left[F(\xi, \eta) + c\right] w \tag{6.27}$$

$$\dot{\eta} = (w_g + w_l)F(\xi, \eta) - F(\xi, \eta)w, \tag{6.28}$$

The feedback controller

$$w = \frac{-1}{F(\xi, \eta) + c}\left(-(w_g + w_l)\left[F(\xi, \eta) + c\right] + v\right) \tag{6.29}$$

reduces equation (6.27) to $\dot{\xi} = v$ and choosing $v = -K_1\xi$ gives

$$\dot{\xi} = -K_1\xi, \tag{6.30}$$

where $K_1 > 0$ results in *exponential stability* of the ξ dynamics. By inserting the control law (6.29) into (6.28) we get

$$\dot{\eta} = \frac{F(\xi, \eta)}{F(\xi, \eta) + c} v = -\mathcal{F} K_1 \xi, \tag{6.31}$$

where

$$0 < \underline{\mathcal{F}} < \mathcal{F} = \frac{F(\xi,\eta)}{F(\xi,\eta)+c} < \overline{\mathcal{F}} < 1. \tag{6.32}$$

Since $0 < \mathcal{F} < 1$ and $\xi \to 0$ known as exponentially fast, η will therefore remain bounded. This is partial exponential stabilization of the system with respects to the riser-base pressure ξ [81].

□

Assumption 2. In order to make the control law realizable, we replace $w_g + w_l$ by inflow rates to the system, $w_{g,in} + w_{l,in} = w_{in}$, such that

$$w = \frac{w_{in}(F(y)+c) + K_1(y_1 - \bar{y}_1)}{F(y)+c} \tag{6.33}$$

The final control signal to the valve is

$$u = \text{sat}\left(\frac{w}{C_v\sqrt{\rho_{rt}(y_2 - P_s)}}\right), \tag{6.34}$$

where C_v and P_s are the choke valve constant and the separator pressure, respectively. The riser friction F_r and the density ρ_{rt} are calculated based on the two pressure measurements y_1 and y_2 and model parameters (see Appendix D).

We can also design a control law that linearizes equation (6.28). Although we are using both y_1 and y_2 for $F(y)$ in (6.28), we use only y_2, the topside pressure, for feedback in the linear part of the controller. The resulting controller is

$$w = \frac{1}{F(y)}\left(w_{in}F(y) + K_2(y_2 - \bar{y}_2)\right), \tag{6.35}$$

and the η-dynamics are exponentially stable. The final control signal to the valve is same as equation (6.34). However, for feedback linearization we need the system to be *minimum phase*, but the linearized 4-state model constitutes two *Right-Half-Plane zeros* from the valve position (input) to the top-side pressure (output) [40]. Although we cannot prove stability of the system using the controller in (6.35), we will try it in experiments.

Stability of composite system

After designing a stabilizing feedback control for the "Riser" subsystem using feedback linearization, we consider the complete pipeline-riser system as a partially linear composite system,

$$\dot{x} = f(x,\xi),\ x \in \mathbb{R}^2,\ \xi \in \mathcal{D} \tag{6.36}$$

$$\dot{\xi} = -K_1 \xi, \tag{6.37}$$

where $f(x, \xi)$ represents dynamics of the "Pipeline" subsystem. We can check the conditions for stabilization of the composite system as stated by [64] and [42]:

"A linear controllable nonlinear asymptotically stable cascade system is globally stabilizable by smooth dynamic state feedback if (a) the linear subsystem is right invertible and weakly minimum phase, (b) the only variables entering the nonlinear subsystem are the outputs and the zero dynamics corresponding to this output."

We use *Hypothesis 1* for stability of the nonlinear (pipeline) subsystem. The two conditions (a) and (b) are satisfied when using the pressure at the riser-base as the output. The riser-base pressure is minimum-phase and it is the output which enters the nonlinear subsystem as shown in Fig. 6.10. Therefore, the composite system is *stabilizable* on the domain $\mathcal{D}$ by using the riser-base pressure as the controlled output. However, the top-side pressure is not minimum-phase and this output does not enter the nonlinear subsystem.

6.3.4 Analogy with conventional cascade control

The proposed control law is very similar to a conventional cascade controller that uses a flow controller as its inner loop and a pressure controller as the outer loop [74]. The control law in equation (6.33) is a nonlinear pressure controller that specifies the set-point of the flow rate. In addition, equation (6.34) determines the valve opening based on the flow rate. Flow controllers are also used in conventional cascaded controllers to remove nonlinearities of the valve. However, the difference is that we do not use any flow measurement, instead the model estimates the flow rate from the two pressure measurements. The virtual control signal w can be considered as an estimate of the flow rate.

6.3.5 Experimental Results

The two pressure measurements at the riser-base and at top of the riser are very noisy because of air bubbles and hydrodynamic slugs which have much faster dynamics than the severe-slugging dynamics. In order to reduce the noise effect on the control signal (input), we used a second-order low-pass filter. The experimental result using the riser-base pressure for feedback-linearization with a valve opening $Z = 30\%$ is shown in Fig. 6.13. The low-pass filter was used for this case and the system could be stabilized without much noise effect.

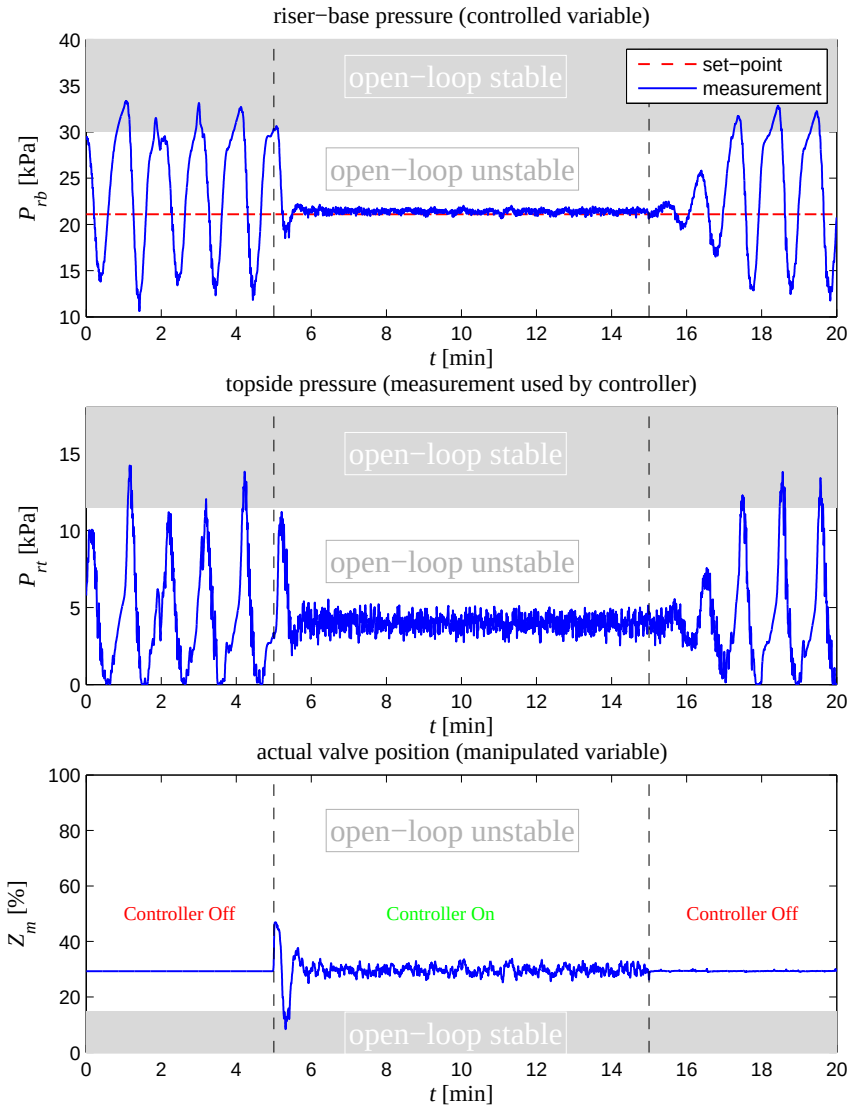

Figure 6.13: Experimental result of using riser-base pressure (P_{rp}) for feedback linearization, $Z = 30\%$

It is desirable to open the top-side choke valve as much as possible to get the maximum production. For example, one experiment was performed with a valve opening $Z = 60\%$ as shown Fig. 6.14. We did not need to re-tune the controller; the control law generates a larger proportional gain to stabilize the system. On the other hand, the low-pass filter adds a time-lag to the control loop, and it limits the controllability. The extra time-lag from the low-pass filter destabilises the closed-loop system when using the large control gain. Therefore, we can not filter out the noise completely; we should keep the system stable in expense of accepting a noisy input signal.

In order to avoid the noise effect, we could use the buffer tank pressure instead of the riser-base pressure. There are no bubbles in the buffer tank and its pressure is very close to the riser-base pressure. Indeed, although the controller law was designed for the riser-base pressure, it works very well using the buffer-tank pressure and with less noise effect as shown in Fig. 6.15.

We could stabilize the system using the controller in (6.35) which has the top-side pressure in the linear part. The maximum achievable valve opening for this case as illustrated in Fig. 6.16 is 20%. This result is same as using a nonlinear observer and state feedback [37].

For comparison, we carried out some experiment using PI controller. First, we considered using pressure drop of the riser $(y_1 - y_2)$ which is the most simple combination of the two pressure measurements we used for feedback-linearizing controller. The pressure drop over the riser was also recommended by [15] as the best control solution. As shown in Fig. 6.17, although the pressure drop over the riser is tightly controlled, both the riser-base pressure and the top-side pressure drift away in the same direction.

Next, we used the riser-base pressure as the controlled variable of PI controller for two valve openings of 30% and 50%. The results are given in Fig. 6.18 and Fig. 6.19 respectively. However, we needed to re-tune the PI controller for the second valve opening, and K_c was changed from -10 to -20.

6.3.6 Controllability Limitations

When using the riser-base pressure for feedback linearization the controller counteracts the nonlinearity of the system and we are able to stabilize the system for very large valve openings. The only limitation regarding the riser-base pressure is that with large valve openings the gain of the system decreases drastically and the controller generates a very large proportional gain to stabilize the system. In this situation, the controller can not differentiate between noises and the unstable dynamics. The controller amplified

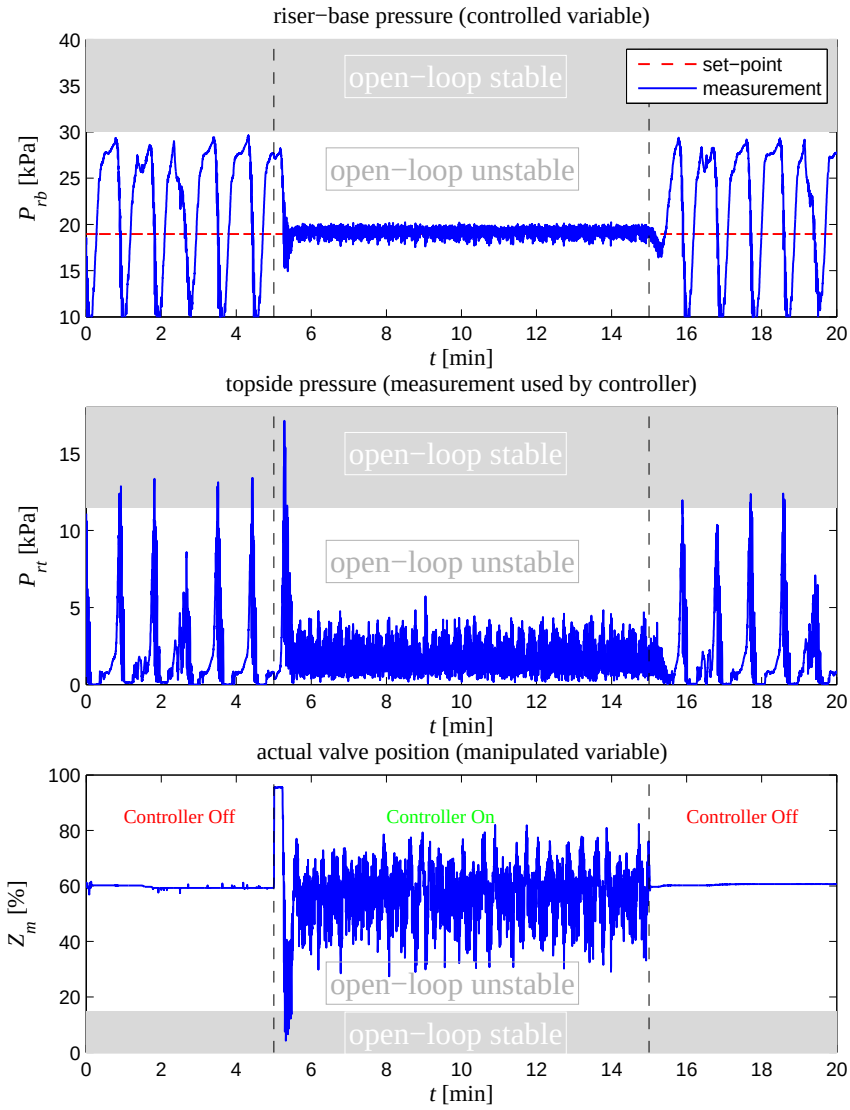

Figure 6.14: Experimental result of using riser-base pressure (P_{rb}) for feedback linearization, $Z = 60\%$

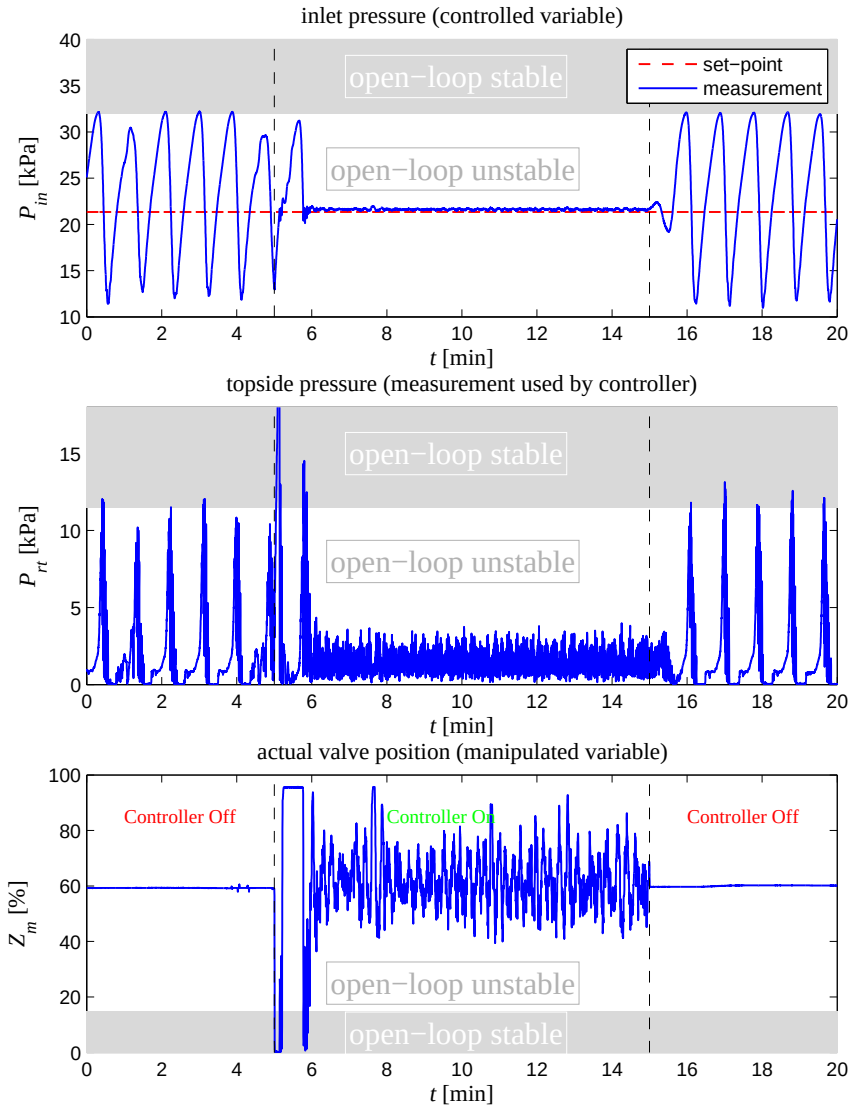

Figure 6.15: Experimental result of using buffer tank pressure (P_{in}) for feedback linearization, $Z = 60\%$

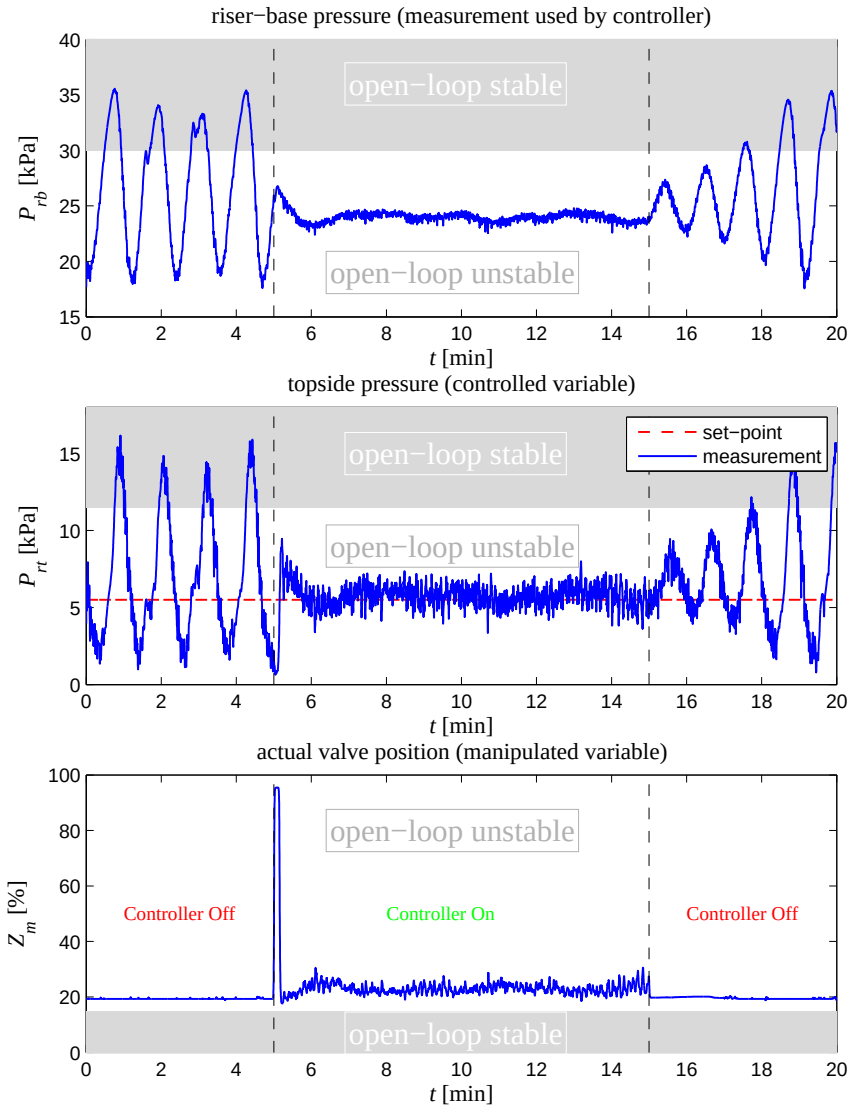

Figure 6.16: Experimental result of using top-side pressure (P_{rt}) for feedback linearization, $Z = 20\%$

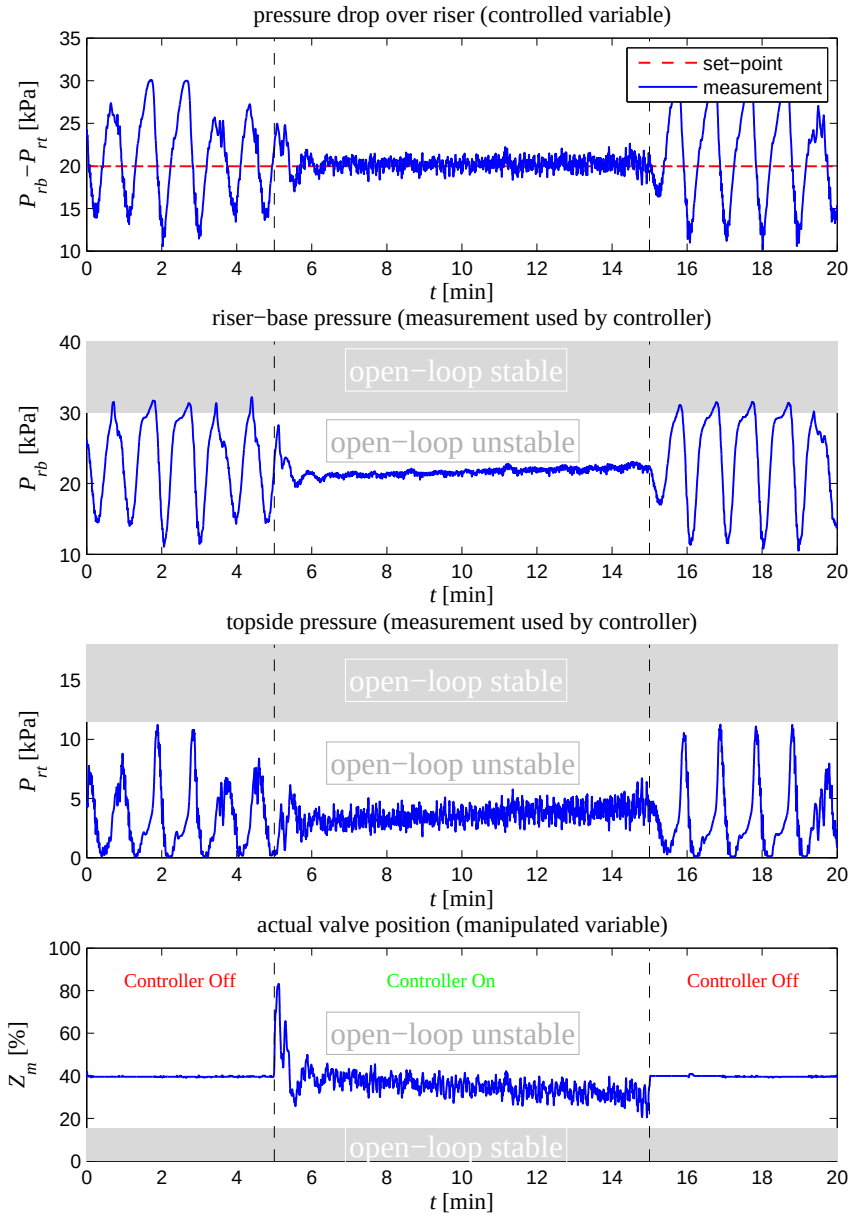

Figure 6.17: Experimental result of using pressure drop over riser ($P_{rb} - P_{rt}$) as controlled variable of a PI controller with $K_c = -5$, $T_i = 120\ s$, $Z = 40\%$

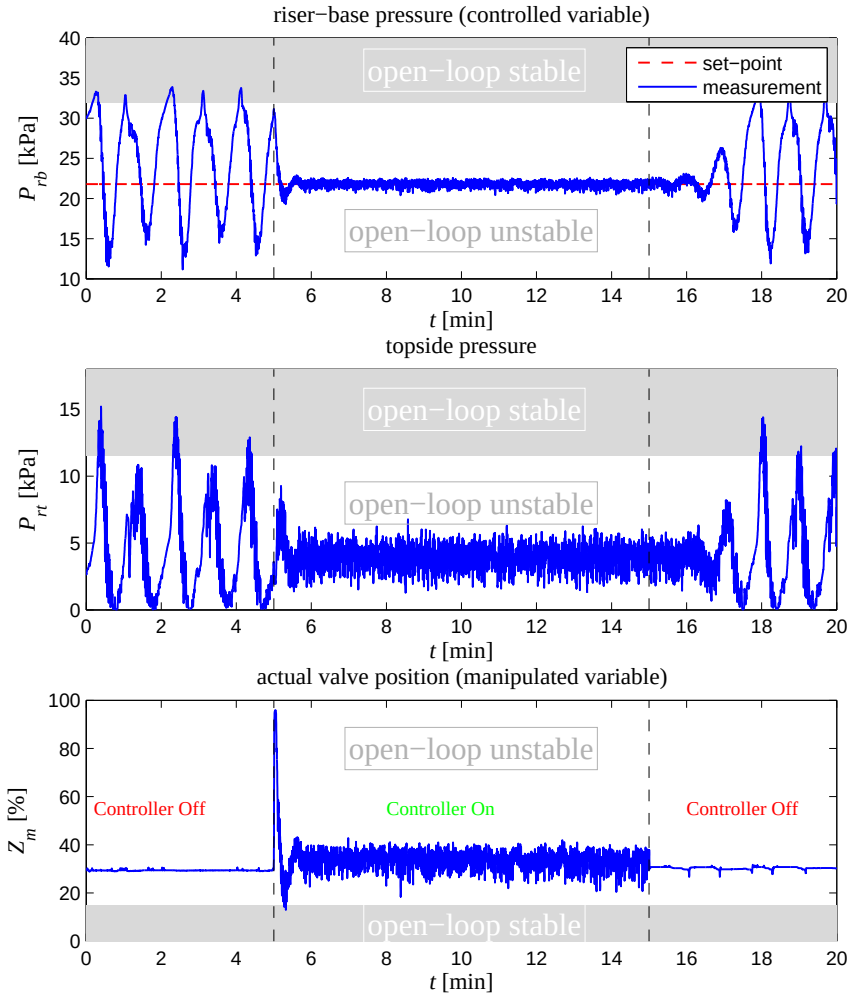

Figure 6.18: Experimental result of using riser base pressure (P_{rb}) as controlled variable of a PI controller with $K_c = -10$, $T_i = 120\ s$, $Z = 30\%$

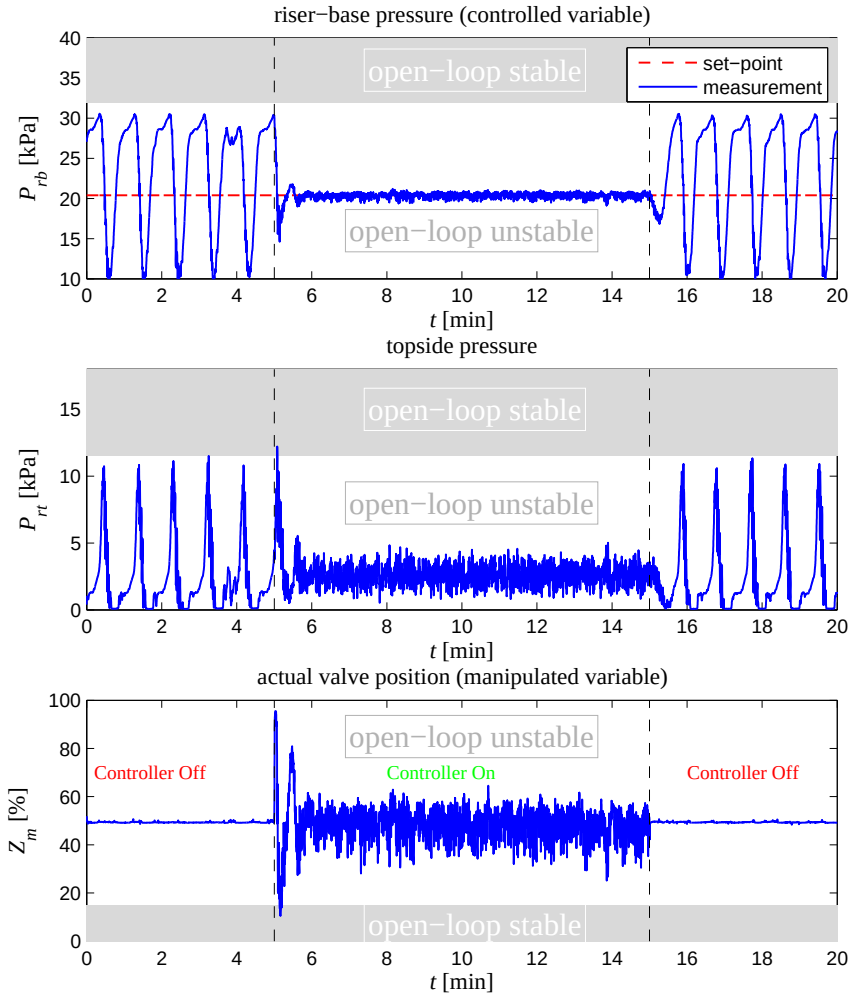

Figure 6.19: Experimental result of using riser base pressure (P_{rb}) as controlled variable of a PI controller with $K_c = -20$, $T_i = 120\ s$, $Z = 50\%$

the noises and the control signal is very aggressive as shown in Fig. 6.14. One problem is how fast our valve can follow the control command signal, another problem is saturation of the valve.

By using the top-side pressure, linear controllers (PID, LQG, $\mathcal{H}_{\text{inf}}$) are not able to stabilize the system, but the nonlinear control law based on feedback linearization could stabilize the system. However, we could stabilize the system using the top-pressure in a very limited range (20% valve opening). Although the nonlinear controller law can counteract the nonlinearity, the fundamental limitations regarding the *non-minimum phase* dynamics [74] are still in place.

6.3.7 Remarks on output-linearizing controller

A nonlinear model-based output-linearizing controller was proposed for anti-slug control. The proof of convergence was shown in theory and experiments. The controller was able to stabilize the system up to very large valve openings without re-tuning.

The advantage of the proposed controller over the previous works is that it directly uses two pressure measurements at the riser-base and at the riser top, not the state variable. We do not have to deal with observers and hope for the *the separation principle* to be applicable.

Furthermore, we showed that there are controllability limitations for the system when using the riser-base pressure and the top pressure for the feedback linearization design. The fundamental limitation related to using the riser-base pressure is the small gain of the system with large valve openings. In addition to nonlinearity, the top-side pressure has still the limitation regarding *non-minimum phase* dynamics which can not be bypassed by any control solution.

6.4 PI Tuning Considering Nonlinearity

Here, we consider a PI controller and change the PI tuning values at different operating points to counteract the linearity of the system. This can be implemented as a gain-scheduling controller or an adaptive controller. The gain-scheduling or adaptation is based on the static gain of the system and the average valve opening.

6.4.1 Simple model for static nonlinearity

The middle line in the bifurcations diagrams (Figure 6.3) represents the desired non-slug flow. The slope of this line ($\frac{\partial y}{\partial u} = \frac{\partial P}{\partial Z}$) represents the

process gain. We found that this curve is mostly related to valve properties. We assume the valve equation as the following:

$$w = C_v f(z)\sqrt{\rho \Delta P} \tag{6.38}$$

where $w[kg/s]$ is the outlet mass flow and $\Delta P[N/m^2]$ is the pressure drop. From the valve equation, the pressure drop over the valve for different valve openings can be written as

$$\Delta P = \frac{\bar{a}}{f(z)^2}, \tag{6.39}$$

where we assume $\bar{a}$ as a constant parameter calculated in Appendix C. Our simple empirical model for the inlet pressure is as follows:

$$P_{in} = \frac{\bar{a}}{f(z)^2} + \bar{P}_{fo} \tag{6.40}$$

Where $\bar{P}_{fo}$ is another constant parameter that is the inlet pressure when the valve is fully open, and it is given in Appendix C. By differentiating (6.40) with respect to z, we get the static gain of the system as a function of valve opening.

$$k(z) = \frac{-2\bar{a}\frac{\partial f(z)}{z}}{f(z)^3} \tag{6.41}$$

For a linear valve (i.e. $f(z) = z$) it reduces to

$$k(z) = \frac{-2\bar{a}}{z^3}, \tag{6.42}$$

where $0 \leq z \leq 1$. Figure 6.20 compares the simple static model in (6.40) and (6.41) to the Olga model.

6.4.2 PI tuning rules based on static model

The PID and PI tuning rules given in Chapter 5 are based on a linear model identified at a certain operating point. However, as we see in Figure 6.20, the gain of the system changes drastically with the valve opening. Hence, a controller working at one operating point may not work at other operating points.

One solution is gain-scheduling with multiple linear controllers based on multiple identified models that we will use in the next Section. Here, we propose simple PI tuning rules based on a single step test. We apply a gain correction to counteract the nonlinearity of the system. For this, we use the

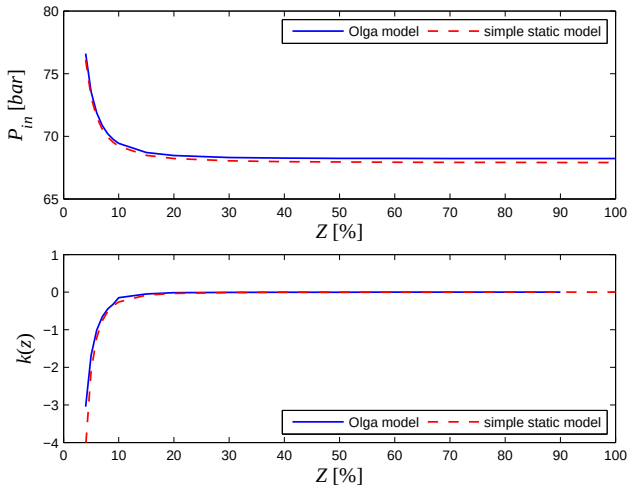

Figure 6.20: Simple static model compared to OLGA case

static model given in (6.41) and the data from a closed-loop step test as in Figure 6.21. We calculate the following constant:

$$\beta = \frac{-\ln\left(\frac{\Delta y_\infty - \Delta y_u}{\Delta y_p - \Delta y_\infty}\right)}{2\Delta t} + \frac{K_{c0}k(z_0)\left(\frac{\Delta y_p - \Delta y_\infty}{\Delta y_\infty}\right)^2}{4t_p}, \tag{6.43}$$

where z_0 is the average valve opening in the closed-loop step test and K_{c0} is the proportional gain used for the test. The PI tuning values as functions of valve opening are given as the following:

$$K_c(z) = \frac{\beta T_{osc}}{k(z)\sqrt{z/z^*}} \tag{6.44}$$

$$\tau_I(z) = 3T_{osc}(z/z^*) \tag{6.45}$$

Where T_{osc} is the period of slugging oscillations when the system is open-loop and z^* is the critical valve opening of the system (at the bifurcation point).

6.4.3 Experimental result

First, we performed a closed-loop step test at $Z = 20\%(z_0 = 0.2)$ where the pressure set-point is 26 kPa. We closed the loop by a proportional controller $K_{c0} = -10$ and changed the set-point by 2 kPa (Figure 6.21). We calculated

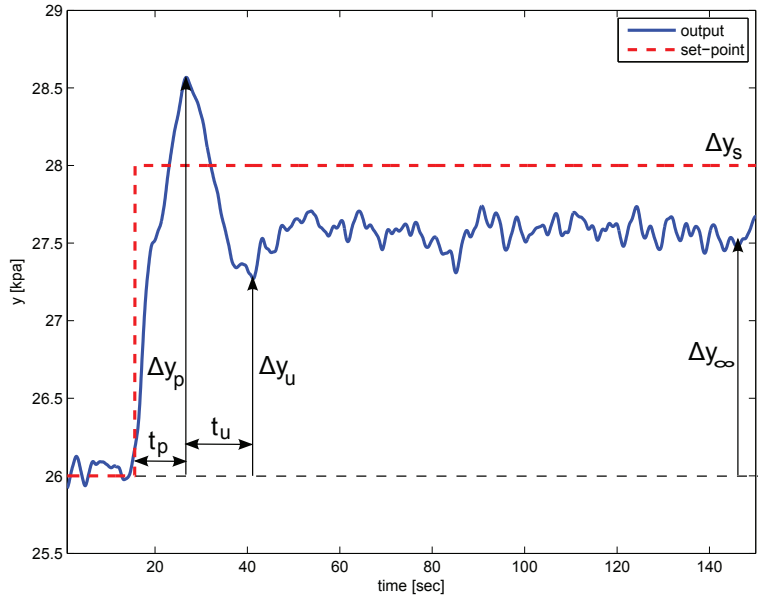

Figure 6.21: Closed-loop step response for stabilized experimental system

$\beta = 0.061$ from (6.43) using the step test information taken from Figure 6.21. The period of the slugging oscillations in open-loop was $T_{osc} = 68$ *sec*. We used the PI tuning given in (6.44) and (6.45) in an adaptive manner to control the system. The valve opening had many variations and it could be used directly; a low-pass filter was used to make it smooth. The result of control using this tuning is shown in Figure 6.22. The controller gains are given in Figure 6.23. This simple adaptive controller could stabilize the system from $Z = 20\%$ to $Z = 50\%$, and it was stable even with $1sec$ added time delay. It can stabilize the system up to $Z = 60\%$ when no time delay is added.

6.4.4 Olga Simulation

Here, we test the PI tuning rules in (6.44) and (6.45) as a gain-scheduling on the Olga case presented in Section 2.3.1. The PI tuning values are given in Table 6.5 and the simulation result is shown in Figure 6.24. The open-loop system switches to slugging flow at 5% valve opening, but by using the proposed PI tuning, the system could be stabilized up to 23.24% valve opening.

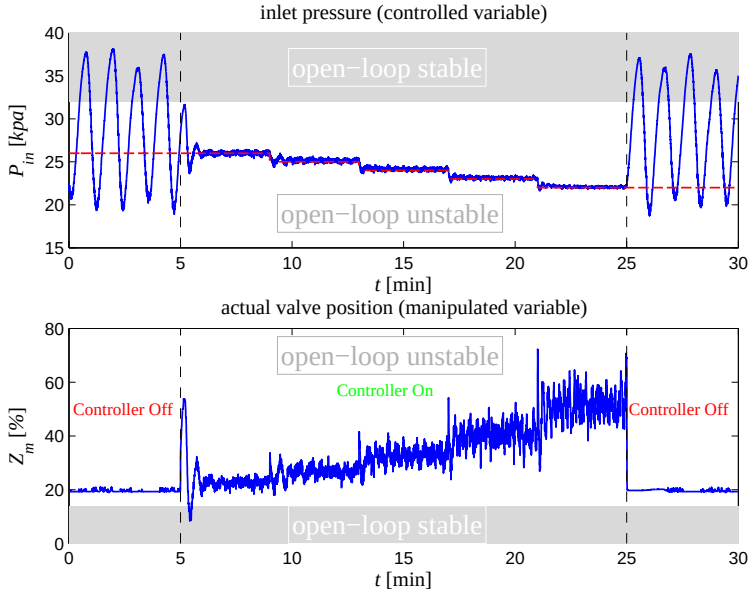

Figure 6.22: Result of control using adaptive PI tuning in experiment 3

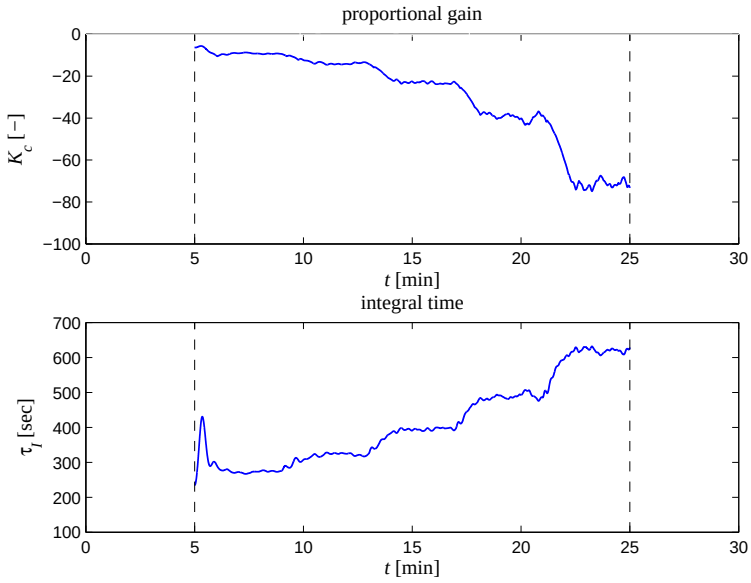

Figure 6.23: Controller gains resulted from adaptive PI tuning in experiment 3

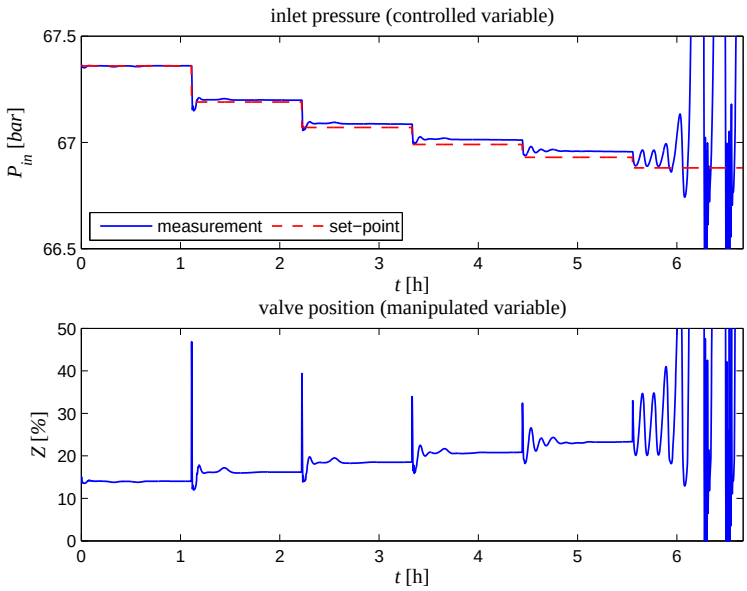

Figure 6.24: Result of control from Olga simulation

6.5 Gain-Scheduling IMC

In Section 6.3, we applied feedback linearization for anti-slug control. However, the feedback linearization design is not robust against modeling errors, since the nonlinearities of the system must be perfectly known in order to cancel them.

An alternative approach in which the mechanistic model is not directly used for the control design is to identify an unstable model of the system by a closed-loop step test. We use the subsea pressure measurement as the

Table 6.5: PI tuning values in Olga simulation

set-point	valve opening	K_c	τ_I
67.36	14	0.5	8400
67.19	16.1	0.7	9600
67.07	18.2	0.94	10800
66.99	20.1	1.23	12000
66.93	23.24	1.56	13200
66.88	–	1.93	14400

controlled output, and the identified model contains two unstable poles and one stable zero.

$$G(s) = \frac{\hat{b}_1 s + \hat{b}_0}{s^2 - \hat{a}_1 s + \hat{a}_0} = \frac{k'(s+\varphi)}{(s-\pi_1)(s-\pi_2)} \tag{6.46}$$

We use the identified model for an IMC (Internal Model Control) design [58]. The feedback version of the IMC controller is in the following form.

$$C(s) = \frac{[\frac{1}{k'\lambda^3}](\alpha_2 s^2 + \alpha_1 s + 1)}{s(s+\varphi)}. \tag{6.47}$$

Where λ is an adjustable filter time-constant. The filter coefficients α_1 and α_2 are calculated by solving the following system of linear equations:

$$\begin{pmatrix} {\pi_1}^2 & \pi_1 & 1 \\ {\pi_2}^2 & \pi_2 & 1 \end{pmatrix} \begin{pmatrix} \alpha_2 \\ \alpha_1 \\ \alpha_0 \end{pmatrix} = \begin{pmatrix} (\lambda\pi_1 + 1)^3 \\ (\lambda\pi_2 + 1)^3 \end{pmatrix} \tag{6.48}$$

Where we choose $\alpha_0 = 1$ to get an integral action in the controller. The closed-loop model identification and the IMC design for the slugging flow system have been presented in Chapter 5 in more details.

Here, we identify three linear models from step tests at three different operating points, $Z = 20\%$, $Z = 30\%$ and $Z = 40\%$, respectively,

$$G_1(s) = \frac{-0.015(\mathrm{s} + 0.26)}{s^2 - 0.045s + 0.0094}, \tag{6.49}$$

$$G_2(s) = \frac{-0.0098(\mathrm{s} + 0.25)}{s^2 - 0.040s + 0.025}, \tag{6.50}$$

$$G_3(s) = \frac{-0.0056(\mathrm{s} + 0.27)}{s^2 - 0.017s + 0.096}. \tag{6.51}$$

Then, we design three IMC controllers to cover operation range of the non-linear system for small, medium and large valve openings.

$$C_1(s) = \frac{-16.15(s^2 + 0.016s + 0.0012)}{\mathrm{s}(\mathrm{s} + 0.26)} \tag{6.52}$$

$$C_2(s) = \frac{-42.20(s^2 + 0.052s + 0.0047)}{\mathrm{s}(\mathrm{s} + 0.25)} \tag{6.53}$$

$$C_3(s) = \frac{-115.11(s^2 + 0.052s + 0.014)}{\mathrm{s}(\mathrm{s} + 0.27)} \tag{6.54}$$

Switching (gain-scheduling) between the three controllers is based on the pressure set-point as given in Table 6.6, and bump-less transfers between controllers are considered.

Table 6.6: Gain-scheduling logic

Pressure set-point	Controller
$P_{set} \geq 24\ kPa$	$C_1(s)$
$24\ kPa > P_{set} > 21.5\ kPa$	$C_2(s)$
$P_{set} \leq 21.5\ kPa$	$C_3(s)$

6.6 Comparing Four Nonlinear Controllers

We compare the four nonlinear controllers presented in the previous sections experimentally. All the experiments are performed on set of descending pressure set-points to observe where the system becomes unstable. A lower pressure set-point which gives a larger valve opening is desirable, but it is more difficult to control. To test the robustness of the controllers, we repeated each experiments for three different values of time delay 1 *sec*, 2 *sec* and 3 *sec*, but we do not show results for 1 *sec* time-day because of space limitation.

Figure 6.25 shows result of using the state-feedback/nonlinear observer scheme for control. It can stabilize the system up to 28% valve opening. However, with 2 *sec* time delay, as in Figure 6.26, it is stable only up to 22% valve opening.

The observer/state-feedback scheme can stabilize the system only when using the top-side pressure P_{rt} as the measurement for the observer, since a high-gain observer diverges when using the subsea pressure P_{in} as the measurement (see Figure 6.8). The reason for this has been explained in Section 6.2.4.

Figure 6.27 shows the experimental result of the adaptive PI controller with 2 *sec* time delay. This controller was able to stabilize the system up to $Z = 60\%$ when no time delay was added, and $Z = 32\%$ with 2 *sec* added time delay.

Figure 6.28 shows result of using the feedback linearization controller. With no time delay, it stabilizes the system up to 60% valve opening. However, with 2 *sec* time delay, as in Figure 6.29, it is stable only up to 25% valve opening.

Figure 6.30 shows result of applying gain scheduling IMC. This scheme stabilizes the system up to 60% valve opening, and even with 2 *sec* time delay (Figure 6.31), it is stable up to 50% valve opening.

Table 6.7 shows the maximum valve opening achieved by using the four controllers with different values of time-delay.

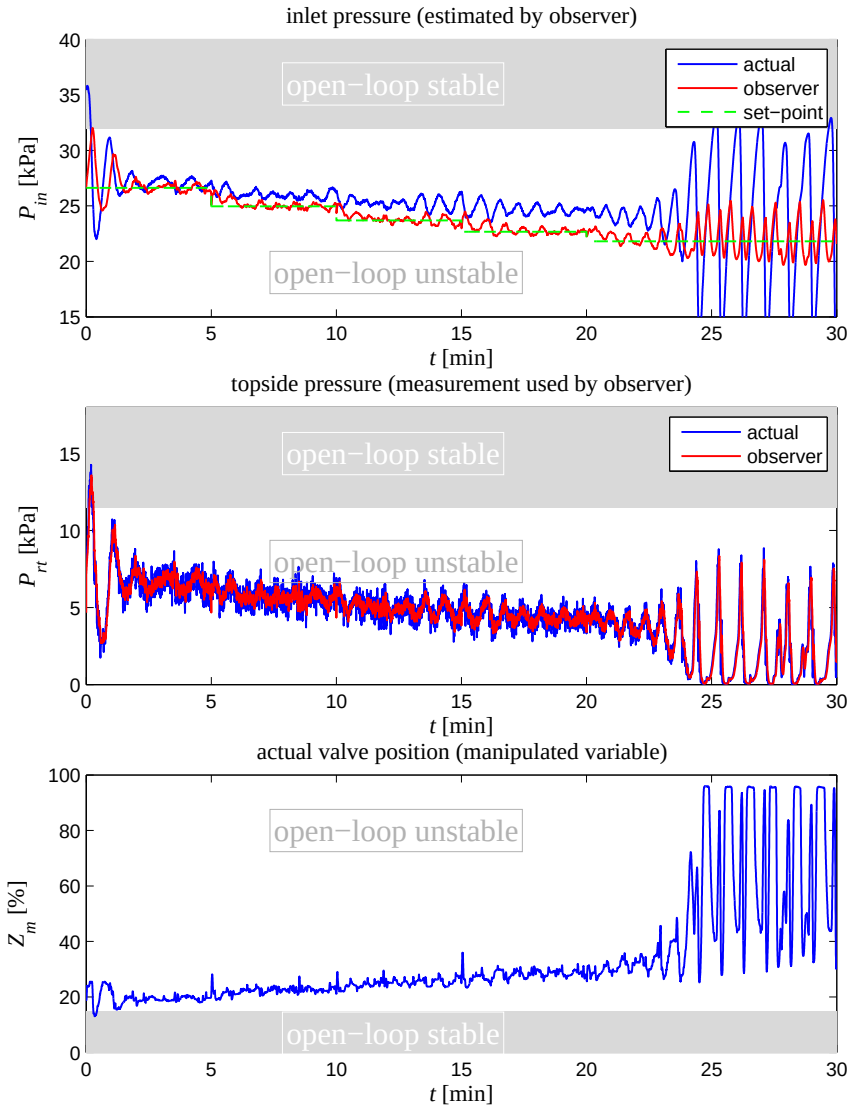

Figure 6.25: Control using High-Gain observer measuring top pressure (P_{rt}) with *0 sec* time delay

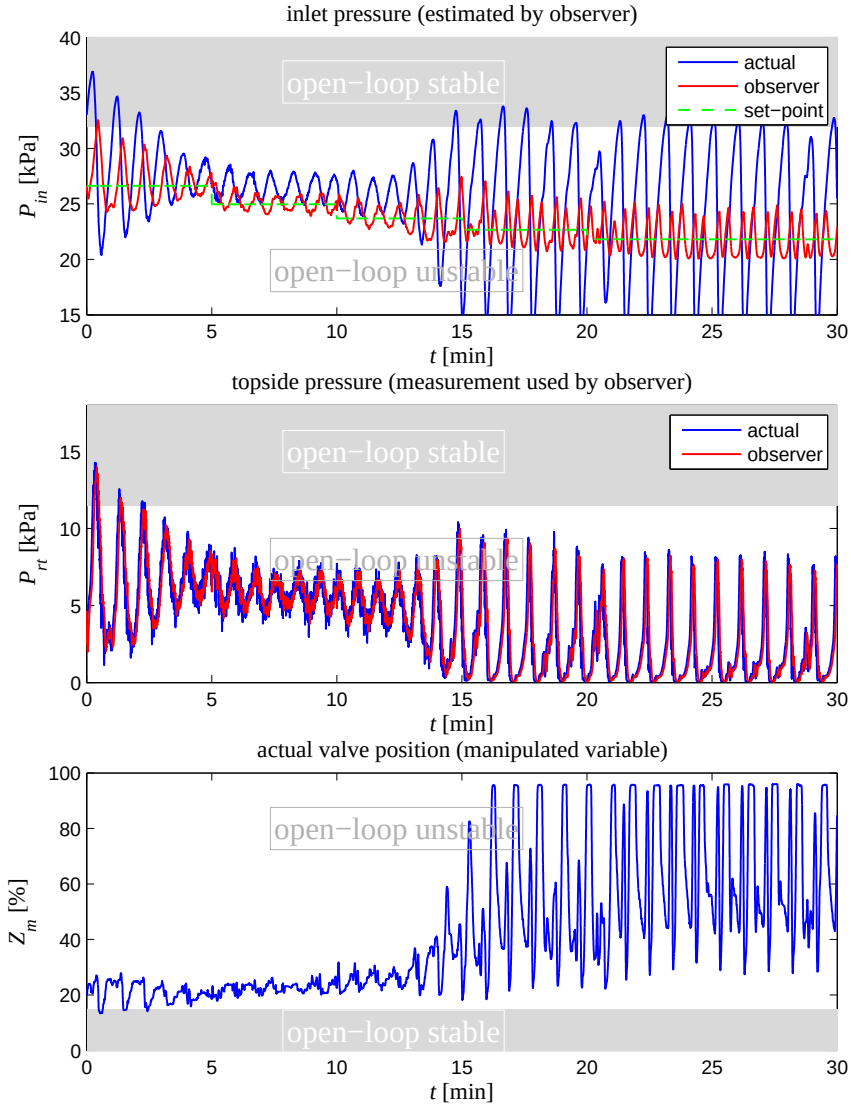

Figure 6.26: Control using High-Gain observer measuring top pressure (P_{rt}) with *2 sec* time delay

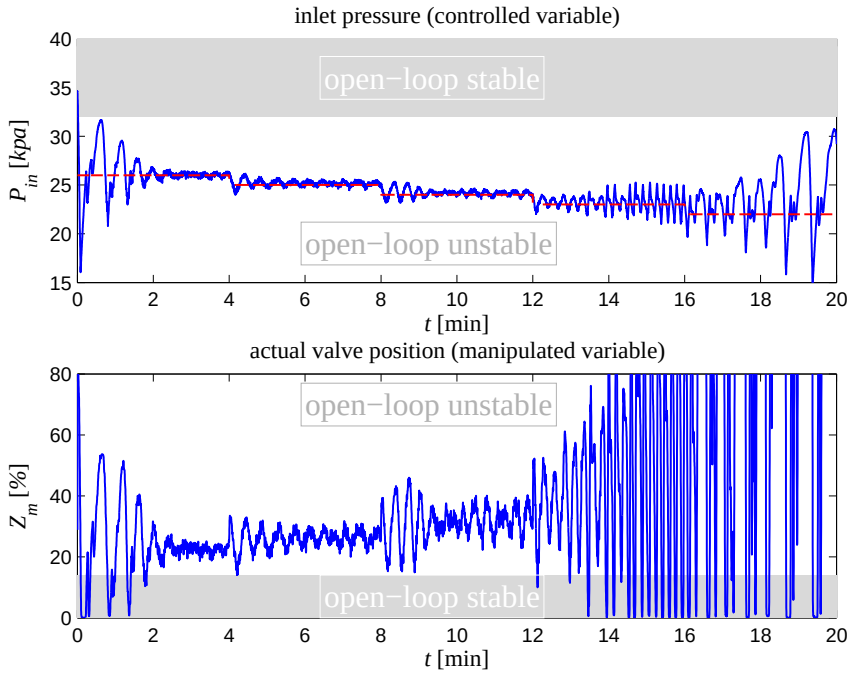

Figure 6.27: Control using adaptive PI controller measuring inlet pressure (P_{in}) with *2 sec* time delay

Table 6.7: Maximum valve opening achieved by using different controllers and different values of time delay

	CV	$\theta = 0$	$\theta = 1$	$\theta = 2$
Gain-scheduling IMC	P_{in}	60%	60%	50%
Adaptive PI	P_{in}	60%	50%	32%
Output linearization	P_{rb} & P_{rt}	60%	40%	25%
Nonlinear observer	P_{rt}	28%	24%	22%

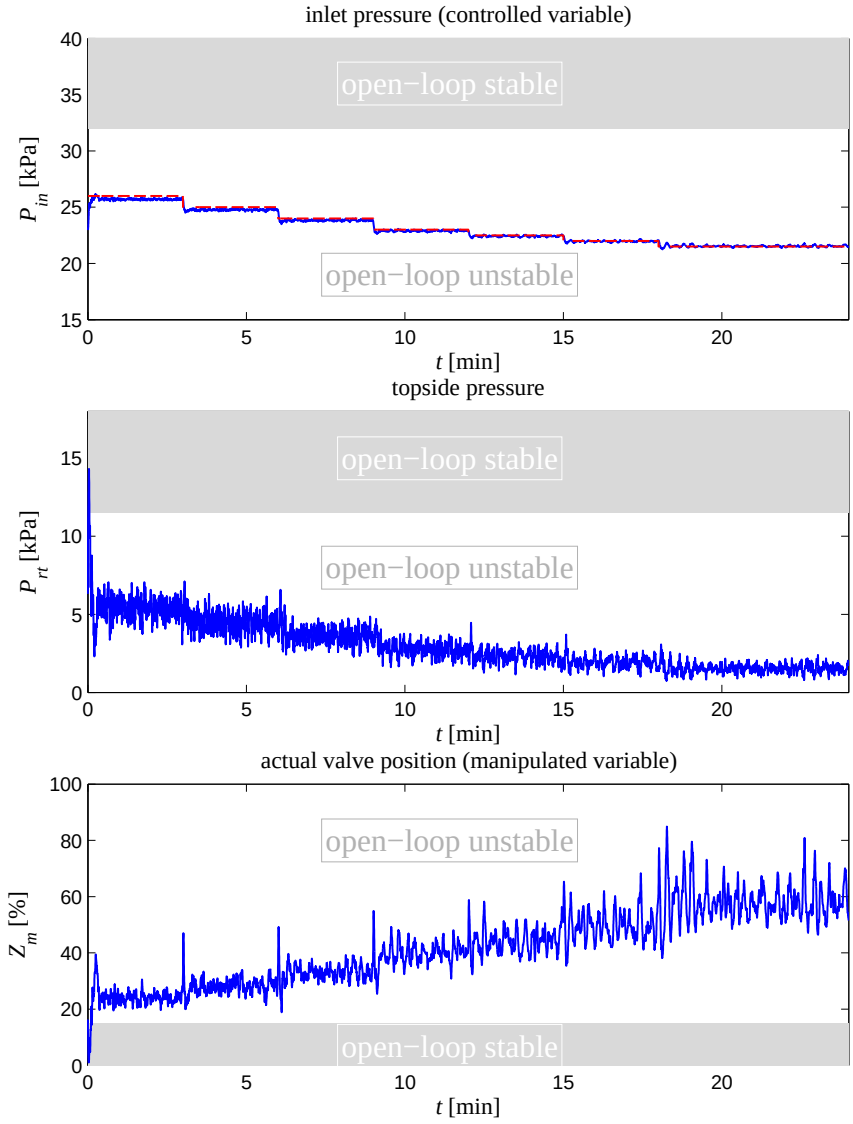

Figure 6.28: Control using nonlinear controller measuring subsea pressure (P_{in}) with *0 sec* time delay

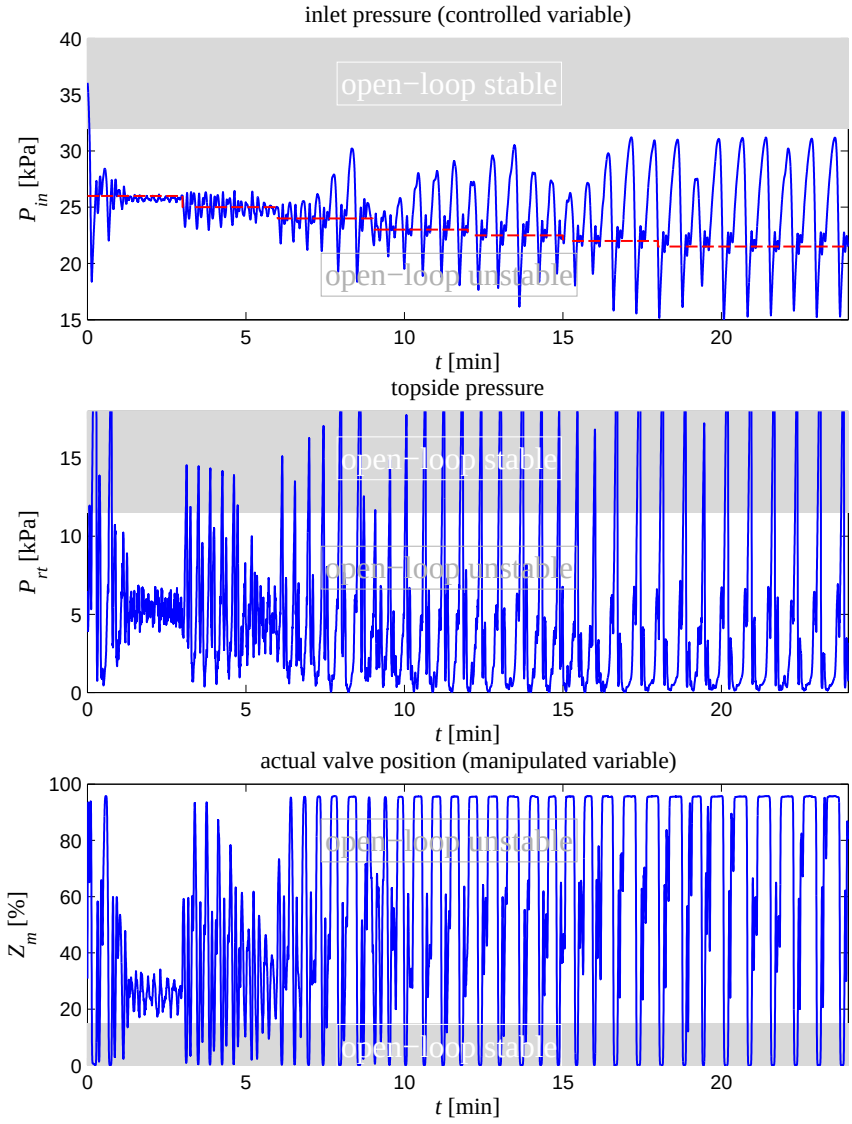

Figure 6.29: Control using nonlinear controller measuring subsea pressure (P_{in}) with *2sec* time delay

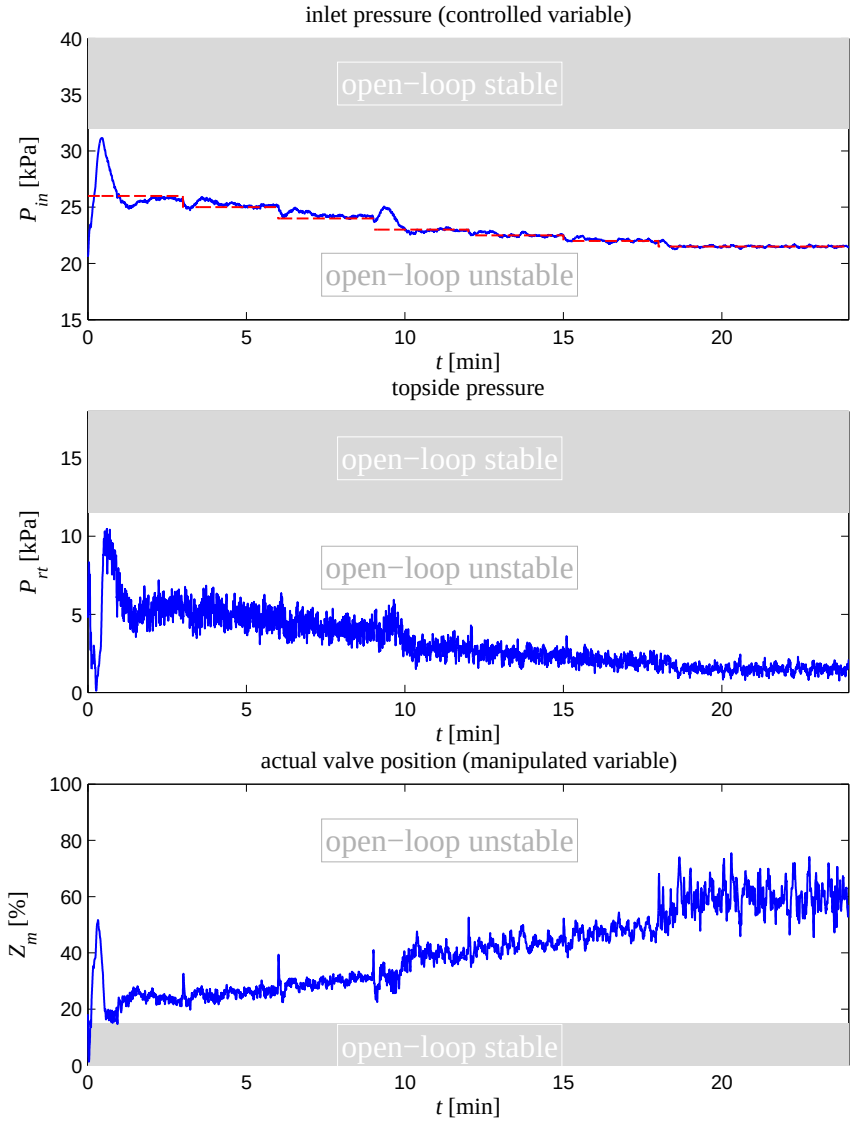

Figure 6.30: Control using IMC controller measuring subsea pressure (P_{in}) with *0 sec* time delay

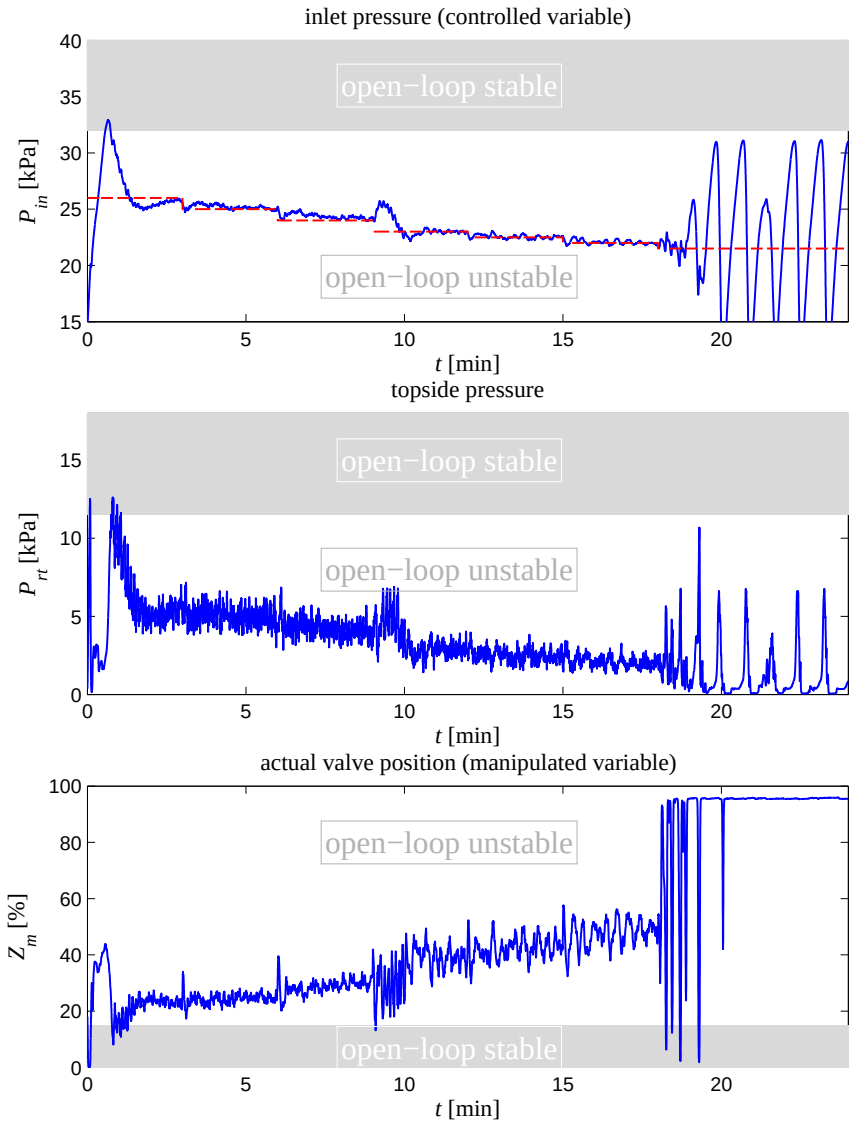

Figure 6.31: Control using IMC controller measuring subsea pressure (P_{in}) with *2 sec* time delay

6.7 Summary

Four nonlinear anti-slug controllers were tested on the same experimental platform under the same conditions. First, we considered two nonlinear controllers based on the mechanistic model, the state-feedback/nonlinear observer and the feedback linearizing controller. Then, we applied PI control with gain adaptation based on a simple model of the static gain. Finally, a gain-scheduling with IMC controllers based on identified models was used. The gain-scheduling IMC was able to stabilize the system up to large valve openings ($Z = 60\%$) even when applying time-delay to control loop ($Z = 50\%$); time-delay in the measurement is a major problem of long flow-lines. The IMC controller takes advantage of derivative action which results in a better phase-margin for stabilizing control, while the two other nonlinear controllers (based on the mechanistic model) are essentially proportional controllers. Other advantages of the IMC scheme are its simplicity and the fact that no mechanistic model is required for the controller design.

The second best controller for this case-study was the adaptive PI tuning that stabilizes the system up to $Z = 60\%$ without delay and $Z = 32\%$ with 2 *sec* delay. the third rank solution was output-linearizing controller which uses two pressure measurements directly, without observer. This controller could stabilize the system for large valve openings ($Z = 60\%$), but it was not robust against time delay.

The high-gain observer was only applicable by using the top-side pressure measurement, in a limited range ($Z = 28\%$). It was not stable when using the the subsea pressure measurement in closed loop.

Chapter 7

CONCLUSIONS AND FUTURE WORK

7.1 Main Contributions

This thesis reports results of the research carried out to improve anti-slug control at offshore oilfields. This research includes modeling, simulations using the OLGA simulator and experiments. The modeling and control structure design have been accomplished for three different offshore processes which severe-slugging flow occurs in (the pipeline-riser systems, the well-pipeline-riser systems and the gas-lifted oil wells). We mainly focused on the pipeline-riser systems in the control part.

The main contributions of the thesis are described below.

7.1.1 Modeling

In Chapter 2, a new four-state model was proposed for the severe-slugging flow in the pipeline-riser systems. The model was compared to five other simple models from the previous works, results from the OLGA simulators, as well as experiments. The proposed model matches well with the OLGA simulations and the experiments. Then, we extended this model to the well-pipeline-riser systems. We compared also the extended model to results from the OLGA simulator that resulted in a good agreement. Furthermore, we presented a modified three-state model for casing-heading instability in gas-lifted oil well and compared to the OLGA simulations. The gas-lift model is not a major contribution of this thesis and we present it in Appendix A.

7.1.2 Control structure design

We focused on finding suitable controlled variables and manipulated variables for anti-slug control in Chapter 3 and 4, respectively. We performed the controllability analysis for the three main processes mentioned above. With the controllability analysis we found the fundamental limitations in anti-slug stabilizing control.

When using the top-side pressure for the anti-slug control, the RHP-plane zeros of the system with this output limit the controllability by large peak on the sensitivity and the complementary sensitivity transfer functions. This problem becomes problematic for larger valve openings. As a result, using the top-side pressure, we can stabilize the system in a limited range. For example, in the experiments the system switches from non-slug flow to slug flow at $Z_1^* = 15\%$, and by using the topside pressure we could stabilize the system only up to $Z_1 = 20\%$. Indeed, this limitation was independent from the controller that we use and even with nonlinear control solutions this limitation cannot be bypassed.

When using a pressure measurement from the seabed the system can be stabilized in a large range ($Z_1 = 60\%$ in experiments). However, this requires a large controller gain for large valve openings. We face two fundamental limitations when controlling a subsea pressure with large valve openings:

- **Input saturation**:
  The gain of the system (G) decreases and finally approaches to zero as the valve opening increases. The loop gain ($L = KG$) should not vary much for different operating points, therefore, the control gain (K) must be increased to stabilize the system with large valve openings.

  $$u = KS(r - G_d d - n)$$

  By using an integral action we are at the steady-state where the complementary sensitivity transfer function is $T \approx 1$.

  $$KS = G^{-1}T \approx G^{-1}$$

  This means that small G translates to a large KS and leads large inputs due to measurement noises or disturbances.

- **Time delay**:
  Time delay causes problem especially when controlling with a large valve opening, because the instability moves further away from the origin ("faster instability") for larger valve openings. One of poles moves

further into the RHP as the valve opening increases and the term $e^{p\theta}$ becomes larger and the peak on the complementary sensitivity transfer function increases. In addition, by increasing the controller gain (K) the delay margin of the control loop (θ_M) decreases, because the crossover frequency ω_c increases for a large controller gain (fast control action).

$$\theta_M = PM/\omega_c$$

□

In Chapter 4, we tested three different manipulated variable (different locations for the control valve) for anti-slug control in a well-pipeline-riser system. We found that a subsea valve located near the riser base is suitable for anti-slug control and its operation range is same as the top-side valve. However, a subsea wellhead valve can not be used to prevent the riser slugging.

For the gas-lifted oil wells, the bottom-hole pressure is the best controlled variable when using the production choke for control. However, the bottom-hole pressure is not measured directly. In addition, we found that combing two topside pressure (the annulus pressure and the tubing pressure) gives satisfactory result. Further, we investigated using the topside gas-lift valve for the control purpose, but it was not an effective manipulated variable for stabilizing control.

7.1.3 PID and PI tuning

In Chapter 5, we proposed PID and PI tuning rules for robust anti-slug control. We found from an order truncation on the four-state model that a second order model is enough for the control design. We considered a model structure with one zero and two unstable poles, then we estimated parameters of the unstable model from a closed-loop step test.

Then, we used the identified unstable model for an IMC design. Finally, the PID and the PI tuning parameters were obtained from the resulted IMC controller. The proposed tuning rules were tested in OLGA simulations and experiments on two experimental rigs which showed applicability and robustness of the proposed tuning rules.

7.1.4 Nonlinear control

Three nonlinear control solutions were tested in Chapter 6. First, we used state-feedback with state estimation by nonlinear observers. Three types

of nonlinear observers were tested by experiments. Secondly, we applied feedback linearization with measured outputs. Finally, we designed a gain-scheduling IMC (Internal Model Control) based on linear models identified from closed-loop step test. We compared these three approaches in terms of robustness (delay margin of the control loop) and operation range (maximum achievable valve opening) in experiments.

Both the gain-scheduling and the feedback-linearization solutions were able to stabilize the system up to $Z_1 = 60\%$. However, the gain-scheduling IMC was the preferred solution. It does not need a physical model of the system and was more robust against time-delay in the subsea pressure measurement.

The state-feedback/solution was only applicable by using the top-side pressure measurement where we have fundamental limitation of the RHP-zero dynamics. We could stabilize the system by this solution in a limited range of $Z_1 = 20\%$. For the stabilizing control we need a fast observer, but fast nonlinear observers diverge when using the the subsea pressure as the measurement. Consequently, the closed-loop system with a fast nonlinear observer and using subsea pressure measurement was not stable.

7.2 Future works

We have used a stable vertical oil well in the well-pipeline-riser case study in order that we could focus on the riser-slugging instability. An extension to this can be using an unstable oil well in the well-pipeline-riser case study. Oil wells can have different geometries other than simply vertical. Some geometries may include low-points that causes flow instabilities in the oil well. In addition, wells with low reservoir pressures and heavy oils are more prone to flow instabilities.

Appendix A

GAS-LIFTED OIL WELL MODEL

Here, we present a modified three-state model for casing-heading instability in gas-lifted oil wells. The model is very similar to the ones used in [1], [2], [18], [19], [20]. We have improved the model by considering a friction term for the pressure drop and the gas production from the oil well. A schematic illustration of a gas-lifted oil wells is shown in Fig. A.1. The state variables are the mass of gas in the annulus ($m_{g,a}$), the mass of gas in the tubing ($m_{g,t}$) and the mass of liquid in the tubing ($m_{l,t}$). We consider also production of gas from the reservoir, which gives the following mass balances.

$$\frac{dm_{g,a}}{dt} = w_{g,in} - w_{g,inj} \tag{A.1}$$

$$\frac{dm_{g,t}}{dt} = w_{g,inj} + w_{g,res} - w_{g,out} \tag{A.2}$$

$$\frac{dm_{l,t}}{dt} = w_{l,res} - w_{l,out} \tag{A.3}$$

In this model, $w_{g,in}$ is the mass flow rate of inlet gas to the annulus and $w_{g,inj}$ is the mass flow of injected gas from the annulus into the tubing. $w_{g,res}$ and $w_{l,res}$ are gas and liquid mass flow rates from the reservoir to the tubing. $w_{g,out}$ and $w_{l,out}$ are the mass flow rates of gas and oil outlet from the tubing, respectively.
There is only gas phase inside the annulus, and pressure at top of the annulus can be calculated by ideal gas law.

$$P_{at} = \frac{RT_a m_{g,a}}{M_g V_a} \tag{A.4}$$

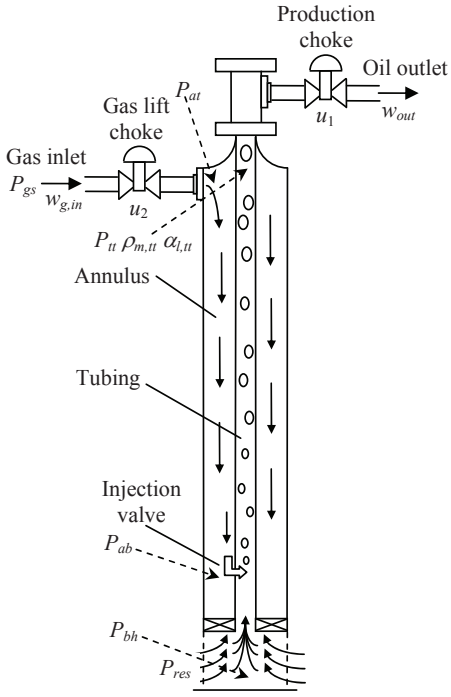

Figure A.1: Schematic presentation of gas-lift oil well

Then, the pressure at bottom of the annulus is given by

$$P_{ab} = P_{at} + \frac{m_{g,a} g L_a}{V_a}, \tag{A.5}$$

Thus, the density of the gas phase at this point is

$$\rho_{g,ab} = \frac{P_{ab} M_g}{R T_a}. \tag{A.6}$$

The inlet gas to the annulus comes from a source tank or a compressor with the pressure P_{gs}, and the density of gas through the gas-lift choke can be written as:

$$\rho_{g,in} = \frac{P_{gs} M_g}{R T_a} \tag{A.7}$$

Therefore, gas mass flow into the annulus is

$$w_{g,in} = K_{gs} u_2 \sqrt{\rho_{g,in} \max(P_{gs} - P_{at}, 0)}. \tag{A.8}$$

Because of high pressure, the fluid from the reservoir is saturated ([3]). Hence, we assume that distance between the bottom-hole and the injection point, L_{bh}, is filled by liquid phase. This must be accounted for in calculating the volume of gas in the tubing. Consequently, the density of gas inside the tubing follows as

$$\rho_{g,t} = \frac{m_{g,t}}{V_t + S_{bh} L_{bh} - m_{l,t}/\rho_l}. \tag{A.9}$$

Pressure at top of tubing using ideal gas law:

$$P_{tt} = \frac{\rho_{g,t} R T_t}{M_g} \tag{A.10}$$

Average mixture density inside tubing:

$$\bar{\rho}_m = \frac{m_{g,t} + m_{l,t} - \rho_l S_{bh} L_{bh}}{V_t} \tag{A.11}$$

Average liquid volume fraction inside tubing:

$$\bar{\alpha}_{l,t} = \frac{m_{l,t} - \rho_l S_{bh} L_{bh}}{V_t \rho_l} \tag{A.12}$$

gor is the constant mass ratio of gas and liquid produced from the reservoir, and gas mass fraction at bottom of the tubing is

$$\alpha^m_{g,b} = gor/(gor + 1). \tag{A.13}$$

Before calculating the inlet mass flow rate from the reservoir by use of the bottom-hole pressure in equation (A.27), the pressure drop due to friction is needed to determine the bottom-hole pressure. However, we need to know the inlet flow rate to calculate the friction term. We evade this problem by using the nominal production rate of the well, $\bar{w}_{nom}$, in calculation of friction terms.
Average superficial velocity of liquid phase in tubing:

$$\bar{U}_{sl,t} = \frac{4(1-\alpha_{g,b}^{m})\bar{w}_{nom}}{\rho_l \pi D_t^2} \tag{A.14}$$

Average superficial velocity of gas phase:

$$\bar{U}_{sg,t} = \frac{4(w_{g,in}+\alpha_{g,b}^{m}\bar{w}_{nom})}{\rho_{g,ab}\pi D_t^2} \tag{A.15}$$

We have not calculated flow rate of the injected gas from the annulus into the tubing yet, instead we use $w_{g,in}$ in equation (A.15); we believe averages of these two variables are equal.
Average mixture velocity in tubing:

$$\bar{U}_{m,t} = \bar{U}_{sl,t} + \bar{U}_{sg,t} \tag{A.16}$$

Reynolds number of flow in tubing:

$$Re_t = \frac{\bar{\rho}_m \bar{U}_{m,t} D_t}{\mu} \tag{A.17}$$

The Haaland equation [26] is used as the friction factor in the tubing.

$$\frac{1}{\sqrt{\lambda_t}} = -1.8\log_{10}\left[\left(\frac{\epsilon/D_t}{3.7}\right)^{1.11} + \frac{6.9}{Re_t}\right] \tag{A.18}$$

Pressure loss due to friction in tubing:

$$\Delta P_{ft} = \frac{\bar{\alpha}_{l,t}\lambda_t \bar{\rho}_{mix}\bar{U}_{m,t}^2 L_t}{2D_t} \tag{A.19}$$

Pressure at bottom of tubing where gas being injected from annulus:

$$P_{tb} = P_{tt} + \bar{\rho}_m g L_t + \Delta P_{ft} \tag{A.20}$$

Mass flow rate of gas injected into tubing:

$$w_{g,inj} = K_{inj}\sqrt{\rho_{g,ab}\max(P_{ab}-P_{tb},0)} \tag{A.21}$$

Liquid velocity at bottom-hole:

$$\bar{U}_{l,b} = \frac{\bar{w}_{nom}}{\rho_l S_{bh}} \tag{A.22}$$

Reynolds number of flow at bottom-hole:

$$Re_b = \frac{\rho_l \bar{U}_{l,b} D_b}{\mu} \tag{A.23}$$

Friction factor at bottom-hole:

$$\frac{1}{\sqrt{\lambda_b}} = -1.8 \log_{10} \left[\left(\frac{\epsilon / D_b}{3.7} \right)^{1.11} + \frac{6.9}{Re_b} \right] \tag{A.24}$$

Pressure loss due to friction from bottom-hole to injection point:

$$\Delta P_{fb} = \frac{\lambda_b \rho_l \bar{U}_{l,b}^2 L_{bh}}{2 D_b} \tag{A.25}$$

Pressure at bottom-hole:

$$P_{bh} = P_{tb} + \rho_l g L_{bh} + \Delta P_{fb} \tag{A.26}$$

Mass flow rate from reservoir to tubing:

$$w_{res} = PI max(P_{res} - P_{bh}, 0) \tag{A.27}$$

Mass flow rate of liquid from reservoir to tubing:

$$w_{l,res} = (1 - \alpha_{g,b}^m) w_{res} \tag{A.28}$$

Mass flow rate of gas from reservoir to the well:

$$w_{g,res} = \alpha_{g,b}^m w_{res} \tag{A.29}$$

Density of gas at bottom of tubing:

$$\rho_{g,tb} = \frac{P_{tb} M_G}{R T_t} \tag{A.30}$$

Liquid volume fraction at bottom of tubing:

$$\alpha_{l,tb} = \frac{w_{l,res} \rho_{g,tb}}{w_{l,res} \rho_{g,tb} + (w_{g,inj} + w_{g,res}) \rho_l} \tag{A.31}$$

With the same assumptions used for the phase fraction of the riser in Section 2.2.8, liquid volume fraction at top of the tubing can be written as

$$\alpha_{l,tt} = 2\bar{\alpha}_{l,t} - \alpha_{l,tb}, \tag{A.32}$$

Then, the mixture density at top of the tubing will be

$$\rho_{tt} = \alpha_{l,tt}\rho_l + (1 - \alpha_{l,tt})\rho_{g,t}. \tag{A.33}$$

Mass flow rate of mixture from production choke:

$$w_{out} = K_{pr} u_1 \sqrt{\rho_{tt} \max(P_{tt} - P_0, 0)} \tag{A.34}$$

Volumetric flow rate of production choke:

$$Q_{out} = w_{out}/\rho_{tt} \tag{A.35}$$

Gas mass fraction at top of tubing:

$$\alpha^m_{g,tt} = \frac{(1 - \alpha_{l,tt})\rho_{g,t}}{\alpha_{l,tt}\rho_l + (1 - \alpha_{l,tt})\rho_{g,t}} \tag{A.36}$$

Mass flow rate of outlet gas from tubing:

$$w_{g,out} = \alpha^m_{g,tt} w_{out} \tag{A.37}$$

Mass flow rate of outlet liquid from tubing:

$$w_{l,out} = (1 - \alpha^m_{g,tt}) w_{out} \tag{A.38}$$

□

The simplified model was fitted to a test case implemented in the OLGA simulator. Constants and parameters used in the model are given in Table A.1. The stability map of the system is shown in Figure A.2 where stability transitions of the OLGA model and the simplified model are compared. It was not possible to add the gas-lift choke to the OLGA model, therefore we used a constant gas source equal to $w_{G,in} = 0.8\ [kg/s]$ in the OLGA model and we fitted the model with the constant gas rate. Then, we added the gas-lift choke valve to the Matlab model so that the simplified model gives $w_{G,in} = 0.8\ [kg/s]$ when the gas-lift choke opening is $u_2 = 0.4$ and the production choke opening is $u_1 = 0.3$. The system switches from stable to unstable at this operating point. Figure A.3 Shows comparison of the bifurcations diagrams of the system where the production valve opening u_1 is considered as the degree of freedom while the gas-lift choke valve is kept constant at $u_2 = 0.4$.

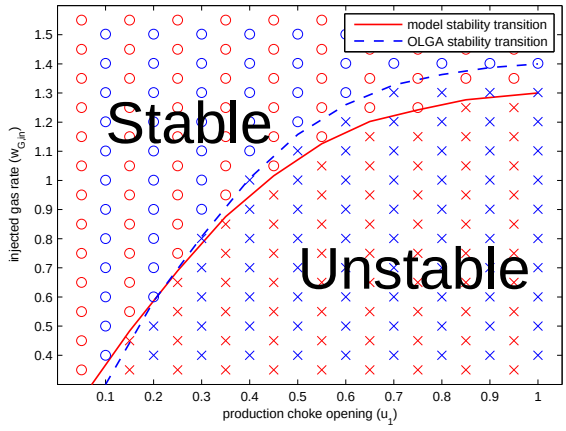

Figure A.2: Stability transition of system, blue markers for OLGA and red markers for simplified model

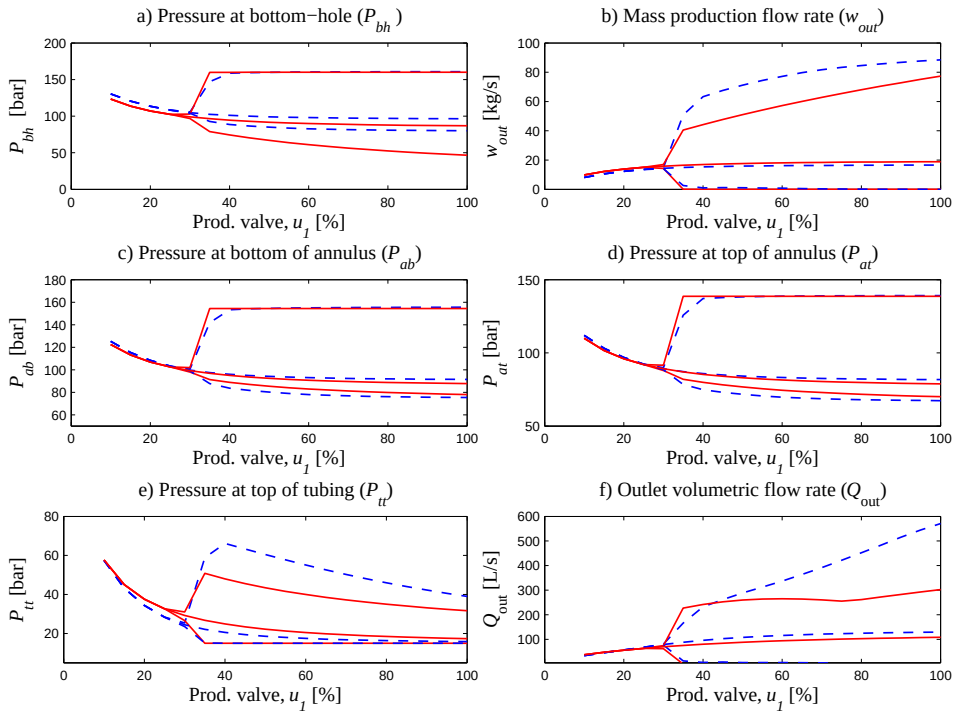

Figure A.3: Bifurcation diagrams of simplified gas-lift model (solid lines) compared to OLGA model (dashed lines)

Table A.1: Parameter values for gas-lift model

Symb.	Description	Values	Units
R	universal gas constant	8314	$J/(kmol.K)$
g	gravity	9.81	m/s^2
μ	viscosity	3.64×10^{-3}	$Pa.s$
ρ_l	liquid density	760	kg/m^3
M_g	gas molecular weight	16.7	gr
T_a	annulus temperature	348	K
V_a	annulus volume	64.34	m^3
L_a	annulus length	2048	m^3
P_{gs}	gas source pressure	140	bar
V_t	tubing volume	25.03	m^3
S_{bh}	cross-section below injection point	0.0314	m^2
L_{bh}	length below injection point	75	m
T_t	tubing temperature	369.4	K
gor	mass gas oil ratio	0	–
P_{res}	reservoir pressure	160	bar
$\bar{w}_{nom}$	nominal mass flow from reservoir	18	kg/s
D_t	tubing diameter	0.134	m
L_t	tubing length	2048	m
PI	productivity index	2.47e-6	$kg/(s.Pa)$
K_{gs}	gas-lift choke cons.	9.98×10^{-5}	–
K_{inj}	injection valve cons.	1.40×10^{-4}	–
K_{pr}	production choke cons.	2.90×10^{-3}	–

Appendix B

MODEL IDENTIFICATION CALCULATIONS

Stable closed-loop transfer function:

$$\frac{y(s)}{y_s(s)} = \frac{K_2(1+\tau_z s)}{\tau^2 s^2 + 2\zeta\tau s + 1} \tag{B.1}$$

The Laplace inverse (time-domain) of the transfer function in (B.1) is given in [83] as

$$y(t) = \Delta y_s K_2 \left[1 + D\exp(-\zeta t/\tau)\sin(Et+\phi)\right], \tag{B.2}$$

where

$$D = \frac{\left[1 - \frac{2\zeta\tau_z}{\tau} + \left(\frac{\tau_z}{\tau}\right)^2\right]^{\frac{1}{2}}}{\sqrt{1-\zeta^2}} \tag{B.3}$$

$$E = \frac{\sqrt{1-\zeta^2}}{\tau} \tag{B.4}$$

$$\phi = \tan^{-1}\left[\frac{\tau\sqrt{1-\zeta^2}}{\zeta\tau - \tau_z}\right] \tag{B.5}$$

By differentiating (B.2) with respect to time and setting the derivative equation to zero, one gets time of the first peak:

$$t_p = \frac{\tan^{-1}\left(\frac{1-\zeta^2}{\zeta}\right) + \pi - \phi}{\sqrt{1-\zeta^2}/\tau} \tag{B.6}$$

And the time between the first peak (overshoot) and the undershoot:

$$t_u = \pi\tau/\sqrt{1-\zeta^2} \tag{B.7}$$

The damping ratio ζ can be estimated as

$$\hat{\zeta} = \frac{-\ln v}{\sqrt{\pi^2 + (\ln v)^2}} \tag{B.8}$$

where

$$v = \frac{\Delta y_\infty - \Delta y_u}{\Delta y_p - \Delta y_\infty} \tag{B.9}$$

Then, using equation (B.7) we get

$$\hat{\tau} = \frac{t_u\sqrt{1-\hat{\zeta}^2}}{\pi}. \tag{B.10}$$

The steady-state gain of the closed-loop system is estimated as

$$\hat{K}_2 = \frac{\Delta y_\infty}{\Delta y_s}. \tag{B.11}$$

We use time of the peak t_p and (B.6) to get an estimate of ϕ :

$$\hat{\phi} = \tan^{-1}\left[\frac{1-\hat{\zeta}^2}{\hat{\zeta}}\right] - \frac{t_p\sqrt{1-\hat{\zeta}^2}}{\hat{\tau}} \tag{B.12}$$

From (B.4), we get

$$\hat{E} = \frac{\sqrt{1-\hat{\zeta}^2}}{\hat{\tau}} \tag{B.13}$$

The overshoot is defined as

$$D_0 = \frac{\Delta y_p - \Delta y_\infty}{\Delta y_\infty}. \tag{B.14}$$

By evaluating (B.2) at time of peak t_p we get

$$\Delta y_p = \Delta y_s \hat{K}_2\left[1 + \hat{D}\exp(-\hat{\zeta}t_p/\hat{\tau})\sin(\hat{E}t_p + \hat{\phi})\right] \tag{B.15}$$

Combining equation (B.11), (B.14) and (B.15) gives

$$\hat{D} = \frac{D_0}{\exp(-\hat{\zeta}t_p/\hat{\tau})\sin(\hat{E}t_p + \hat{\phi})}. \tag{B.16}$$

We can estimate the last parameter by solving (B.3):

$$\hat{\tau}_z = \hat{\xi}\hat{\tau} + \sqrt{\hat{\zeta}^2\hat{\tau}^2 - \hat{\tau}^2\left[1 - \hat{D}^2(1-\hat{\zeta}^2)\right]} \tag{B.17}$$

Then, we back-calculate to parameters of the open-loop unstable model. The steady-state gain of the open-loop model is

$$\hat{K} = \frac{\Delta y_\infty}{K_{c0}\,|\Delta y_s - \Delta y_\infty|} \tag{B.18}$$

From this, we can estimate the four model parameters in equation (B.5) are

$$\hat{a}_0 = \frac{1}{\hat{\tau}^2(1 + K_{c0}\hat{K}_p)} \tag{B.19}$$

$$\hat{b}_0 = \hat{K}_p \hat{a}_0 \tag{B.20}$$

$$\hat{b}_1 = \frac{\hat{K}_2 \hat{\tau}_z}{K_{c0}\hat{\tau}^2} \tag{B.21}$$

$$\hat{a}_1 = -2\hat{\zeta}/\hat{\tau} + K_{c0}\hat{b}_1, \tag{B.22}$$

where $\hat{a}_1 > 0$ gives an unstable system.

Appendix C

STATIC NONLINEARITY PARAMETERS

From equation (6.38) we have

$$\bar{a} = \frac{1}{\bar{\rho}}\left(\frac{\bar{w}}{C_v}\right)^2 \tag{C.1}$$

Where C_v is the known valve constant, $\bar{w}$ is the steady-state average outlet flow rate and $\bar{\rho}$ is the steady-state average mixture density. The average outlet mass flow is approximated by constant inflow rates.

$$\bar{w} = w_{g,in} + w_{l,in} \tag{C.2}$$

In order to estimate the average mixture density $\bar{\rho}$, we perform the following calculations, assuming a fully open valve.
Average gas mass fraction:

$$\bar{\alpha} = \frac{w_{g,in}}{w_{g,in} + w_{l,in}} \tag{C.3}$$

Average gas density at top of the riser from ideal gas law:

$$\bar{\rho}_g = \frac{(P_s + \Delta P_{v,\min})M_g}{RT} \tag{C.4}$$

where P_s is the constant separator pressure, and $\Delta P_{v,\min}$ is the (minimum) pressure drop across the valve that exists with a fully open valve. In the numerical simulations $\Delta P_{v,\min}$ is assumed to be zero but in our experiments it was 2 kPa.
Liquid volume fraction:

$$\bar{\alpha}_l = \frac{(1-\bar{\alpha})\bar{\rho}_g}{(1-\bar{\alpha})\bar{\rho}_g + \bar{\alpha}\rho_L}. \tag{C.5}$$

Average mixture density:

$$\bar{\rho} = \bar{\alpha}_l \rho_l + (1 - \bar{\alpha}_l)\bar{\rho}_g \tag{C.6}$$

In order to calculate the constant parameters $\bar{P}_{fo}$ in (6.40), we use the fact that if the inlet pressure is large enough to overcome a riser full of liquid, slugging will not happen. [78] used the same concept for stability analysis, also this was observed in our experiments. we define the critical pressure as

$$P^*_{in} = \rho_L g L_r + P_s + \Delta P_{v,\min} \tag{C.7}$$

This pressure is associated with the critical valve opening at the bifurcation point z^*. From (6.40), we get $\bar{P}_{fo}$ as the following:

$$\bar{P}_{fo} = P^*_{in} - \frac{\bar{a}}{f(z^*)^2} \tag{C.8}$$

Appendix D

CALCULATION OF FRICTION AND DENSITY

Here, we calculate the friction and the density which are need by the non-linear controller in equation (6.34).

Gas mass fraction:

$$\alpha = \frac{w_{g,in}}{w_{g,in} + w_{l,in}} \tag{D.1}$$

Gas density:

$$\rho_g = \frac{y_2 M_G}{R T_r} \tag{D.2}$$

Liquid volume fraction:

$$\alpha_{lt} = \frac{\rho_g w_l}{\rho_g w_l + \rho_l w_g} \tag{D.3}$$

Mixture density at top of riser:

$$\rho_{rt} = \alpha_{lt}.\rho_l + (1 - \alpha_{lt})\rho_g \tag{D.4}$$

Liquid superficial velocity:

$$\bar{U}_{sl} = \frac{w_{l,in}}{\rho_l A_r} \tag{D.5}$$

Gas superficial velocity:

$$\bar{U}_{sg} = \frac{w_{g,in}}{\rho_g A_r} \tag{D.6}$$

Mixture velocity:

$$\bar{U}_m = \bar{U}_{sl} + \bar{U}_{sg} \tag{D.7}$$

Average density in riser:

$$\bar{\rho} = \frac{y_1 - y_2}{c L_r A_r} \tag{D.8}$$

Reynolds number of flow in riser:

$$Re = \frac{\bar{\rho}\bar{U}_m D_r}{\mu} \tag{D.9}$$

An explicit approximation of the implicit Colebrook-White equation proposed by [26] is used as the friction factor in the riser.

$$\frac{1}{\sqrt{\lambda}} = -1.8 \log_{10} \left[\left(\frac{\epsilon/D_r}{3.7} \right)^{1.11} + \frac{6.9}{Re} \right] \tag{D.10}$$

Pressure loss due to friction in riser:

$$F_r = \frac{\alpha_{lt} \lambda \bar{\rho} \bar{U}_m^2 L_r}{2 D_r} \tag{D.11}$$

REFERENCES

[1] Aamo, O., Eikrem, G., Siahaan, H., Foss, B., 2005. Observer design for multiphase flow in vertical pipes with gas-lift - theory and experiments. Journal of Process Control 15 (3), 247 – 257.

[2] Aamo, O. M., Eikrem, G. O., Siahaan, H., Foss, B., 2004. Observer design for gas lifted oil wells. In: American Control Conference. pp. 1552–1557.

[3] Ahmed, T., 2006. Reservoir Engineering Handbook, Third Edition. Elsevier, Oxford, UK.

[4] Bai, Y., Bai, Q., 2005. Subsea Pipelines and Riser. Elsevier Science Ltd, Oxford.

[5] Bendlksen, K. H., Malnes, D., Moe, R., Nuland, S., 1991. Dynamic two-fluid model olga. theory and application. SPE Production Engineering 6 (2), 171–180.

[6] Boizot, N., Busvelle, E., Gauthier, J.-P., 2010. An adaptive high-gain observer for nonlinear systems. Automatica 46 (9), 1483–1488.

[7] Brill, J. P., Beggs, H. D., 1991. Two-Phase Flow In Pipes, 6th Edition, Third Printing. University of Tulsa, Tulsa, Oklahoma.

[8] Chen, J., June 2000. Logarithmic integrals, interpolation bounds and performance limitations in mimo feedback systems. IEEE Transactions on Automatic Control 45 (6), 1098–1115.

[9] Cossé, R., 1993. Basics Of Reservoir Engineering. Institut français du pétrole (IFP), Paris.

[10] Courbot, A., 1996. Prevention of severe slugging in the dunbar 16 inches multiphase pipeline. In: Proceedings of the Annual Offshore Technology Conference. Vol. 4. pp. 445–452, *SPE no.* 8196.

[11] Devold, H., 2010. Oil and gas production handbook, An introduction to oil and gas production, 2nd Edition. ABB Oil and Gas, Oslo.

[12] Di Meglio, F., 2011. Production de pétrole: étude dynamique et contrôle des écoulements à bouchons. Phd. thesis, l'Ecole des mines de paris.

[13] Di Meglio, F., Kaasa, G.-O., Petit, N., 2009. A first principle model for multiphase slugging flow in vertical risers. In: Joint 48th IEEE Conference on Decision and Control and 28th Chinese Control Conference. Shanghai, China, pp. 8244–8251.

[14] Di Meglio, F., Kaasa, G.-O., Petit, N., Alstad, V., 2010. Reproducing slugging oscillations of a real oil well. In: 49th IEEE Conference on Decision and Control. Atlanta, Georgia, USA, pp. 4473–4479.

[15] Di Meglio, F., Kaasa, G.-O., Petit, N., Alstad, V., 2012. Model-based control of slugging: advances and challenges. In: IFAC Workshop on Automatic Control in Offshore Oil and Gas Production. Trondheim, Norway, pp. 109–115.

[16] Doyle, J., Glover, K., Khargonekar, P., Francis, B., aug 1989. State-space solutions to standard $\mathcal{H}_2$ and $\mathcal{H}_\infty$ control problems. IEEE Transactions on Automatic Control 34 (8), 831–847.

[17] Eikrem, G. O., 2008. Eikrem riser model.
URL `http://www.nt.ntnu.no/users/skoge/diplom/prosjekt08/tuvnes/`

[18] Eikrem, G. O., Aamo, O. M., Siahaan, H., Foss, B., 2004. Anti-slug control of gas-lift wells - experimental results. In: 6th IFAC Symposium on Nonlinear Control Systems. Stuttgart, Germany, pp. 1–8.

[19] Eikrem, G. O., Foss, B., Imsland, L., Hu, B., Golan, M., 2002. Stabilization of gas lifted wells. In: 15th IFAC World Congress. Barcelona, Spain, pp. 1489–1489.

[20] Eikrem, G. O., Imsland, L., Foss, B., 2004. Stabilization of gas lifted wells based on state estimation. In: IFAC International Symposium on Advanced Control of Chemical Processes. Hong Kong, China, pp. 1–6.

[21] Fard, M. P., Godhavn, J.-M., Sagatun, S. I., 2006. Modelling of severe slug and slug control with olga, spe 84685. SPE Journal of Production & Operations.

[22] Glover, K., 1986. Robust stabilization of linear multivariable systems: relations to approximation. International Journal of Control 43 (3), 741–766.

[23] Glover, K., Doyle, J. C., 1988. State-space formulae for all stabilizing controllers that satisfy an $\mathcal{H}_\infty$-norm bound and relations to relations to risk sensitivity. Systems and Control Letters 11 (3), 167–172.

[24] Glover, K., McFarlane, D., 1989. Robust stabilization of normalized coprime factor plant descriptions with h_∞-bounded uncertainty. IEEE Transactions on Automatic Control 34 (8), 821–830.

[25] Godhavn, J.-M., Fard, M. P., Fuchs, P. H., 2005. New slug control strategies, tuning rules and experimental results. Journal of Process Control 15, 547–557.

[26] Haaland, S. E., 1983. Simple and explicit formulas for the friction factor in turbulent pipe flow. Journal of Fluids Engineering 105 (1), 89–90.

[27] Havre, K., Skogestad, S., 1998. Effect of rhp zeros and poles on the sensitivity functions in multivariable systems. Journal of Process Control 8 (3), 155–164.

[28] Havre, K., Skogestad, S., 2001. Achievable performance of multivariable systems with unstable zeros and poles. International Journal of Control 48, 1131–1139.

[29] Havre, K., Skogestad, S., August 2003. Selection of variables for stabilizing control using pole vectors. IEEE Transaction on Automatic Control 48 (8), 1393–1398.

[30] Havre, K., Stornes, K., Stray, H., 2000. Taming slug flow in pipelines. ABB Review 4, 55–63.

[31] Hu, B., Golan, M., 2003. Gas-lift instability resulted production loss and its remedy by feedback control: dynamical simulation results. In: SPE International Improved Oil Recovery Conference in Asia Pacific. SPE no. 84917-MS, Kuala Lumpur, Malaysia, pp. 513–521.

[32] Irmann-Jacobsen, T. B., 2012. Flow assurance - a system perspective. MEK4450 Offshore Technology Course, universitet i Oslo, Matematisk Institutt.

[33] Isidori, A., 1999. Nonlinear Control Systems II, 1st Edition. Springer-Verlag, London.

[34] Jahanshahi, E., Skogestad, S., Auguest 2011. Simplified dynamical models for control of severe slugging in multiphase risers. In: 18th IFAC World Congress. Milan, Italy, pp. 1634–1639.

[35] Jahanshahi, E., Skogestad, S., 2013. Closed-loop model identification and pid/pi tuning for robust anti-slug control. In: 10th IFAC International Symposium on Dynamics and Control of Process Systems. Mumbai, India.

[36] Jahanshahi, E., Skogestad, S., 2013. Comparison between nonlinear modelbased controllers and gain-scheduling internal model control based on identified model. In: 52nd IEEE Conference on Decision and Control. Florence, Italy.

[37] Jahanshahi, E., Skogestad, S., Grøtli, E. I., 2013. Anti-slug control experiments using nonlinear observer. In: American Control Conference. Washington D.C., pp. 1056–1062.

[38] Jahanshahi, E., Skogestad, S., Grøtli, E. I., 2013. Nonlinear model-based control of two-phase flow in risers by feedback linearization. In: 9th IFAC Symposium on Nonlinear Control Systems. Toulouse, France, pp. 301–306.

[39] Jahanshahi, E., Skogestad, S., Hansen, H., 2012. Control structure design for stabilizing unstable gas-lift oil wells. In: Advanced Control of Chemical Processes. Vol. 8. Singapore, pp. 93–100.

[40] Jahanshahi, E., Skogestad, S., Helgesen, A. H., May 2012. Controllability analysis of severe slugging in well-pipeline-riser systems. In: IFAC Workshop - Automatic Control in Offshore Oil and Gas Production. Trondheim, Norway, pp. 101–108.

[41] Jahanshahi, E., Skogestad, S., Lieungh, M., 2013. Subsea solution for anti-slug control of multiphase risers. In: European Control Conference. Zürich, Switzerland, pp. 4094–4099.

[42] Jankovic, M., Sepulchre, R., Kokotovic, P., dec 1996. Constructive Lyapunov stabilization of nonlinear cascade systems. IEEE Transactions on Automatic Control 41 (12), 1723 –1735.

[43] Jansen, B., Dalsmo, M., Nøkleberg, L., Havre, K., Kristiansen, V., Lemetayer, P., 1999. Automatic control of unstable gas lifted wells. In: SPE Annual Technical Conference and Exhibition. Houston, Texas, pp. 1–9.

[44] Jansen, F., Shoham, O., Taitel, Y., 1996. The elimination of severe slugging - experiments and modeling. International Journal of Multiphase Flow 22 (6), 1055 – 1072.

[45] Johal, K., 2012. Flow Assurance for Oil-Gas Fields Production Transport, fisrt Edition. Fluids in Motion Limited, London.

[46] Joshi, N. B., Muhammad, M., Creek, J., McFadden, J., 2003. Flow assurance: A challenging path to well completions and productivity. In: Offshore Technology Conference. Houston, Texas, pp. 1142–1146.

[47] Julier, S. J., Uhlmann, J. K., 1997. A new extension of the kalman filter to non-linear systems. In: AeroSense: The 11th Int. Symp. A.D.S.S.C.

[48] Kaasa, G.-O., Alstad, V., Zhou, J., Aamo, O. M., 2007. Nonlinear model-based control of unstable wells. Journal of Modeling, Identification and Control 28 (3), 69–79.

[49] Kaasa, G.-O., Alstad, V., Zhou, J., Aamo, O. M., 2008. Attenuation of slugging in unstable oil wells by nonlinear control. In: 17th IFAC World Congress. COEX, Korea, South, pp. 6251–6256.

[50] Kalman, R. E., Falb, P. L., Arbib, M. A., 1969. Topics in mathematical system theory. McGraw-Hill Book Co., New York.

[51] Khalil, H. K., 2002. Nonlinear Systems, Third Edition. Prentice Hall, Upper Saddle River, New Jersey.

[52] Krima, H., Cao, Y., Lao, L., May 2012. Gas injection for hydrodynamic slug control. In: IFAC Workshop, Automatic Control in Offshore Oil and Gas Production. Vol. 1. Trondheim, Norway, pp. 116–121.

[53] Larsen, R., Lund, A., Argo, C., June 2003. Cold flow - a practical solution. In: 11th International Conference on Multiphase Flow. San Remo,Italy, pp. 313–331.

[54] Lieungh, M., June 2012. Stabilizing slug control using sub-sea choke valve. Master thesis, Norwegian University of Science and Technology, Deoartment of Chemical Engineering.

[55] Martins Da Silva, C., Dessen, F., Nydal, O. J., 2010. Dynamic multiphase flow models for control. In: BHR Group - 7th North American Conference on Multiphase Technology. pp. 221–236.

[56] Meglio, F. D., Petit, N., Alstad, V., Kaasa, G.-O., 2012. Stabilization of slugging in oil production facilities with or without upstream pressure sensors. Journal of Process Control 22 (4), 809 – 822.

[57] Mokhatab, S., Poe, W. A., Speight, J. G., 2006. Chapter 3 - raw gas transmission. In: Handbook of Natural Gas Transmission and Processing. Gulf Professional Publishing, Burlington, pp. 81 – 188.

[58] Morari, M., Zafiriou, E., 1989. Robust Process Control. Prentice Hall, Englewood Cliffs, New Jersey.

[59] Nilsen, A. S., 2012. Simplified first principle model for severe-slugging flow in s-shaped risers. Master project, Nowegian University of Science and Technology.

[60] Ogazi, A., Cao, Y., Yeung, H., Lao, L., 2010. Slug control with large valve openings to maximize oil production. SPE Journal 15 (3), 812–821.

[61] Ogazi, A., Ogunkolade, S., Cao, Y., Lao, L., Yeung, H., 2009. Severe slugging control through open loop unstable pid tuning to increase oil production. pp. 17–32.

[62] Ogazi, I., Cao, Y., Lao, L., Yeung, H., 2011. Production potential of severe slugging control systems. In: 18th IFAC World Congress. Vol. 18. Milano, Italy, pp. 10869–10874.

[63] Pickering, P. F., Hewitt, G. F., Watson, M. J., Hale, C. P., June 2001. The prediction of flows in production risers - truth & myth? In: IIR Conference. Aberdeen, pp. 1–16.

[64] Saberi, A., Kokotovic, P., Sussmann, H., dec 1989. Global stabilization of partially linear composite systems. In: Proceedings of the 28th IEEE Conference on Decision and Control, 1989. pp. 1385 –1391 vol.2.

[65] Sayda, A., Taylor, J., 2007. Modeling and control of three-phase gravilty separators in oil production facilities. In: American Control Conference, 2007. ACC '07. pp. 4847–4853.

[66] Schlumberger, 2013. The schlumberger oilfield glossary. http://www.glossary.oilfield.slb.com.

[67] Schmidt, Z., Brill, J., Beggs, D., 1980. Riser-base gas injection into the se forties line. SPE Journal 20, 407–414.

[68] Schmidt, Z., Brill, J. P., Beggs, H. D., 1979. Choking can eliminate severe pipeline slugging. Oil & Gas Journal 12, 230–238.

[69] Sinegre, L., 2006. Etude des instabilits dans les puits activs par gas-lift. Ph.D. thesis, Ecole des Mines de Paris.

[70] Sivertsen, H., 2008. Stabilizing of desired flow regimes using active control. Ph.D. thesis, Norwegian University of Science and Technology, NTNU.

[71] Sivertsen, H., Alstad, V., Skogestad, S., 2009. Medium-scale experiments on stabilizing riser-slug flow. SPE Projects, Facilities & Construction 4 (4), 156–170, SPE no. 120040.

[72] Skofteland, G., Godhavn, J. M., Kulset, T., 2007. Implementation of a slug control system for subsea wells in an integrated operation environment. In: 13th International Conference on Multiphase Production Technology. Edinburgh, UK., pp. 225–236.

[73] Skogestad, S., 2009. Chemical And Energy Process Engineering. CRC Press, Taylor & Francis Group, Boca Raton, FL.

[74] Skogestad, S., Postlethwaite, I., 2005. Multivariable Feedback Control: Analysis and Design. Wiley & Sons, Chichester, West Sussex, UK.

[75] Storkaas, E., 2005. Stabilizing control and controllability: Control solutions to avoid slug flow in pipeline-riser system. Ph.D. thesis, Norwegian University of Science and Technology, NTNU.

[76] Storkaas, E., Skogestad, S., 2003. A low-dimensional dynamic model of severe slugging for control design and analysis. In: 11th International Conference on Multiphase flow. BHR Group, San Remo, Italy, pp. 117–133.

[77] Storkaas, E., Skogestad, S., 2007. Controllability analysis of two-phase pipeline-riser systems at riser slugging conditions. Control Engineering Practice 15 (5), 567–581.

[78] Taitel, Y., 1986. Stability of severe slugging. International Journal of Multiphase Flow 12 (2), 203–217.

[79] Time, R. W., May 2011. Flow assurance and multiphase flow. Seminar at Aker Solutions, Stavanger.

[80] Tuvnes, H., 2008. Final year project: Severe well slugging and reservoir-well interactions, modeling and simulations. Tech. rep., Norwegian University of Science and Techology.

[81] Vorotnikov, V. I., 1997. Partial Stability and Control, 1st Edition. Birkhäuser, Boston.

[82] Yocum, B., April 1973. Offshore riser slug flow avoidance: Mathematical models for design and optimization. In: SPE European Meeting. Society of Petroleum Engineers, London, United Kingdom, p. SPE 4312.

[83] Yuwana, M., Seborg, D. E., May 1982. A new method for on-line controller tuning. AIChE Journal 28 (3), 434–440.